Response to Review 1

Thank you for the helpful comments and suggestions. We appreciate your time for reviewing our paper. We have addressed all of your comments as detailed below:

p2 line 29: The authors may want to consider the publication of Peeters et al. PCCP 2014, if they mention new gas-phase chemistry of isoprene.

Yes, good point, we had included the Wennberg et al., 2018 review paper as a summary of these advances in gas-phase chemistry, but to be more thorough we have added the following to include some examples of both recent and important experimental and theoretical studies. We assume you are referring to the Peeters et al. PCCP 2009 and Peeters et al. J. Phys. Chem. A., 2014 papers.

> "Additionally, there have been major recent advances in our understanding of isoprene gas-phase oxidation (Wennberg et al., 2018, and references therein) including theoretical (e.g., Peeters et al., 2009, 2014; Kjaergaard et al., 2012) and experimental (e.g., Teng et al., 2017; Nguyen et al., 2015; Lee et al., 2014; Jacobs et al., 2014) studies. This improved understanding of isoprene gas-phase chemistry influences the processes governing isoprene SOA formation and informs the experimental design of the present work."

p3, Fig 1: I would suggest to add reference for the chemical scheme that is shown. What is the importance of the 1,5-H shift reaction that is shown in the scheme for conditions of high NO in these experiments?

Yes, we added a reference for both Figure 1 and Figure 2 and we removed the peroxy radical undergoing a 1,5-H shift to Figure 1. We do not detect the organic nitrate from this reaction, which is likely because this 1,5-H shift will not occur at the high levels of NO in these experiments. For clarity, we also add further detail describing Figure 1 in the introduction.

In the Figure 1 and 2 caption:

> "largely based on schemes in Wennberg et al. (2018)"

And in the introduction:

> "The formation of some organic nitrate SOA-precursors are summarized in Figure 1, which is largely adapted from schemes presented in Wennberg et al. (2018) with the exception of the isoprene dihydroxy nitrooxy alkoxy radical 1,5 H-shift. Wennberg et al. (2018) suggests the importance of a similar peroxy radical 1,5 H-shift, which will not form in the present experiments due to the high levels of NO. However, based on past studies largely on alkane oxidation (Orlando et al., 2003; Atkinson, 2007), the equivalent alkoxy radical 1,5 H-shift is expected to occur and has the potential to form low-volatility nitrates as further described in Section 5.1."

p5 l6: I assume the specification of the Milli-Q water is meant to be 18 M Ohm.

Yes, thanks we have updated this to "ultrapure water (18 M Ω, Millipore Milli-Q)"

p5 l18: I would suggest to add the mean diameter of the seed aerosol for information.

Yes, this has been added:

> "The seed aerosol particle number concentration had an approximately lognormal diameter distribution centered on average ~100 nm."

p7 l13: The author mention that in only few experiments NO_2 was directly detected and in other NO_2 was modelled. How was the model-measurement agreement of NO_2 in the experiments, when NO_2 was measured?

Yes, unfortunately the luminol NO_2/acyl peroxynitrate analyzer, which has less interferences than the Teledyne NO_x analyzer was not operational for all experiments. In Figure S3, we show an example of a LV and 2MGA pathway experiment for modeled and measured NO_2. The NO_2 is reasonably well captured by the model, but as is explained in the supplement remaining biases are likely caused by measurement interferences or unaccounted for wall deposition of NO_x reservoir species. We had added reference to this Figure in Section 3 of the main text, but we also now reference this Figure in the instrument section as well:

> "The NO_2 measured by the luminol NO_2/acyl peroxynitrate analyzer compares reasonably well with the simulated NO_2 from the kinetic model (Figure S3)."

p8 l26: I would suggest to mention the parameters that were constrained by measurements in the model.

Yes, this has been added:

> "As listed in Table 1, the kinetic model was initialized for each experiment with the measured initial concentration of VOC, NO, NO_2, and CH_3ONO as well as the measured average temperature and relative humidity."

p12 l1-9: What does the unreasonable result of the correction of DMA data for wall loss mean for the uncertainty of yields determined for similar conditions in this work?

The unreasonable result of the correction of DMA data described in this paragraph only applies to humid experiments and is why we do not report any DMA data from the humid experiments. We add the following to this paragraph to make this clearer.

> "Thus, in this work, only the AMS results will be discussed for the humid experiments and SOA yields are only reported for experiments performed under dry conditions (Table 1). None of the dry experiments exhibited the odd behavior observed in the humid experiments, and the AMS results confirm that under dry conditions minimal nitric acid partitioned to the aerosols (Figure S10). For the dry experiments, the uncertainties are well characterized by the dry control experiments presented in Figure 3."

p14: Fig 5: The figure does not very clearly support the statement that SOA mass yield depends on the initial seed aerosol correction. There are essentially two values for the range from 1000 to 2000 and from 2500 to 6000 m2/cm3. Could you please

comment?

Yes, we have rephrased this in the text to be clearer and offer some further explanation. We interpret Figure 5 as having three regions: 0, 1000-1500, and 2500-6000 um2/cm3 instead of the two you specify. As seed aerosol increases, the SOA mass yield increases until a plateau is reached. This non-linear nature is expected especially for the isoprene SOA precursors as described below:

> "Similar to previous studies (e.g., Zhang et al. (2014)), at a certain point increased seed surface area no longer substantially impacts the SOA yield (i.e., Figure 5 after 2500 μm^2 cm^{-3}). This point will heavily depend on the system and the saturation mass concentration (C*) of the SOA precursors. As shown in Table S2, the isoprene SOA precursors are mostly classified as IVOCs and SVOCs (Donahue et al., 2012). Reaching a point where most of the vapors are in particles relative to the chamber wall is expected for IVOCs and SVOCs, which have moderate vapor wall losses in Teflon chambers especially under dry conditions (Zhang et al., 2014; Huang et al., 2018)."

p25 l27-30: Does the statement that SOA from the LV pathway is moderately higher than from 2MGA takes into account the differences in the turnover of the OH oxidation of the precursors of the two pathways?

Yes, this is exactly why we do not directly compare the measured SOA yields from the LV and 2MGA pathways. As described in Section 5.5, we use the kinetic model at atmospheric conditions to estimate the contribution of both the LV and 2MGA pathways to the total. We have also added the following two sentences to make this clearer:

> "In this study, direct comparison of the results from the 2MGA and LV pathways is difficult due to the difference in the extent of oxidation between the two regimes caused by the use of different VOC precursors and the variation in OH levels (Table 1). Thus, the kinetic model is used here to estimate the contribution of each pathway to the total under consistent oxidant levels."

Response to Review 2

Thank you for the helpful comments and suggestions. We appreciate your time for reviewing our paper. We have addressed all of your comments as detailed below:

Major: 1. The authors concluded in the abstract that the LV pathway which produces organic nitrates and dinitrates likely contribute to isoprene SOA under high-NO conditions more substantially than previously thought under typical atmospheric conditions. But some components of the typical atmospheric conditions were not thoroughly discussed. For example, how does hydrolysis of the organic nitrates affect this contribution? How would aerosol acidity affect the contribution from the 2MGA pathway? Would low particle surface areas in real atmosphere impede partitioning of the products that the authors discussed? In addition, as the authors have claimed themselves that the yields of these LV organic nitrates are highly uncertain, the MCM model assumes a yield of 10.4%. Estimation of LV pathway yield using this model is thus also highly uncertain. The results from this model that LV pathway yield of ~0.15 is rather hypothetic and I suggest leave it out of the abstract. Moreover, the partitioning behavior can be very different in the atmosphere compared to the chamber studies.

First, the 0.15 SOA yield is measured from the experiments (Figure 5), and not estimated from the kinetic model, so we leave this in the abstract, but revise the sentence as stated below:

> "the experimentally measured SOA mass yield from the LV pathway is ~0.15"

We understand your concern that we too quickly extrapolate the impact of our results to the atmosphere. We agree that more detailed particle-phase box and regional/global modeling, which is out of scope of this work, would be necessary to fully understand the impact of our experimental results on SOA formed in the atmosphere, which we have already explained in Section 5.5. The modeling here is only meant to begin the process of comparing the SOA contribution from the two pathways. It is impossible to fully describe all of this in an abstract. Thus, we remove the rough attempt to approximate the contribution of each pathway to the atmosphere from the abstract and instead include a broader statement based only on our experimental results, which is the primary focus of this work. The simplified approximation is still included in Section 5.5 and in the conclusion, and we have included more explanation of the limitations of the simplified kinetic model used in this work in Section 5.5. As related to Major comment 2, this modeling is necessary in order to compare the two regimes under similar OH levels, from the same VOC precursor, and under atmospherically relevant conditions.

We change the last two sentences of the abstract to the following:

> "The isoprene SOA mass yield from the LV pathway measured in this work is significantly higher than previous studies have reported suggesting that low-volatility compounds such as organic nitrates and dinitrates may contribute to isoprene SOA under high-NO_x conditions significantly more than previously thought, and thus deserve continued study."

We add more detail in Section 5.5 and updated our approach to account for changes in the concentration of organic aerosol between chamber experiments and the ambient atmosphere. These revisions in our approach do not change the overall results significantly, but hopefully add more confidence:

> "To estimate the aerosol contribution from the LV pathway, we assume that SOA production from the LV pathway scales with the production of isoprene dihydroxy dinitrates. Organic aerosol concentrations are higher in chamber experiments than the ambient atmosphere. By using low levels of VOC precursors compared to previous studies, this study attempts to reduce the organic aerosol concentrations to produce results more relevant to the ambient atmosphere. However, due to limitations in the DMA sensitivity, reducing the organic aerosol concentrations further to ambient levels is not possible. The ratio of the measured SOA yield (Figure 5) versus the simulated gas-phase dihydroxy dinitrate SOA precursor yield (Figure S4) is about 5. F_P is decreased by a factor of 2 for the dihydroxy dinitrates when C_{OA} is reduced from ~25 μg cm^{-3} in the chamber to ~4μg cm^{-3} measured in the Southeast U.S. (Zhang et al., 2018). Thus, we multiply the dihydroxy dinitrate SOA precursors by 2.5 and we convert to mass by multiplying by the molecular weight of dihydroxy dinitrate. MCM v3.3.1 assumes a nitrate yield of 0.087-0.104 from NO reacting with the peroxy radical derived from OH + isoprene hydroxy nitrate. Low-volatility nitrates such as dihydroxy hydroperoxy nitrates form when HO_2 reacts with the peroxy radical derived from OH + isoprene hydroxy nitrate. Such products would not form in the chamber conditions used in this work where NO levels remained above 100 ppb, but would form in the ambient atmosphere. Considering these low-volatility species from mixed chemical regimes would further increase the SOA mass generated from the LV pathway.
>
> For the 2MGA pathway, we convert to mass by multiplying gas-phase HMML by the molecular weight of 2-MGA (120 g/mol), 2-MGA-nitrate (165 g/mol), and 2-MGA-sulfate (200 g/mol), which are the expected condensed-phase products under the high humidity levels in the atmosphere. Laboratory studies confirm that 2-MGA forms under humid conditions and some of the 2-MGA partitions to the gas-phase as expected based on its volatility (Nguyen et al., 2015). For simplicity, we assume most of the HMML forms 2-MGA-nitrate and 2-MGA-sulfate, but acknowledge further experimental and modeling studies are needed to fully understand HMML/2-MGA aqueous phase chemistry.
>
> Then based on the gas-phase SOA precursor distribution from the kinetic model and assumptions above, under typical atmospheric conditions the fraction of the total SOA mass from isoprene OH-initiated oxidation under high-NO_x conditions is ~0.7 from the LV pathway and ~0.3 from the 2MGA pathway. This assumes that the dihydroxy dinitrates are valid surrogates for the isoprene SOA. Considering many multi-functional isoprene derived organic nitrates have been detected in ambient aerosol (Lee et al., 2016), all SOA precursors in Table S2 with $F_P > 0.05$ at 26°C are combined and converted to mass. Extrapolating these to ambient organic aerosol concentrations is more difficult because these compounds are more likely to exist in the particle phase because of accretion reactions and not volatility. When these products are assumed to exist entirely in the particle-phase and no factor is applied to correct for differences in organic aerosol

> concentration or for these products only representing about 1/3 of the isoprene SOA yield measured in this study (Figure S4), the LV pathway is estimated to contribute to ~0.6 of the SOA formed under high-NO_x conditions."

Also in Section 5.5, we added more detail explaining the need for additional experiments and modeling to more completely extrapolate the chamber SOA yields to the atmosphere, which is out of the scope of our current work.

> "Additional studies addressing organic nitrate hydrolysis and aerosol acidity are also necessary to fully understand the relative impact of the two pathways on SOA formation. Additionally, the kinetic model used in this work only estimates gas-phase potential SOA precursors. Future analysis using a more complex model that explicitly simulates both the gas and particle phases would be useful for extrapolating the SOA yields measured here to the ambient atmosphere, which typically has lower organic aerosol concentrations than chamber experiments. This would need to be combined with additional analysis of the chemical constituents in the particle phase. From past work (Kleindienst et al., 2009; Xu et al., 2014; D'Ambro et al., 2017) demonstrating that isoprene derived SOA under high-NO_x conditions is lower in volatility than that derived under low-NO_x conditions and the C* values estimated in this work (Table S2), accretion reactions appear to be important even in the LV pathway experiments. The degree to which accretion reactions occur in the LV pathway experiments to form even lower volatility products is quite uncertain and will greatly impact future analysis on how best to extrapolate isoprene SOA yields measured in chambers to the ambient atmosphere."

We also revise the concluding statement slightly:

> "we now estimate based on the simple assumptions discussed in Section 5.5 that the LV pathway produces moderately more SOA mass than the 2MGA pathway due to the high isoprene SOA yield from the LV pathway measured in this work."

We also better explain why adding additional inorganic seed aerosol is necessary to compete with vapor wall losses in Section 4.2:

> "With the addition of inorganic seed aerosol like ammonium sulfate, vapor species are expected to partition more to particles relative to the chamber wall (Zhang et al., 2014). The gas-particle equilibrium is not expected to be dependent on the concentration of inorganic seed aerosol, but instead is dependent on the concentration of organic aerosol. Depending on the saturation mass concentration (C*), as the concentration of organic aerosol rises, vapors are present more in the particle-phase relative to the gas-phase (Seinfeld and Pandis, 2016). C* and the fraction of a compound expected to be in the particle phase (F_P) were estimated for a variety of organic nitrates and dinitrates in MCM v3.3.1 at 13, 26, and 32°C (Table S2)."

We would welcome future collaboration using the dataset described in this work to aid in development of regional and global models to more thoroughly determine the SOA contribution from the LV and 2MGA pathways. This is out of scope for the present work, which focuses on measurement of SOA yields, but we have added a statement in the Data Availability section to encourage future work in this direction:

> “We welcome future collaboration with those who wish to use this data set for additional modeling purposes (e.g., creating volatility basis set parameters for global/regional models or for evaluating the results with a more complex box-model that includes aerosol chemistry). Please contact Rebecca Schwantes (rschwant@ucar.edu).”

2. Validation is needed to explain why the authors only studied the 2MGA pathway using methacrolein as the initial VOC. I understand that the authors tried to tailor the conditions to separate the two pathways and measure SOA yield from each pathway. This is a really good idea. But then, a direct comparison between the two pathways is also needed, which is more straightforward and reasonable to start with isoprene and vary NO/NO$_2$ between different experiments. For example, using the many analytical tools in the authors’ lab, they can show that as NO/NO$_2$ decreases, the gas-phase (CIMS) and particle-phase (AMS) organic nitrates and dinitrates decrease, while the HMML and 2MGA increase. Comparing with the isolated experiments, quantification of the two pathways is probably possible too. In this way, the same OH oxidation extent and seed particle surface area will be used and variations can be better controlled. Although the 2MGA pathway from isoprene and methacrolein oxidation is the same mechanistically, in direction isoprene photooxidation experiment, the 2MGA pathway products are formed in later generation and that may change the dynamics (e.g., OH availability at different times) in the SOA formation. Also, how signature SOA product ions (both CIMS and AMS) from the LV pathway and the 2MGA pathway in the same isoprene photooxidation experiments as NO/NO$_2$ ratio varies is a more desired and direct way to present the results.

Previous studies have already clearly demonstrated the impact of changing the NO$_2$/NO ratio on the SOA yield from methacrolein and isoprene (e.g., Chan et al. 2010). The purpose of this study was not to repeat their results, but to attempt to completely separate the regimes and assess how the SOA from these two unique regimes respond to changing chamber conditions. From this we were able to understand more than past experiments. For example, if we had not completely separated the regimes, we would not have determined that low-volatility nitrates contribute appreciably to SOA formation as long as the experiments use high seed aerosol surface areas to limit the impact of vapor wall losses. We also would not have understood that the AMS is significantly more sensitive to aerosol from the 2MGA pathway and not the LV pathway. We potentially could have misinterpreted the results if we had only used the combined approach you describe above.

Unfortunately, the “combined” approach you describe above will result in mixed regimes throughout. The low-volatility nitrates from isoprene oxidation will form regardless of the NO$_2$/NO ratio (see Figure 1 – none of these reactions are dependent on NO$_2$). Even during methacrolein oxidation (Figure 2), organic nitrates are not formed in the competing pathway for the acyl peroxy radical reaction with NO versus NO$_2$. So your statement that “as NO/NO$_2$ decreases, the gas-phase (CIMS) and particle-phase (AMS) organic nitrates and dinitrates decrease, while the HMML and 2MGA increase” is not true. As NO/NO$_2$ decreases, the organic nitrates and dinitrates from isoprene oxidation will largely be unaffected and HMML and 2MGA will increase. This is why we started with methacrolein as the precursor VOC for the 2MGA pathway experiments. If we had started with isoprene, the 2MGA pathway experiments would have both nitrates and dinitrates from the LV pathway and 2MGA aerosol.

We add further description in Section 2 to explain this further:

> "In order to completely separate the LV and 2MGA pathways, methacrolein had to be used as the VOC precursor for the 2MGA pathway experiments. If isoprene was used, even at the high NO_2/NO ratios used in the 2MGA pathway experiments, the SOA precursors from the LV pathway would form resulting in a mixed regime (i.e., chemistry in Figure 1 is not dependent on NO_2 concentration). In each case, the effect of seed surface area, temperature, and humidity on the SOA yield was independently determined."

You also suggest we use the CIMS and the AMS to differentiate the influence of these two pathways. Unfortunately, as we were performing these experiments, we realized that this was not possible due to limitations of both instruments. The CIMS can measure the organic nitrates, but we do not have sensitivities for many of these low-volatility nitrates to be quantitative. Additionally, the CF_3O^- CIMS cannot measure HMML. HMML, being a reactive alpha-lactone, is likely easily lost in the inlet or on sampling tubing and/or is not stable with the CF_3O^- ion chemistry. The AMS, which is most important for understanding the relative contribution of both pathways to SOA, is significantly more sensitive to aerosol from the 2MGA pathway than the LV pathway as explained in Section 5.3. Thus, the AMS cannot be used to separate the influence of the two pathways in mixed experiments as it realistically only measures aerosol from one of the regimes. As done here, the AMS can confirm that the two regimes are fully separated. So unfortunately, due to limitations in the CIMS and AMS techniques, we cannot separate the regimes as you suggest. You are correct that direct comparison to account for variation of OH and the extent of oxidation is important for comparing the two regimes. This is why we only use the kinetic model to directly compare the two regimes (Section 5.5) in this work. Additionally, based on the analysis of these chamber results, likely the best approach to improving isoprene SOA parameterizations in models is to parameterize the 2MGA and LV pathways separately. As explained further below, this work sets up the experimental basis for this approach. We add further description in Section 5.5 to explain this:

> "This work was not only designed to independently study SOA formation from the two high-NO_x regimes (the 2MGA and LV pathways), but also to suggest alternative methods for parameterizing isoprene SOA under high-NO_x conditions in regional and global models. Because obtaining constant NO_2/NO ratios similar to the ambient atmosphere is near impossible for a chamber study (e.g., temporal variation in Figure S3), creating isoprene SOA parameterizations based on NO_2/NO ratio that realistically extrapolate to the ambient atmosphere is not realistic. Instead, this work highlights a potential alternative. Aerosol from the 2MGA pathway could be incorporated directly from gas-phase HMML formation and aerosol from the LV pathway could be included either from formation of surrogate compounds such as isoprene dihydroxy dinitrates or with a volatility basis set scheme. By treating the SOA from these two independent regimes separately, this study sets up the experimental basis for such an approach.

> In this study, direct comparison of the results from the 2MGA and LV pathways is difficult due to the difference in the extent of oxidation between the two regimes caused by the use of different VOC precursors and the variation in OH levels (Table 1). Thus, the kinetic model is used here to estimate the contribution of each pathway to the total under consistent oxidant levels."

Finally, the results reported here are novel because we were able to completely separate the LV and 2MGA pathways and test how varying chamber conditions impacted the two regimes independently. These novel results were missed by other past studies, which took the "combined" approach you suggest. We have added further explanation of this in Section 5.4:

> "As shown in Table 2, a variety of NO_x regimes (i.e., non-consistent NO_2/NO ratios) are all labeled as high-NO_x in these past studies. Each study likely produces SOA in varying degrees from the LV and 2MGA pathways, which greatly complicates direct comparison between these past studies. By varying a large number of conditions and completely separating SOA production between the 2MGA and LV pathways, our results lend insight into the variation in these past experiments."

3. Page 12, line 22. It is very interesting that SOA yield does not vary too much as temperature changes between 13 and 32 C. The authors mention two reconciling effects: enhanced vapor wall loss and enhanced organic nitrate yields from RO2 + NO reaction under lower temperatures. Can the authors provide some quantitative constraints on these two effects? How different are the organic nitrate yields and wall loss rates under this range of temperatures? Another point to add, is that at lower temperature, more semi-volatile species may partition into the particle phase. I think this is a major effect. Previous studies using very similar temperature range and found a difference of 2-10 times in SOA yields (Clark et al., 2016 ES&T; Takekawa et al., 2003 Atmos. Environ.; Sheehan and Bowman, 2001 ES&T.). Some of these studies use isoprene, some use hydrocarbons that likely produce less volatile SOA than isoprene. The authors should think about addressing this question. Is it because the LV SOA have surprisingly low volatility that they are already mostly in the particle-phase at 30C? Can the authors estimate the vapor pressure of the nitrate and dinitrate compounds and see if this hypothesis make sense? Note that there are only two experiments at different temperatures and the lower temperature experiment started forming SOA much earlier than the higher temperature experiment. But they ended up forming similar SOA mass. From that perspective, there is a clear temperature influence. I hope the authors can address this question with more detailed discussion. The same case for the 2MGA pathway. The authors found little temperature influence on SOA mass yield. But again, that was based on only one high temperature and one low temperature experiment. The two experiments have very different seed particle surface areas too. The data provided are not sufficient to draw conclusions on temperature effects.

Thank you for pointing out the Clark et al., 2016 ES&T paper. We have now included this in Table 3 (now Table 2) and added a column for chamber volume. We explain how our results compare to this paper in Section 4.2, 4.3 and 5.4. Given that the SOA yields measured from experiments at 13 and 32 deg C were not significantly different for the LV or 2MGA pathway, we chose not to perform additional temperature experiments. Unfortunately, 13 deg C is near the limit of the Caltech chamber's temperature capability, so lower temperature experiments are not possible. Thank you for the recommendation of estimating the C* values. We have now estimated the C* and estimated fraction of a compound in the particle phase (F_P) at 13, 29, and 32°C (Table S2) for all organic nitrates and dinitrates from MCM v3.3.1 relevant to the LV pathway. We include a description of how these C* and F_P values were calculated in Section S1 of the supplement and briefly in Section 3. We also include substantial updates as explained below referencing these C* values and addressing your concerns above:

Explanation of C* values in Section 3:

> "Saturation mass concentration (C*) and fraction of each compound in the particle phase (F_P) at 13, 26, and 32°C are estimated for relevant organic nitrates and dinitrates produced in MCM v3.3.1 and listed in Table S2. C* was calculated with the vapor pressure estimated from Nannoolal et al. (2004, 2008) using the online calculator located at: http://www.aim.env.uea.ac.uk/aim/ddbst/pcalc_main.php. F_P was calculated from the C* values and gas-particle equilibrium theory as further explained in Section S1 (Seinfeld and Pandis, 2016)."

We update Section 4.2:

> "Without sufficient seed aerosol, low-volatility nitrates partition primarily to the chamber walls, and the resulting SOA yields are biased low. With the addition of inorganic seed aerosol like ammonium sulfate, vapor species are expected to partition more to particles relative to the chamber wall (Zhang et al., 2014). The gas-particle equilibrium is not expected to be dependent on the concentration of inorganic seed aerosol, but instead is dependent on the concentration of organic aerosol. Depending on the saturation mass concentration (C*), as the concentration of organic aerosol rises, vapors are present more in the particle-phase relative to the gas-phase (Seinfeld and Pandis, 2016). C* and the fraction of a compound expected to be in the particle phase (F_P) were estimated for a variety of organic nitrates and dinitrates in MCM v3.3.1 at 13, 26, and 32°C (Table S2).
>
> Similar to previous studies (e.g., Zhang et al. (2014)), at a certain point increased seed surface area no longer substantially impacts the SOA yield (i.e., Figure 5 after 2500 μm^2 cm^{-3}). This point will heavily depend on the system and the saturation mass concentration (C*) of the SOA precursors. As shown in Table S2, the isoprene SOA precursors are mostly classified as IVOCs and SVOCs (Donahue et al., 2012). Reaching a point where most of the vapors are in particles relative to the chamber wall is expected for IVOCs and SVOCs, which have moderate vapor wall losses in Teflon chambers especially under dry conditions (Zhang et al., 2014; Huang et al., 2018).
>
> As expected the isoprene dihydroxy dinitrates had the lowest C* values and high F_P at all temperatures. Based on the kinetic model, even assuming all of the isoprene dihydroxy dinitrates exist in the particle-phase, the SOA formed would be much less than that detected in this study (Figure S4). This is likely caused by too low production of the isoprene dihydroxy dinitrates and/or the importance of other SOA precursors. There are many additional compounds largely produced from hydroxy aldehyde oxidation or alkoxy [1,5]-H-shifts (Figure 1) with F_P at 26°C between 0.05 and 0.4 (Table S2). The vapor pressures may be over-predicted for these specific compounds, but past studies

suggest that in general, vapor pressure estimation methods like Nannoolal et al. (2004, 2008) under-predict rather than over-predict vapor pressure (Kurten et al., 2016). From the C* calculations (Table S2), none of the multi-functional organic nitrates are expected to be appreciably in the particle phase. However, in a recent study, Lee et al. (2016) detected many multi-functional organic nitrates in aerosols in the ambient atmosphere, which has lower organic aerosol concentrations than chamber studies. Possibly, MCM under-predicts the formation of these IVOC and SVOC products (Figure S4), such that even if only a fraction exists in the particle-phase relative to the gas-phase, an appreciable mass of aerosol still forms and/or these results suggest that volatility is not the only driver for aerosol formation from the LV pathway. All of the multi-functional nitrates here with estimated F_P at 26°C between 0.05 and 0.4 have at least one hydroxy or aldehyde group (Table S2). Alcohols and aldehydes are well known to combine in particles to produce hemiacetals, whose vapor pressure is significantly lower than that of the initial reactants (Kroll and Seinfeld, 2008). Several past studies have confirmed that NO_x in general, but not necessarily linearly, decreases the volatility of isoprene SOA (Kleindienst et al., 2009; Xu et al., 2014; D'Ambro et al., 2017). This decrease in volatility is likely due to accretion reactions. Whether the accretion reactions from hemiacetal formation versus those from 2MGA oligomerization are responsible for the decrease in volatility is yet unknown.

Differences in the SOA yield at 10h of photooxidation by varying temperature (13-32°C) lie within the experimental uncertainty. SOA forms earlier (i.e. with less isoprene reacted) at 13°C than at 26 or 32°C at comparable seed surface areas. This is consistent with the C* values estimated in Table S2 and the above explanation demonstrating the likelihood of accretion reactions. Vapors that are only moderately in the particle phase at 26°C (e.g., FP = 0.05-0.4) will exist more appreciably in the particle phase at 13°C (e.g., FP = 0.2-0.8). From the above discussion, we expect many of these compounds are SOA precursors not based only on their volatility, but also due to their potential to react in the particle phase to form lower volatility products such as hemiacetals. Thus, if accretion reactions are the main factor, reducing temperature is expected to increase the rate of SOA production, but not necessarily to impact the overall SOA yield.

Clark et al. (2016) have also measured isoprene SOA formation under high-NOx conditions at varying temperatures. Under the high-NO_x conditions of their study, SOA is produced from both the 2MGA and LV pathways combined. Similarly to our study, Clark et al. (2016) do not find appreciable differences for temperatures from 27-40°C. Contrary, to our work, Clark et al. (2016) found that reducing the temperature to 5°C increases the SOA yield by a factor of 4. Unfortunately, there are no experiments between 5°C and 27°C to determine whether this shift is exponential or linear, so direct comparison of our results at 13°C is difficult. Under the high-NO_x conditions used by Clark et al. (2016), at colder temperatures MPAN will be more stable and so more HMML will form, which produces more SOA. Under this mixed regime, determining how much of the SOA increase is due to the LV versus the 2MGA pathway for direct comparison to this study is difficult. Additionally, Clark et al. (2016) start with significantly more isoprene than in our experiment, which enhances the concentration of

> organic aerosol, which will increase the fraction of a compound in the particle phase relative to the gas phase.
>
> While vapor wall losses of LV compounds are expected to increase at colder temperatures (Zhang et al., 2015; Schwantes et al., 2017), the organic nitrate yields are also expected to be enhanced under colder temperatures (Orlando and Tyndall, 2012). Thus, the effects of these two temperature-dependent processes might cancel. The increase in organic nitrate yield is expected to be moderate. For example, ~30% increase from 32 to 13°C is estimated for the yield of isoprene hydroxy nitrates (Wennberg et al., 2018). The loss of vapors to the walls could be much higher at colder temperatures, but this is hard to constrain as vapor wall deposition is dependent on the compound itself and the chamber used. The chamber used by Clark et al. (2016) (90 m^3) is larger than our chamber (21 m^3). Vapor wall losses are expected to be lower in larger chambers, which have a lower chamber surface area to volume ratio (Zhang et al., 2015). Significant seed aerosol is added into our chamber to reduce the influence of vapor wall deposition, but vapor wall deposition could certainly explain some of the differences at cold temperatures between our results and those from Clark et al. (2016).
>
> Consistent with past work (e.g., Kroll et al. (2005); Ng et al. (2006)), aerosol from the LV pathway is produced only after most of the isoprene is consumed, implying that aerosol from the LV pathway largely forms from later-generation chemistry (Figure 4). As shown in Figure 4, generally, SOA formation begins earlier (i.e., with less isoprene reacted) in experiments with larger seed aerosol. This is consistent with vapors partitioning more to particles relative to the chamber wall when seed aerosol is enhanced."

We also update Section 4.3 and update Figure 7. In Figure 7, two of the experiments have nearly identical seed surface areas. For ease of viewing we had shifted one over. We have reduced the size of this shift. The seed surface areas for the three temperature experiments (13, 26, and 32°C) are within 600 um^2/cm^3 of each other. This seems sufficient to demonstrate that temperature does not greatly impact the SOA yield in the 2MGA pathway at high NO_2/NO levels.

> "At the high NO_2/NO ratios used in this work, temperature does not impact SOA mass yield beyond given uncertainties (Figure 7). Based on known gas-phase chemistry, past studies (e.g., Clark et al. (2016)) with more moderate NO_2/NO ratios than that used in this work are expected to measure an enhanced SOA yield under colder temperatures due to a reduction in MPAN thermal decomposition and thereby an increase in HMML formation."

We also update Section 5.4:

> "As shown in Table 2, the range for isoprene SOA yields under high-NO_x conditions even from the two most recent studies at comparable temperatures spans over an order of magnitude (0.004 at ~21°C for Bregonzio-Rozier et al. (2015) and 0.1 at 27°C for Clark et al. (2016)). Our results are most consistent with those of Clark et al. (2016). As shown in Table 2, a variety of NO_x regimes (i.e., non-consistent NO_2/NO ratios) are all labeled as high-NO_x in these past studies. Each study likely produces SOA in varying degrees from the LV and 2MGA pathways, which greatly complicates direct comparison between

> these past studies. By varying a large number of conditions and completely separating SOA production between the 2MGA and LV pathways, our results lend insight into the variation in these past experiments.
>
> Many of the past SOA yield measurements were performed with no seed aerosol. Consistent with past results, when no seed aerosol was injected into the chamber (experiments D1 and M1), the SOA mass yield for the LV pathway (0 from isoprene) and 2MGA pathway (0.1 from methacrolein) were quite low. Past experiments performed with no seed aerosol were only measuring SOA from the 2MGA pathway, which is highly dependent on the NO_2/NO ratio (Chan et al., 2010), which varied greatly between these past studies. Clark et al. (2016), who measured high SOA yields (0.1 at 27°C) in unseeded experiments is the exception. Possibly, the larger chamber volume (90 m^3) used by Clark et al. (2016) compared to most studies listed in Table 2 reduced vapor wall losses and contributed to the enhanced SOA yield. However, other chamber characteristics might also be important because Zhang et al. (2011) measured quite low isoprene SOA yields (0.007-0.03) using a chamber larger than the one used in the Clark et al. (2016) study.
>
> While the zero or low seed aerosol loading experiments in this study generally compare well with the past, SOA yields measured here using higher initial seed surface areas are substantially greater than most studies, especially for the LV pathway. The SOA yield from the LV pathway is ~0.15 in this study, while past isoprene SOA yields are largely ~0.07 with the exception of studies optimizing for high $RO_2 + NO_2$ reactions (Chan et al., 2010) or mixed regimes - $RO_2 + HO_2$/NO (Xu et al., 2014). The SOA yield from the LV pathway in this work is even larger than the SOA yield from Clark et al. (2016) (0.1 at 27°C), which includes SOA from both the LV and 2MGA pathways. Possibly the larger chamber volume used by Clark et al. (2016) reduces vapor wall losses, but not to the extent that enhanced seed surface area does in this work."

4. The authors use "low-volatility" to describe the organic nitrates. But they should also justify this by providing some estimates of the vapor pressures or C* of the molecules in Figure 1.

As explained in Major comment 3, we have estimated C* values for relevant organic nitrates and dinitrates in MCM v3.3.1. These are listed now in Table S2. In the introduction, we also define how we use low-volatility throughout the text:

> "Throughout the text we use low-volatility as a general term representing gas-phase compounds with a potential to exist partially in the particle phase. In this work, low-volatility compounds include the following volatility classes from Donahue et al. (2012): IVOC (Intermediate), SVOC (Semi-), LVOC (Low), and ELVOC (Extremely Low). When referring to specific volatility classes, the acronyms defined above are used."

Minor: 1. Title and abstract: HMML is formed not only under high-NO, but also high-NO_2 (MPAN is their precursor). It is thus inaccurate to term "high-NO" as the condition. As the authors also point out in the text, NO_2/NO ratio is an important indicator of the two pathways. From the experimental list, NO and NO_2 are indeed adjusted to optimize

different conditions. Thus, it seems more appropriate to use "high NO_x" rather than "high-NO" in this manuscript.

We had chosen high-NO here based only on the first step of isoprene oxidation by OH. This peroxy radical will not react with NO_2. This then defines the scope of our work, which is all subsequent chemistry past the isoprene hydroxy peroxy radical + NO reaction. However, we do understand your more general interpretation too, which is based on all peroxy and acyl peroxy radicals in the system reacting with either NO or NO_2.

Thus, we change all instances of high-NO to high-NO_x in the paper unless we are particularly referring to only high-NO or high-NO_2 conditions, and we also add further explanation in the introduction:

> "There are many definitions for high-NO_x conditions (Wennberg, 2013). Here we test two different high-NO_x chemical regimes. Experiments targeting the LV pathway are designed such that all peroxy radicals including acyl peroxy radicals dominantly react with NO and experiments targeting the 2MGA pathway are designed such that all acyl peroxy radicals dominantly react with NO_2 and all other peroxy radicals dominantly react with NO."

2. Page 3, line 2. The 2MGA pathway should refer to particle-phase products (2-MGA, its oligomers, and its organosulfates) from further oxidation of MPAN or uptake of HMML.

Yes, we updated this as suggested to include more detail:

> "representing aerosol formed from 2MGA, its oligomers, its organosulfates, and its organonitrates (blue compounds in Figure 2)"

3. Page 5, line 27. Whether the NO_2 signal can be interferences from nitrous acid or CH_3ONO can be easily tested using the standards.

Yes, we know CH_3ONO and nitrous acid are interferences based on standards. As suggested we adjust the text to be more descriptive:

> "(e.g., known interferences include organic nitrates, nitrous acid, and CH_3ONO)."

4. Page 12, line 14. It is unclear what is referred to as "the 2-MGA precursor" here. Is it MACR? MPAN? HMML? This information was obtained from the kinetic mechanism. I think the author should at least provide the simulations in the supporting information and mention it in the main text.

We understand your confusion and have completely revised this so that the use of the kinetic mechanism is more straightforward. Originally, we had added "tracers" for both the 2MGA (HMML + MAE) and LV pathway (dihydroxy dinitrates) into the mechanism. Given your comment, we have decided to change this. We have made some small changes to the MCM v3.3.1 mechanism to be more consistent with recommendations from the Caltech isoprene mechanism (Wennberg et al. 2018). We have listed all changes to MCMv3.3.1 in the original Table 2, which has been moved to the supplement (now Table S1) due to length. We have added text summarizing these changes in Section 3:

> "Updates include inorganic reactions needed for chamber studies with large NO_x levels (e.g., CH_3ONO photolysis) and small changes to the isoprene chemistry based largely on Wennberg et al. (2018) and consistent with Figures 1 and 2. As shown in Table S1, these updates include: the first generation isoprene hydroxy nitrate yields, the rates and branching ratios for the oxidation of the first generation isoprene hydroxy nitrates, and the HMML yield from the MPAN + OH reaction. In some cases, δ-isoprene hydroxy alkoxy radicals in MCM v3.3.1 decompose through peroxy radical H-shifts directly to products that would not form under the high-NO conditions in this work. For simplicity, we change these reactions, so that the δ-isoprene hydroxy alkoxy radicals form unity yields of hydroxy aldehydes."
>
> Now that we have directly updated HMML formation in the mechanism, we can refer to HMML rather than the 2-MGA precursor throughout the text. We have updated this in Section 4.2, Section 4.3, Section 5.5, and in S1 of the Supplement.

5. Page 12, line 26-27. Exceptions are when temperature was low and initial seed particle surface area was high.

We have already explained that the low temperature experiment forms aerosol earlier (see major comment 3). Here we add an explanation for the higher seed surface area experiments as well:

> "As shown in Figure 4, generally, SOA formation begins earlier (i.e., with less isoprene reacted) in experiments with larger seed aerosol. This is consistent with vapors partitioning more to particles relative to the chamber wall when seed aerosol is enhanced."

6. Page 12, line 31. Based on the earlier description, the kinetic model combines MCM and some other gas-phase reactions that are listed in Table 2. So the kinetic model seems to be a pure gas-phase model. It is thus unclear when the authors mentioned that the kinetic model can predict the SOA mass yield. This sentence needs to be re-phrased to something like: "The kinetic model predicts that the formation of gas-phase dinitrates from experiment D7 is similar to the other experiments". Then the followed issue is whether this single species can represent the overall SOA in the studied condition. The authors may want to also compare other proposed LV-pathway products from the model.

Yes, we revised this sentence:

> "The kinetic model predicts that the production of important gas-phase SOA precursors from the LV pathway (e.g., isoprene dihydroxy dinitrates), when corrected for total isoprene reacted, is similar in experiment D7 to the other experiments (Figure S4)."

We now discuss how other potential SOA precursors may also influence the isoprene SOA yield in Section 4.2 (see response to major comment 3). Figure S4 has also been updated. Unfortunately, use of the dihydroxy dinitrates as a surrogate for SOA from the LV pathway is necessary because the exact composition is unknown. We add to section 5.5, another approach using all of the compounds in Table S2 with $F_P > 0.05$ at 26°C. This produces similar results to using dihydroxy dinitrates as the surrogate for LV pathway SOA and hopefully adds confidence to this approach.

> "This assumes that the dihydroxy dinitrates are valid surrogates for the isoprene SOA. Considering many multi-functional isoprene derived organic nitrates have been detected in ambient aerosol (Lee et al., 2016), all SOA precursors in Table S2 with $F_P > 0.05$ at 26°C are combined and converted to mass. Extrapolating these to ambient organic aerosol concentrations is more difficult because these compounds are more likely to exist in the particle phase because of accretion reactions and not volatility. When these products are assumed to exist entirely in the particle-phase and no factor is applied to correct for differences in organic aerosol concentration or for these products only representing about 1/3 of the isoprene SOA yield measured in this study (Figure S4), the LV pathway is estimated to contribute to ~0.6 of the SOA formed under high-NO_x conditions."

7. Page 15, line 9. The authors may also want to consider that organosulfate formation in the presence of ammonium sulfate seed particles.

Yes, we have added the following sentence to account for this:

> "Alternatively, the presence of higher ammonium sulfate seed aerosol may also increase organosulfate formation, which could impact SOA composition and yield."

8. Page 15, line 15. HMML/reacted MACR = 0.25 does not mean the SOA yield from HMML uptake is 0.25. HMML is a $C_4H_6O_3$ lactone. If you think about its vapor pressure, it is probably on the more volatile side of the SVOC range. It will have a large fraction in the gas phase.

Yes, we have now added in more detail here:

> "HMML, based on volatility alone, would exist mostly in the gas phase, but because HMML is very reactive (e.g., oligomerization or reaction with inorganic ions in the particle phase), HMML quickly produces aerosol (Kjaergaard et al., 2012; Nguyen et al., 2015). Based on HMML production simulated by the kinetic mechanism under the conditions used in these experiments, ~0.21 SOA mass yield from methacrolein is expected purely from the mass contained in HMML (MW = 102 g/mol, Figure S4). At first, the molecular weight of HMML itself is used because this is the mass of the majority of the oligomer monomers."

9. Page 17, line 30 to Page 18, line 2. The description is unclear. A brief but better explanation (better than just saying "highly uncertain") is needed here to explain why the Lee et al. used upper limit yields 10 times higher than their measurements? Are there other studies supporting the yields?

Lee et al. 2014 based these uncertainties on carbon closure. We recognize that this might not be the best approach especially considering that the uncertainties in the sensitivities of the measured compounds could also explain the lack of carbon closure (Lee et al., 2014, Interactive comment on "Kinetics of the reactions of isoprene-derived hydroxynitrates: gas phase epoxide formation and solution phase hydrolysis" by M. I. Jacobs et al.). Thus, we revise this sentence to be more general:

> "One study, Lee et al. (2014), was able to quantify the yield of dinitrates from the first-generation isoprene hydroxy nitrate standards. Assuming a sensitivity similar to the isoprene hydroxy nitrate standards, Lee et al. (2014) measured a dinitrate yield of 0.03-0.04 from OH-initiated oxidation of the δ-1-hydroxy,4-nitrate isomer."

10. Page 18, line 17. The Lee et al., 2016 PNAS study provide some constraints on isoprene nitrate yields and should be cited here.

Yes, we had already cited this paper in Section 5.3 and the conclusions, but we now cite this paper here too:

> "Many multi-functional isoprene derived organic nitrates have been detected in ambient aerosol (Lee et al., 2016)."

11. Figures 9 and 10. What do the rest unlabeled ions represent?

We add "in gray" to the description in Figure 9 and 10 to clarify that all of the mass spectra are in gray and then specific m/z are labeled in the various colors. The aerosol mass spectrometer produces spectra with a high degree of fragmentation. Thus, as has been done by previous studies on isoprene oxidation (e.g., Chan et al. 2010 for 2-MGA and 2-MGA oligomers aerosol and Lin et al. (2012) for IEPOX aerosol), we only characterize the ions that form distinctly high peaks.

12. Page 25, line 23. The authors provided evidence that MAE is not a product from MPAN oxidation, but then use MCM which assumes MAE has a 21% yield from MPAN oxidation, to estimate contribution to the 2MGA pathway. Why not modify the MCM model and provide an estimate that the authors are more confident about?

We have now modified MCM v3.3.1, see Table S1 for a list of reactions and a description of these changes in Section 3. See the response to minor comment 4 for more detail.

13. The CIMS data are shown for the LV pathway. CIMS can also measure HMML in the 2MGA pathway and I'm curious why the data were not shown.

Unfortunately, the CF_3O^- CIMS, used in this work, cannot measure HMML. HMML, being a reactive alpha-lactone, is likely easily lost in the inlet or on sampling tubing and/or is not stable with the CF_3O^- ion chemistry.

Low-volatility compounds contribute significantly to isoprene SOA under high-NO_x conditions

Rebecca H. Schwantes[1,5], Sophia M. Charan[2], Kelvin H. Bates[2,6], Yuanlong Huang[1], Tran B. Nguyen[3], Huajun Mai[1], Weimeng Kong[2], Richard C. Flagan[2], and John H. Seinfeld[2,4]

[1]Division of Geological and Planetary Sciences, California Institute of Technology, 1200 East California Boulevard, Pasadena, California 91125, United States
[2]Division of Chemistry and Chemical Engineering, California Institute of Technology, 1200 East California Boulevard, Pasadena, California 91125, United States
[3]Department of Environmental Toxicology, University of California - Davis, Davis, California 95616, United States
[4]Division of Engineering and Applied Science, California Institute of Technology, Pasadena, California 91125, USA
[5]Current Affiliation: National Center for Atmospheric Research, Boulder, Colorado, 80307, USA
[6]Current Affiliation: Faculty of Arts and Sciences, Harvard University, Cambridge, MA 02138, USA

Correspondence to: Rebecca H. Schwantes (rschwant@ucar.edu)

Abstract. Recent advances in our knowledge of the gas-phase oxidation of isoprene, the impact of chamber walls on secondary organic aerosol (SOA) mass yields, and aerosol measurement analysis techniques warrant re-evaluating SOA yields from isoprene. In particular, SOA from isoprene oxidation under high-NO_x conditions forms via two major pathways: 1) low-volatility nitrates and dinitrates (LV pathway) and 2) hydroxymethyl-methyl-α-lactone (HMML) reaction on a surface or the condensed phase of particles to form 2-methyl glyceric acid and its oligomers (2MGA pathway). These SOA production pathways respond differently to reaction conditions. Past chamber experiments generated SOA with varying contributions from these two unique pathways, leading to results that are difficult to interpret. This study examines the SOA yields from these two pathways independently, which improves the interpretation of previous results and provides further understanding of the relevance of chamber SOA yields to the atmosphere and regional/global modeling. Results suggest that low-volatility nitrates and dinitrates produce significantly more aerosol than previously thought; the experimentally measured SOA mass yield from the LV pathway is ~~$\simeq$~~ $\sim$0.15. Sufficient seed surface area at the start of the reaction is needed to limit the effects of vapor wall losses of low-volatility compounds and accurately measure the complete SOA mass yield. Under dry conditions, substantial amounts of SOA are formed from HMML ring-opening reactions with inorganic ions and HMML organic oligomerization processes. However, the lactone organic oligomerization reactions are suppressed under more atmospherically relevant humidity levels, where hydration of the lactone is more competitive. This limits the SOA formation potential from the 2MGA pathway to HMML ring-opening reactions with water or inorganic ions under typical atmospheric conditions. ~~Due to the high~~ The isoprene SOA mass yield from the LV pathway measured in this work ~~, we now roughly estimate that the LV pathway produces moderately more SOA mass than the 2MGA pathway under typical atmospheric conditions (RH = 70%, T = 298K, NO_2/NO = 6, NO = 0.05 ppb, isoprene = 5 ppb, and OH = 1.5 x 10^6 molec cm^{-3}). This suggests that in the atmosphere~~ is significantly higher than previous studies have reported suggesting that low-volatility compounds such as organic nitrates and dinitrates may contribute to isoprene SOA under high-NO_x conditions significantly more than previously thought, and thus deserve continued study.

1 Introduction

In the atmosphere, submicrometer particulate matter is composed of a significant fraction of organic aerosol (Zhang et al., 2007). There are two forms of organic aerosol: primary, which is directly emitted into the atmosphere, and secondary, which is formed when gas-phase compounds partition to the particle phase. Processes governing secondary organic aerosol (SOA) formation are particularly complex (Kroll and Seinfeld, 2008; Hallquist et al., 2009). SOA yields, the ratio of the mass of SOA formed to the mass of the parent volatile organic compound (VOC) reacted, are measured in environmental chambers and are used in models to reduce the complexity of SOA formation.

Isoprene is the dominant non-methane biogenic VOC emitted into the atmosphere. Because of the large flux of isoprene ($\sim$535 Tg yr^{-1}) into the atmosphere (Guenther et al., 2012), oxidation of isoprene is a significant source of SOA even though SOA yields measured in chambers are relatively low (Carlton et al., 2009). Despite numerous experimental studies of isoprene SOA formation under varying conditions (Pandis et al., 1991; Edney et al., 2005; Kroll et al., 2005; Dommen et al., 2006; Kleindienst et al., 2006; Kroll et al., 2006; Ng et al., 2006; Paulot et al., 2009; Chan et al., 2010; Chhabra et al., 2010; Surratt et al., 2010; Nguyen et al., 2011; Zhang et al., 2011, 2012; Lin et al., 2013; Nguyen et al., 2014b; Xu et al., 2014; Krechmer et al., 2015; Lambe et al., 2015; Nguyen et al., 2015; Bregonzio-Rozier et al., 2015, etc.) (Clark et al., 2016), a consensus on the magnitude of SOA formed from isoprene oxidation by the hydroxyl radical (OH) is still lacking (Carlton et al., 2009; Bregonzio-Rozier et al., 2015) (Clark et al., 2016). This lack of consensus in the experimental data leads recent global modeling studies (Marais et al., 2016; Stadtler et al., 2018) to implement SOA schemes that produce significantly different overall isoprene SOA yields. Isoprene SOA yields have been shown to depend on a variety of factors including RO_2 fate, NO_2/NO ratio, relative humidity, degree of oxidation, temperature, seed surface area, particle acidity, and chamber irradiation source (Carlton et al., 2009). These experimental conditions have not always been controlled or reported, which is likely a major reason for the variability seen in past isoprene SOA yields. By measuring isoprene SOA yields while controlling for seed surface area, RO_2 fate, NO_2/NO ratio, relative humidity, and temperature, we seek to resolve uncertainties in SOA formation in past yields.

Recent advances have improved our understanding of how chamber SOA yields should be measured and analyzed. This includes accounting carefully for particle wall deposition (Loza et al., 2012), vapor wall deposition (Zhang et al., 2014; Ehn et al., 2014), and particle coagulation (Nah et al., 2017). Advances have also taken place in the data processing of aerosol size distribution measurements by the differential mobility analyzer coupled to a condensation particle counter (DMA-CPC), the main instrument used to measure SOA yields (Mai and Flagan, 2018; Mai et al., 2018). Because isoprene SOA yields tend to be relatively small, the DMA data inversion technique and correction for CPC response time are quite important.

Additionally, there have been major recent advances in our understanding of isoprene gas-phase oxidation ~~(Wennberg et al., 2018) and~~ (Wennberg et al., 2018, and references therein) including theoretical (e.g., Peeters et al., 2009, 2014; Kjaergaard et al., 2012) and experimental (e.g., Teng et al., 2017; Nguyen et al., 2015; Lee et al., 2014; Jacobs et al., 2014) studies. This improved understanding of isoprene gas-phase chemistry influences the processes governing isoprene SOA formation ~~. The present work~~and informs the experimental design of the present work. This work focuses on the production of SOA from OH-initiated isoprene oxidation under high-NO_x conditions, which occurs via two major chemical pathways (Figures 1 and 2). The first we define throughout as the low volatility (LV) pathway representing all aerosol formed from the equilibrium gas/particle partitioning of compounds with sufficiently low volatility, which mostly include functionalized nitrates and dinitrates (e.g., red compounds in Figure 1). The second we define as the 2-methyl glyceric acid (2MGA) pathway representing aerosol formed from 2MGA~~and its oligomers~~, its oligomers, its organosulfates, and its organonitrates (blue compounds in Figure 2). There are many definitions for high-NO_x conditions (Wennberg, 2013). Here we test two different high-NO_x chemical regimes. Experiments targeting the LV pathway are designed such that all peroxy radicals including acyl peroxy radicals dominantly react with NO and experiments targeting the 2MGA pathway are designed such that all acyl peroxy radicals dominantly react with NO_2 and all other peroxy radicals dominantly react with NO.

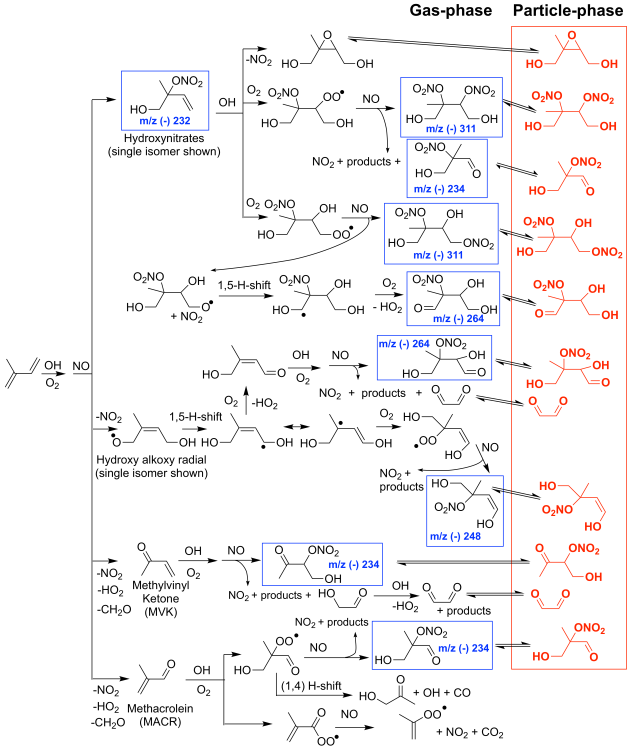

Figure 1. Simplified chemical mechanism of isoprene OH-initiated oxidation under high-NO conditions, largely based on schemes in Wennberg et al. (2018), emphasizing SOA generated from the LV pathway, which includes low-volatility organic nitrates and dinitrates in red. Compounds detected in the gas phase by the chemical ionization mass spectrometer (CIMS) are highlighted with a blue square.

Aerosol from the LV pathway is believed to be composed largely of isoprene dihydroxy dinitrates, which are produced from the first-generation hydroxy nitrate reacting with OH to form a peroxy radical that then reacts with NO. The gas-phase yield of isoprene dihydroxy dinitrates is quite uncertain (Lee et al., 2014). In general, the nitrate yields from highly functionalized RO_2 radicals have not been well studied (Wennberg et al., 2018) due mostly to difficulties in measuring such low

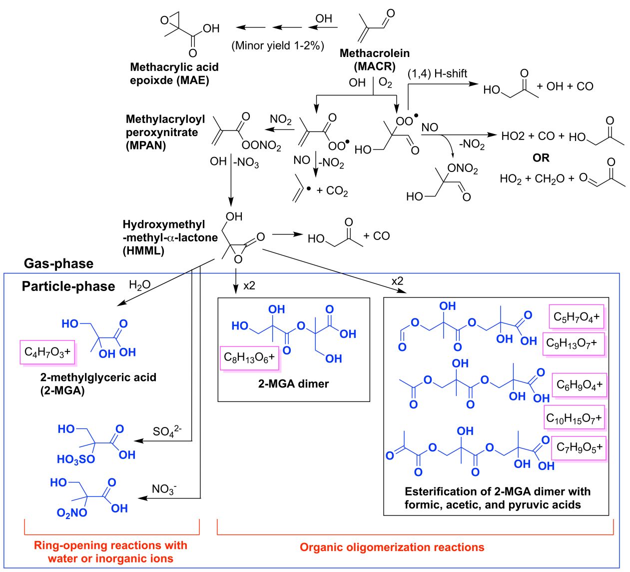

Figure 2. Simplified chemical mechanism of methacrolein OH-initiated oxidation under high-NO_2 conditions, largely based on schemes in Wennberg et al. (2018), emphasizing SOA generated from the 2MGA pathway including 2-methylglyceric acid (2MGA) and its oligomers in blue. Aerosol mass spectrometer (AMS) fragments likely corresponding to each compound are boxed in magenta.

volatility compounds. The formation of some organic nitrate SOA-precursors are summarized in Figure 1, which is largely adapted from schemes presented in Wennberg et al. (2018) with the exception of the isoprene dihydroxy nitrooxy alkoxy radical 1,5 H-shift. Wennberg et al. (2018) suggests the importance of a similar peroxy radical 1,5 H-shift, which will not form in the present experiments due to the high levels of NO. However, based on past studies largely on alkane oxidation (Orlando et al., 2003; Atkinson, 2007), the equivalent alkoxy radical 1,5 H-shift is expected to occur and has the potential to form low-volatility nitrates as further described in Section 5.1.

Throughout the text we use low-volatility as a general term representing gas-phase compounds with a potential to exist partially in the particle phase. In this work, low-volatility compounds include the following volatility classes from Donahue et al. (2012): IVOC (Intermediate), SVOC (Semi-), LVOC (Low), and ELVOC (Extremely Low). When referring to specific volatility classes, the acronyms defined above are used.

Aerosol from the 2MGA pathway forms when methacrolein is oxidized under high-NO_2 conditions to form methylacryloyl peroxynitrate (MPAN). MPAN reacts with OH to form hydroxymethyl-methyl-α-lactone (HMML), and HMML either decomposes in the gas phase to form hydroxy acetone or interacts with a wet surface to form 2-MGA (Kjaergaard et al., 2012; Nguyen et al., 2015). A minor channel to form methacrylic acid epoxide (MAE) also exists from methacrolein oxidation (Lin et al., 2013), but not from pure MPAN oxidation (Nguyen et al., 2015). Nguyen et al. (2015) demonstrated that MAE does not easily undergo ring-opening reactions to form particles. Thus, the yield of MAE from MACR oxidation reported in Lin et al. (2013) should be adjusted to include only MAE detected in the gas phase, which corresponds to a yield of ∼1-2%.

Because SOA formed from the LV and 2MGA pathways is chemically distinct in both route of formation and composition, the experiments reported here probed these chemical pathways separately. This experimental design is aimed to resolve inconsistencies associated with previously reported isoprene SOA yields (Carlton et al., 2009) and improve our understanding of isoprene SOA formation. Additionally, we seek to report updated isoprene SOA yields as well as trace the SOA yields to known gas-phase SOA precursors.

2 Experimental Methods

Chamber experiments were performed to study SOA formation from isoprene oxidation under high-NO_x conditions from two distinct pathways: 1) low-volatility nitrates and dinitrates (LV pathway) and 2) 2-MGA and its oligomers (2MGA pathway). Experiments targeting the LV pathway were performed using isoprene as the precursor and an NO_2/NO ratio < 1.5 was maintained throughout the entire experiment (as verified by the kinetic mechanism) in order to favor the formation of nitrates and dinitrates and limit the formation of MPAN (Figure 1). Experiments targeting the 2MGA pathway were performed using methacrolein as the precursor and an NO_2/NO ratio > 11 was maintained throughout the entire experiment (as verified by the kinetic mechanism) with the exception of experiment M9, which maintained an NO_2/NO ratio > 8. This high NO_2/NO ratio accentuated the formation of MPAN, and thereby 2MGA (Figure 2) and was important for reducing variability between the experiments. If a lower NO_2/NO ratio was used, small fluctuations in the initial NO_2 or NO would result in large differences in the NO_2/NO ratio. In order to completely separate the LV and 2MGA pathways, methacrolein had to be used as the VOC precursor for the 2MGA pathway experiments. If isoprene was used, even at the high NO_2/NO ratios used in the 2MGA pathway experiments, the SOA precursors from the LV pathway would form resulting in a mixed regime (i.e., chemistry in Figure 1 is not dependent on NO_2 concentration). In each case, the effect of seed surface area, temperature, and humidity on ~~SOA formation was~~ the SOA yield was independently determined.

2.1 Experimental Conditions

Experiments (see Table 1) were conducted in the Caltech dual chamber facility using a 21 m^3 Teflon chamber. Prior to each experiment, the chamber was flushed with dry, purified air for 24 h. For humid experiments, the chamber was humidified prior to all injections. 25°C ultrapure water (18 MΩ, ~~Milipore~~Millipore Milli-Q) was recirculated through a Nafion membrane humidifier (FC200, Permapure LLC) while purified air was flowed through the humidifier and into the chamber. First, isoprene (99% purity) or methacrolein (95% purity) was injected into a glass bulb using a gas-tight syringe and was carried by a flow of dry nitrogen into the chamber.

Second, methyl nitrite (CH_3ONO) was injected into the chamber. CH_3ONO was synthesized using the technique described in Taylor et al. (1980) and Chan et al. (2010) and stored in liquid nitrogen. Prior to each experiment, an evacuated glass bulb was filled with CH_3ONO to the desired pressure, as measured by a capacitance manometer (MKS Baratron^{TM}). This bulb was then backfilled with nitrogen and flushed into the chamber. The bulb pressure was used to calculate the CH_3ONO mixing ratio in the chamber (see Table 1). After CH_3ONO was injected, pulses of purified air were added to the chamber to enhance

Table 1. Initial conditions and SOA yield for all experiments

Expt #	$[\mathrm{VOC}]_0$ (ppb)	$[\mathrm{NO}]_0$ (ppb)	$[\mathrm{NO_2}]_0$ (ppb)	$[\mathrm{CH_3ONO}]_0$ (ppb)	$[\mathrm{Aer\ Vol}]_0$ ($\mu\mathrm{m}^3\ \mathrm{cm}^{-3}$)	$[\mathrm{Aer\ SA}]_0$ ($\mu\mathrm{m}^2\ \mathrm{cm}^{-3}$)	Avg T (°C)	Avg RH (%)	OH (molec cm^{-3})	SOA Yield
Dry Control Experiments										
C1	NA	NA	NA	NA	37	788	25.1	10.7	NA	NA
C2	NA	NA	NA	NA	109	2130	25.2	8.3	NA	NA
C3	NA	NA	NA	NA	183	3360	24.7	5.6	NA	NA
C4	NA	NA	NA	NA	375	5390	25.5	7.3	NA	NA
Experiments optimized for LV pathway (VOC precursor is isoprene)										
D1	59	585	6	118	0	0	25.6	5.0	2.6E6	0
D2	58	526	20	117	54	1170	26.4	5.6	2.5E6	0.04
D3	57	519	17	117	183	3420	25.9	7.5	2.5E6	0.17
D4	58	518	18	116	337	5770	26.4	7.9	2.4E6	0.16
D5	55	506	20	117	159	2830	12.8	16.4	1.7E6	0.15
D6	56	541	16	118	152	2660	32.4	5.9	2.7E6	0.16
D7	40	527	18	117	197	3580	25.9	8.1	2.6E6	0.18
D8	60	519	20	118	109	1790	25.5	44.7	2.3E6	NA
D9	55	489	20	119	166	2750	25.6	78.1	2.5E6	NA
D10	58	516	17	111	85	1580	25.8	5.1	2.2E6	0.04
D11	56	490	17	115	264	4770	25.8	5.2	2.4E6	0.16
Experiments optimized for 2MGA pathway (VOC precursor is methacrolein)										
M1	49	14	376	234	0	0	25.8	6.3	4.3E6	0.10
M2	48	15	365	235	82	1640	25.9	8.9	4.7E6	0.34
M3	46	23	345	236	118	2260	25.1	6.8	4.7E6	0.52
M4	50	17	356	235	50	1040	12.9	12.6	3.4E6	0.27
M5	58	18	375	235	87	1740	31.8	4.5	5.1E6	0.34
M6	52	12	334	235	104	1720	25.6	47.1	4.4E6	NA
M7	53	14	339	233	134	2340	25.6	67.4	4.6E6	NA
M8	56	18	352	236	141	2510	25.4	81.0	4.3E6	NA
M9	57	29	298	229	95	1910	25.9	5.1	4.7E6	0.24

Acronyms are defined as follows: VOC = volatile organic compound, NO = nitric oxide, $\mathrm{NO_2}$ = nitrogen dioxide, $\mathrm{CH_3ONO}$ = methyl nitrite, Temp. = temperature, and RH = relative humidity. OH (hydroxyl radical) is estimated from the VOC decay over the first 3 h of each experiment. The $[\mathrm{Aer\ Vol}]_0$ is the particle wall loss corrected seed volume at the start of photooxidation, which is used to determine the uncertainty in the particle wall loss correction as explained in Section 4.1. The $[\mathrm{Aer\ SA}]_0$ is the surface area of the seed aerosol at the start of photooxidation not corrected for particle wall loss, and is used to understand how the SOA yield changes depending on the surface area of the suspended particles (e.g., Figure 5). The SOA yield is the mass fraction after 10 h of photooxidation.

mixing. Once the chamber was adequately mixed, NO (501 ppm in N_2, Scott Specialty Gases) or NO_2 (488 ppm in N_2, Scott Specialty Gases) was injected into the chamber through a calibrated mass flow controller. Again the chamber was mixed by pulses of purified air.

Seed particles were generated from an atomizer using 0.06 M $(NH_4)_2SO_4$ seed solution. The seed aerosol was directed through a soft x-ray neutralizer (TSI Model 3088) prior to injection into the chamber to ensure a consistent initial particle charge distribution for all experiments. For humid experiments, the seed aerosol was directed through a wet-wall denuder after exiting the neutralizer in order to ensure the particles were deliquesced. After seed injection, mixing air was turned on for 1 min to enhance mixing. The seed aerosol particle number concentration had an approximately lognormal diameter distribution centered on average ~100 nm.

After injecting all gas-phase precursors and seed aerosol, photooxidation was delayed by 1 h for experiments with no initial seed aerosol and 4 h for experiments with initial seed aerosol. The rate of particle wall deposition was measured for each experiment during this 4 h delay. Although NO_2 was not intentionally added for the LV pathway experiments, a modest NO_2 signal was observed to form during the 4 h delay and is reported in Table 1. This "NO_2" signal may be NO_2 itself or an interference in the NO_x monitor from an NO_y compound (e.g., known interferences include organic nitrates, nitrous acid, and CH_3ONO). The small signal of NO_2, or other NO_y compound, is not expected to influence the results given the significantly larger initial NO levels (Table 1). When NO_2 or CH_3ONO were injected into the chamber, an NO signal was observed on the NO_x monitor. As the NO_x monitor has few interferences for NO, a small fraction of NO was likely formed from NO_2 or CH_3ONO photolysis in the Teflon injection lines. Thus, the slight increase of NO with the NO_2 and CH_3ONO injection was assumed and reported to be initial NO (Table 1).

The Caltech chamber uses Ultraviolet (UV) broadband lights with the main emission peak centered at ~350 nm. Only 10% of full light capacity ($j_{NO2\ 10\%} = 4 \times 10^{-4}\ s^{-1}$) was used for these experiments because CH_3ONO photolyzes rapidly, and the lower light intensity minimizes chamber temperature increases (~0.4 °C on average) caused by the UV lights. In all experiments, OH was produced by the photolysis of CH_3ONO as shown ~~by~~ in the following reactions:

$$\mathrm{CH_3ONO + h\nu \rightarrow CH_3O + NO} \quad \text{(R1)}$$

$$\mathrm{CH_3O + O_2 \rightarrow CH_2O + HO_2} \quad \text{(R2)}$$

$$\mathrm{HO_2 + NO \rightarrow OH + NO_2} \quad \text{(R3)}$$

Relative to other OH precursors, CH_3ONO has a low Henry's law constant (15 M atm^{-1}, calculated by theory) (Sander, 2015). During experiments with high RH, unlike other OH precursors, CH_3ONO is not expected to enhance OH production in the particle phase beyond atmospherically relevant levels.

2.2 Instrumentation

Temperature and relative humidity (RH) were measured using a Vaisala HMM211 probe. NO and NO_2 were monitored using a Teledyne NO_x analyzer (T200). Because the Teledyne NO_x monitor detects CH_3ONO, organic nitrates, and other NO_y compounds as NO_2, only initial NO_2 measurements can be constrained with this instrument. For some experiments, NO_2 was also monitored using a luminol NO_2/acyl peroxynitrate analyzer developed by Fitz Aerometric Technologies. This instrument separates NO_2 via chromatography at room-temperature using a deactivated DB-5 column. NO_2 then reacts with luminol to produce a chemiluminescence response (Gaffney et al., 1998). The NO_2 measured by the luminol NO_2/acyl peroxynitrate analyzer compares reasonably well with the simulated NO_2 from the kinetic model (Figure S3).

A gas chromatograph with a flame ionization detector (GC-FID, HP 6890N, column HP-Plot-Q) was used to measure the decay of isoprene and methacrolein. The GC-FID was calibrated with ∼50-60 ppm of isoprene or methacrolein generated from analytical standards (Aldrich 95-99% purity) and cross-calibrated by fourier transform infrared absorption (FT-IR) spectroscopy (pathlength 19 cm) using the absorption cross sections measured by Pacific Northwest National Laboratory (PNNL) for isoprene or methacrolein (Sharpe et al., 2004). Linearity in the GC-FID calibration was determined to an error of ∼1% across a factor of 150 in dilution.

Aerosol organic and inorganic composition was recorded in-situ using a high-resolution time-of-flight aerosol mass spectrometer (HR-AMS, Aerodyne Research, Inc.). The HR-AMS switched every 1 min between the high-resolution W-mode and the lower-resolution, higher-sensitivity V-mode. The data were analyzed with Igor Pro (Wave Metrics, Inc.), utilizing the Squirrel 1.56D and PIKA 1.15D analysis toolkits (from http://cires1.colorado.edu/jimenez-group/ToFAMSResources/ToFSoftware/index.html). In-line filter runs conducted prior to each experiment were used to correct for air interferences (Aiken et al., 2008). Bulk SOA elemental composition was calculated following the methods and recommendations of Aiken et al. (2008) and Canagaratna et al. (2015).

Aerosol volume and number concentration were monitored using a differential mobility analyzer (DMA, TSI 3081 column) coupled with a condensation particle counter (CPC, TSI 3010), which measures all particles with a diameter between 20-800 nm. The voltage scan used by the DMA was 1 min hold at 15 V, 4 min increase to 9850 V, 1 min hold at 9850 V, and 0.5 min decrease back to 15 V. Only the upscan data were used for the analysis. The longer upscan and hold times used here, compared to previous studies (e.g., Loza et al. (2012) and Zhang et al. (2014)), reduced biases caused by mixing in the CPC. Such CPC mixing biases particularly impact the measurement of large particles, which are important in SOA yield experiments as they contribute significantly to the total SOA volume.

The DMA data analysis includes an improved data inversion and a correction for particle mixing in the condensation particle counter, which influences the CPC response time (Mai and Flagan, 2018; Mai et al., 2018). The inversion technique is applicable only to particles $\leq$ 600 nm. Particle concentration between 600-800 nm was calculated assuming a non-linear least squares ~~Gaussian~~ lognormal fit applied to particles from 400-600 nm. For experiments with no initial seed aerosol, the inversion inconsistently determined the presence of particles beyond 400 nm. Such large particles are unlikely to be the result of nucleation and more likely to represent an artifact of the inversion; thus, only particles <400 nm were used in the analysis of these experiments. Corrections to the DMA data for coagulation and particle wall loss are addressed in Section 4.1.

Isoprene oxidation products were measured using a CF_3O^- chemical ionization mass spectrometer (CIMS), which utilizes a custom-modified triple quadrupole mass analyzer (Varian 1200) (St. Clair et al., 2010). CF_3O^- interacts with a gas-phase compound (A) to form a complex that is detected at the molecular weight of A + 85 or, in some cases, to fragment. Various fragmentation products can form as explained in previous work (e.g., Paulot et al. (2009); Praske et al. (2015); Schwantes et al. (2017)). In this work, the CIMS results are only used to identify the presence of highly functionalized organic nitrates and not for quantification, so only signals from the complex (i.e., A • CF_3O^-) and not from fragmentation are reported.

3 Kinetic Mechanism

All relevant reactions included in the Master Chemical Mechanism (MCM) v3.3.1 (http://mcm.leeds.ac.uk/MCM) were used in the current kinetic model (Jenkin et al., 1997; Saunders et al., 2003). Isoprene oxidation chemistry was recently updated in MCM v3.3.1 by Jenkin et al. (2015). Additional reactions included in the kinetic model, but not in MCM v3.3.1 are listed in Table S1. Updates include inorganic reactions needed for chamber studies with large NO_x levels (e.g., CH_3ONO photolysis) ~~, are listed in Table ??.~~ and small changes to the isoprene chemistry based largely on Wennberg et al. (2018) and consistent with Figures 1 and 2. As shown in Table S1, these updates include: the first generation isoprene hydroxy nitrate yields, the rates and branching ratios for the oxidation of the first generation isoprene hydroxy nitrates, and the HMML yield from the MPAN + OH reaction. In some cases, δ-isoprene hydroxy alkoxy radicals in MCM v3.3.1 decompose through peroxy radical H-shifts directly to products that would not form under the high-NO conditions in this work. For simplicity, we change these reactions, so that the δ-isoprene hydroxy alkoxy radicals form unity yields of hydroxy aldehydes. BOXMOX, a box-model software package using the Kinetic PreProcessor (Knote et al., 2015), was used to simulate the chamber experiments.

~~Additional reactions and reaction rates included in the kinetic model, but not in MCM v3.3.1 Reaction Reaction Rate Source cm^3 molecule^{-1} s^{-1} $CH_3ONO + h\nu \rightarrow HCHO + HO_2 +$~~ As listed in Table 1, the kinetic model was initialized for each experiment with the measured initial concentration of VOC, NO, NO~~(1.4-2.3) x 10^{-4} s^{-1} NA ^{a} $CH_3ONO + OH \rightarrow H_2O + HCHO + NO$ 3 x 10^{-13} * 0.5 Nielsen (1991), Cox (1980), Jenkin (1988) CH~~, and CH$_3$~~ONO + OH $\rightarrow$ HCHO + HO_2 + HONO 3 x 10^{-13} * 0.5 Nielsen (1991), Cox (1980), Jenkin (1988) $HO_2 + NO_2 \rightarrow$ HONO 5 x 10^{-16} JPL HO_2 + HCHO $\rightarrow$ $HOCH_2OO$ 9.7 x 10^{-15} exp(625/T) IUPAC $HOCH_2OO \rightarrow HO_2$ + HCHO 2.4 x 10^{12} exp(-7000/T) s^{-1} IUPAC $HOCH_2OO + HO_2 \rightarrow$ HMHP 5.6 x 10^{-15} exp(2300/T) * 0.5 IUPAC $HOCH_2OO + HO_2 \rightarrow$ HCOOH 5.6 x 10^{-15} exp(2300/T) * 0.3 IUPAC $HOCH_2OO + HO_2 \rightarrow HCOOH + HO_2 + OH$ 5.60 x 10^{-15} exp(2300/T) * 0.2 IUPAC $HOCH_2OO \rightarrow$ HCOOH 7 x 10^{-13} * RO_2 IUPAC $HOCH_2OO \rightarrow CH_2(OH)_2$ 7 x 10^{-13} * RO_2 IUPAC $HOCH_2OO \rightarrow HCOOH + HO_2$ 5.50 x 10^{-12} * 2 * RO_2 IUPAC $HOCH_2OO + NO \rightarrow HCOOH + HO_2 + NO_2$ 5.60 x 10^{-12} IUPAC HMHP + OH $\rightarrow HOCH_2OO$ 3.1 x 10^{-11} * 0.12 Jenkin (2007) HMHP + OH $\rightarrow$ HCOOH + OH 3.1 x 10^{-11} * 0.88 Jenkin (2007) HMHP + h$\nu \rightarrow HCOOH + HO_2 + OH$ 2.0 x 10^{-7} s^{-1} JPL OH + OH $\rightarrow$ O 6.2 x 10^{-14} $(T/298)^{2.6}$ exp(945/T) IUPAC $OH + NO_2 + M \rightarrow HOONO + M$ Termolecular IUPAC $HOONO + M \rightarrow OH + NO_2 + M$ Termolecular IUPAC $OH + OH + M \rightarrow H_2O_2 + M$ Termolecular IUPAC $OH + NO_2$~~

~~+ M $\rightarrow$ HNO_3 + M ^{b} Termolecular IUPAC $NO_2 + O_3 \rightarrow NO_3$ ^{c} 1.4 x 10^{-13} exp(-2470/T) *0.97 Cantrell (1985) $NO_2 + O_3 \rightarrow NO$ ^{c} 1.4 x 10^{-13} exp(-2470/T) *0.03 Cantrell (1985) $NO_2 + NO_2 + M \rightarrow N_2O_4 + M$ Termolecular IUPAC $N_2O_4 + M \rightarrow NO_2 + NO_2 + M$ Termolecular IUPAC~~ ONO as well as the measured average temperature and relative humidity.

Saturation mass concentration (C*) and fraction of each compound in the particle phase (F_P) at 13, 26, and 32°C are estimated for relevant organic nitrates and dinitrates produced in MCM v3.3.1 and listed in Table S2. C* was calculated with the vapor pressure estimated from Nannoolal et al. (2004, 2008) using the online calculator located at: http://www.aim.env.uea.ac.uk/aim/ddbst/pcalc_main.php. F_P was calculated from the C* values and gas-particle equilibrium theory as further explained in Section S1 (Seinfeld and Pandis, 2016).

As shown in Table 1, the inferred OH concentration was larger in experiments with higher temperatures. Because the temperature dependence of the CH_3ONO absorption cross section and quantum yield are not well established, the CH_3ONO photolysis rate constant was calculated from the CH_3ONO decay curve as measured by the GC-FID. Unfortunately, the GC-FID sensitivity to CH_3ONO was low, so only the 2MGA experiments produced a sufficiently large signal for this approach. The average CH_3ONO photolysis rate constant from experiments M1-M3, M4, M5, and M6-M8 were used for dry ∼25°C (1.9 x 10^{-4} s^{-1}), dry ∼13°C (1.4 x 10^{-4} s^{-1}), dry ∼32°C (2.3 x 10^{-4} s^{-1}), and humid ∼25°C (1.9 x 10^{-4} s^{-1}) experiments, respectively. This approach accurately captured the reaction of isoprene and methacrolein with OH in all experiments (Figures S1 and S2), which implies that the simulated OH in the kinetic model is reasonably accurate even over varying temperature. All other photolysis rate constants are calculated from the absorption cross sections and quantum yields reported in Burkholder et al. (2015) and Jenkin et al. (2015). Additionally, the kinetic model captures NO and NO_2 reasonably well for both the LV and 2MGA pathway experiments (Figure S3).

4 Results

First, corrections for particle coagulation and particle wall deposition, which are required for accurate calculation of SOA yields, are addressed (Section 4.1). Next, SOA produced from the LV (Section 4.2) and 2MGA (Section 4.3) pathways are discussed.

4.1 Corrections for Particle Coagulation and Particle Wall Deposition

Past studies reporting particle wall deposition coefficients apply the measured particle number decay rate in each size bin to produce a wall deposition coefficient, (β(D_p,t)), that is a function of particle size (D_p) (Loza et al., 2012). Because larger seed particle number and surface area concentrations were used in these experiments, corrections to β(D_p,t) that account for coagulation are needed (Pierce et al., 2008; Nah et al., 2017). The current work uses an approach similar to that of Nah et al. (2017) and Sunol et al. (2018) with updates to account for electrostatic charges on the chamber walls as described by Charan et al. (2018). To reduce the experimental uncertainty associated with these processes, particle wall deposition was calculated during each experiment. This approach accounted for the day-to-day fluctuations in particle coagulation processes, chamber wall charging, and chamber mixing. We summarize these approaches and describe any changes required for this analysis in Section S2 of the Supplement.

Four particle wall loss experiments were performed under dry conditions (RH <10%) at varying seed surface areas as controls to verify the technique used to correct for particle wall loss, particle coagulation, and electrostatic charges on the chamber walls. These particle wall deposition experiments were performed by injecting ammonium sulfate seed into the chamber, as described in Section 2.1. Mixing air was added, and the ammonium sulfate seed aerosol was monitored in the dark chamber for at least 14 h. These controls confirmed that the wall loss correction calculated over the first 3.5 h could be extrapolated for an additional 10 h. Beyond 10 h, the wall loss correction was more uncertain, so results only from the first 10 h of each experiment are reported. The percent change between the aerosol volume over 10 h and the aerosol volume at the start of the control experiment was between +4% and -6% for all dry control experiments (Figure 3).

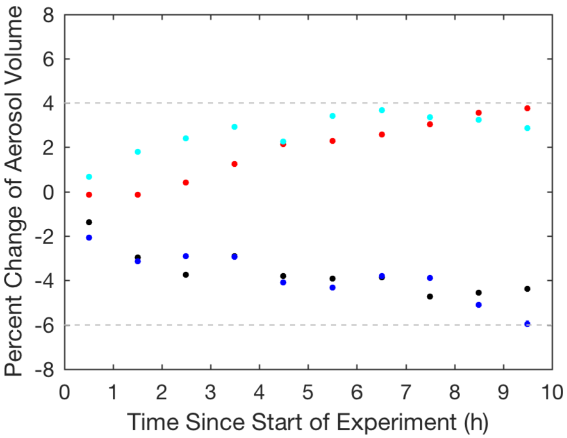

Figure 3. Percent change between the corrected aerosol volume over 10 h and the corrected aerosol volume at the start of photooxidation (60 min averages) for the following particle wall deposition control experiments: C1 (V = 37 $\mu m^3 cm^{-3}$, ●), C2 (V = 109 $\mu m^3 cm^{-3}$, ●), C3 (V = 183 $\mu m^3 cm^{-3}$, ●), and C4 (V = 375 $\mu m^3 cm^{-3}$, ●), respectively where V is the initial corrected particle volume.

The results of these control experiments verified the robustness of the correction technique and provided an estimate for the uncertainty. The reported uncertainty for the particle wall deposition correction is +4% and -6% of the corrected aerosol volume at the start of photooxidation. Experiments with larger seed aerosol volumes exhibit larger uncertainty in the reported SOA yield. However, such experiments are necessary despite the extra uncertainty, as larger seed surface areas minimize low biases in SOA yields due to vapor wall deposition of low-volatility compounds (Zhang et al., 2014; Ehn et al., 2014). For experiments with no initial seed aerosol, particle wall loss corrections were applied assuming the particles coagulated and deposited similarly to the lowest aerosol loading control experiment (C1). No uncertainty for the particle wall deposition correction was added to these experiments because the uncertainty derived here is applicable only to experiments with initial seed aerosol.

In experiments C1-C4, D1-D9, and M1-M8, electrostatic charges on the chamber walls were inferred to be present. After these experiments were completed, new Teflon chambers were acquired with negligible electrostatic charges on the chamber walls (Charan et al., 2018) likely due to their smaller volume (18 m^3). Three additional new experiments (D10, D11, and M9) were completed using one of these new Teflon chambers to confirm that we had accurately corrected for the chamber wall charging effects. For the LV pathway experiments (Section 4.2), results for the new experiments were quite similar and within uncertainties of the old experiments. The new 2MGA pathway experiment produced slightly lower SOA yields than the old experiments, but not necessarily because of the chamber wall charging corrections as described in Section 4.3.

Five control experiments were also performed under humid conditions. The DMA cannot measure hydrated particles owing to arcing in the DMA column at high RH. Thus, a Nafion dryer was used to dry particles before measurement. For the coagulation correction, the volume of the hydrated seed was calculated based on the dry DMA particle measurement, the RH in the chamber, and the hygroscopic growth curve for ammonium sulfate measured by Sjogren et al. (2007). The percent change for the aerosol volume was higher and less consistent in the humid control experiments than in the dry control experiments. Also, the optimized value of the electric field ($\bar{E}$) was higher in many of the humid experiments than in the dry experiments (Section ~~S1, Table S1~~S2, Table S3). Increased humidity is expected to decrease the electrostatic charges on the chamber walls (e.g., Ribeiro et al. (1992)), but the inferred $\bar{E}$ suggests the opposite. Possibly, the humidifying process enhanced the electrostatic charges on the chamber walls, or nitric acid, which is enhanced in the particle phase in the humid experiments under high-NO_x conditions, impacts the coagulation or particle wall loss processes.

The AMS data confirm that during the humid experiments, nitric acid partitioned to the particle phase and that organic aerosol was produced during photooxidation for all experiments. Nevertheless, the particle wall loss corrected volume measured by the DMA decayed below zero during photooxidation in the humid experiments. Potentially, this DMA volume decay suggests that nitric acid present in the particle phase changes the particle coagulation or wall loss characteristics. Even if we understood the impact of nitric acid on the particle coagulation or wall loss corrections, assessing how much of the particle growth is due to nitric acid versus organics would be difficult with the DMA, which measures only total aerosol volume and not composition. Further chamber characterization is required in order to assess isoprene SOA yields measured by the DMA from humid experiments under high-NO_x conditions. Thus, in this work, only the AMS results will be discussed for the humid experiments ~~.~~ and SOA yields are only reported for experiments performed under dry conditions (Table 1). None of the dry experiments exhibited the odd behavior observed in the humid experiments, and the AMS results confirm that under dry conditions minimal nitric acid partitioned to the aerosols (Figure S10). For the dry experiments, the uncertainties are well characterized by the dry control experiments presented in Figure 3.

4.2 SOA Formation From the LV Pathway

The SOA mass yields from isoprene for all LV pathway experiments (i.e., experiments targeting low-volatility compounds) are shown in Figures 4 and 5. To convert aerosol volume measured by the DMA to aerosol mass, a density of 1.4 g cm^{-3} was assumed, consistent with past work (Dommen et al., 2006; Kroll et al., 2005, 2006; Bregonzio-Rozier et al., 2015). The kinetic mechanism suggests that in all experiments targeting the LV pathway, formation of ~~the 2-MGA precursor~~ HMML was $<$

~~0.14~~ 0.12 ppb even in experiments performed under cold conditions (13°C). The AMS results also confirm that 2MGA and its oligomers are not present in the LV pathway experiments (Section 5.2). Thus, the kinetic mechanism and AMS results verify that the experimental design correctly separates the two chemical regimes and 2-MGA is not substantially adding to the aerosol mass in the LV pathway experiments.

Aerosol growth in the absence of seed aerosols was not observed in the LV pathway experiments (Figure 4). As expected, SOA formed from gas/particle partitioning in the LV pathway exhibited a large dependence on seed surface area (Figure 5). Without sufficient seed aerosol, low-volatility nitrates partition primarily to the chamber walls, and the resulting SOA yields are biased low. ~~Differences in SOA yield~~ With the addition of inorganic seed aerosol like ammonium sulfate, vapor species are expected to partition more to particles relative to the chamber wall (Zhang et al., 2014). The gas-particle equilibrium is not expected to be dependent on the concentration of inorganic seed aerosol, but instead is dependent on the concentration of organic aerosol. Depending on the saturation mass concentration (C*), as the concentration of organic aerosol rises, vapors are present more in the particle-phase relative to the gas-phase (Seinfeld and Pandis, 2016). C* and the fraction of a compound expected to be in the particle phase (F_P) were estimated for a variety of organic nitrates and dinitrates in MCM v3.3.1 at 13, 26, and 32°C (Table S2).

Similar to previous studies (e.g., Zhang et al. (2014)), at a certain point increased seed surface area no longer substantially impacts the SOA yield (i.e., Figure 5 after 2500 $\mu m^2\ cm^{-3}$). This point will heavily depend on the system and the saturation mass concentration (C*) of the SOA precursors. As shown in Table S2, the isoprene SOA precursors are mostly classified as IVOCs and SVOCs (Donahue et al., 2012). Reaching a point where most of the vapors are in particles relative to the chamber wall is expected for IVOCs and SVOCs, which have moderate vapor wall losses in Teflon chambers especially under dry conditions (Zhang et al., 2014; Huang et al., 2018).

As expected the isoprene dihydroxy dinitrates had the lowest C* values and high F_P at all temperatures. Based on the kinetic model, even assuming all of the isoprene dihydroxy dinitrates exist in the particle-phase, the SOA formed would be much less than that detected in this study (Figure S4). This is likely caused by too low production of the isoprene dihydroxy dinitrates and/or the importance of other SOA precursors. There are many additional compounds largely produced from hydroxy aldehyde oxidation or alkoxy [1,5]-H-shifts (Figure 1) with F_P at 26°C between 0.05 and 0.4 (Table S2). The vapor pressures may be over-predicted for these specific compounds, but past studies suggest that in general, vapor pressure estimation methods like Nannoolal et al. (2004, 2008) under-predict rather than over-predict vapor pressure (Kurten et al., 2016). From the C* calculations (Table S2), none of the multi-functional organic nitrates are expected to be appreciably in the particle phase. However, in a recent study, Lee et al. (2016) detected many multi-functional organic nitrates in aerosols in the ambient atmosphere, which has lower organic aerosol concentrations than chamber studies. Possibly, MCM under-predicts the formation of these IVOC and SVOC products (Figure S4), such that even if only a fraction exists in the particle-phase relative to the gas-phase, an appreciable mass of aerosol still forms and/or these results suggest that volatility is not the only driver for aerosol formation from the LV pathway. All of the multi-functional nitrates here with estimated F_P at 26°C between 0.05 and 0.4 have at least one hydroxy or aldehyde group (Table S2). Alcohols and aldehydes are well known to combine in particles to produce hemiacetals, whose vapor pressure is significantly lower than that of the initial reactants (Kroll and Seinfeld, 2008). Several past studies have confirmed that NO_x in general, but not necessarily linearly, decreases the volatility of isoprene SOA

(Kleindienst et al., 2009; Xu et al., 2014; D'Ambro et al., 2017). This decrease in volatility is likely due to accretion reactions. Whether the accretion reactions from hemiacetal formation versus those from 2MGA oligomerization are responsible for the decrease in volatility is yet unknown.

Differences in the SOA yield at 10h of photooxidation by varying temperature (13-32°C) lie within the experimental uncertainty. SOA forms earlier (i.e. with less isoprene reacted) at 13°C than at 26 or 32°C at comparable seed surface areas. This is consistent with the C* values estimated in Table S2 and the above explanation demonstrating the likelihood of accretion reactions. Vapors that are only moderately in the particle phase at 26°C (e.g., F_P = 0.05-0.4) will exist more appreciably in the particle phase at 13°C (e.g., F_P = 0.2-0.8). From the above discussion, we expect many of these compounds are SOA precursors not based only on their volatility, but also due to their potential to react in the particle phase to form lower volatility products such as hemiacetals. Thus, if accretion reactions are the main factor, reducing temperature is expected to increase the rate of SOA production, but not necessarily to impact the overall SOA yield.

Clark et al. (2016) have also measured isoprene SOA formation under high-NO_x conditions at varying temperatures. Under the high-NO_x conditions of their study, SOA is produced from both the 2MGA and LV pathways combined. Similarly to our study, Clark et al. (2016) do not find appreciable differences for temperatures from 27-40°C. Contrary, to our work, Clark et al. (2016) found that reducing the temperature to 5°C increases the SOA yield by a factor of 4. Unfortunately, there are no experiments between 5°C and 27°C to determine whether this shift is exponential or linear, so direct comparison of our results at 13°C is difficult. Under the high-NO_x conditions used by Clark et al. (2016), at colder temperatures MPAN will be more stable and so more HMML will form, which produces more SOA. Under this mixed regime, determining how much of the SOA increase is due to the LV versus the 2MGA pathway for direct comparison to this study is difficult. Additionally, Clark et al. (2016) start with significantly more isoprene than in our experiment, which enhances the concentration of organic aerosol, which will increase the fraction of a compound in the particle phase relative to the gas phase.

While vapor wall losses of LV compounds are expected to increase at colder temperatures (Zhang et al., 2015) (Schwantes et al., 2017), the organic nitrate yields are also expected to be enhanced under colder temperatures (Orlando and Tyndall, 2012). Thus, the effects of these two temperature-dependent processes might cancel. The increase in organic nitrate yield is expected to be moderate. For example, ~30% increase from 32 to 13°C is estimated for the yield of isoprene hydroxy nitrates (Wennberg et al., 2018). The loss of vapors to the walls could be much higher at colder temperatures, but this is hard to constrain as vapor wall deposition is dependent on the compound itself and the chamber used. The chamber used by Clark et al. (2016) (90 m^3) is larger than our chamber (21 m^3). Vapor wall losses are expected to be lower in larger chambers, which have a lower chamber surface area to volume ratio (Zhang et al., 2015). Significant seed aerosol is added into our chamber to reduce the influence of vapor wall deposition, but vapor wall deposition could certainly explain some of the differences at cold temperatures between our results and those from Clark et al. (2016).

Consistent with past work (e.g., Kroll et al. (2005); Ng et al. (2006)), aerosol from the LV pathway is produced only after most of the isoprene is consumed, implying that aerosol from the LV pathway largely forms from later-generation chemistry

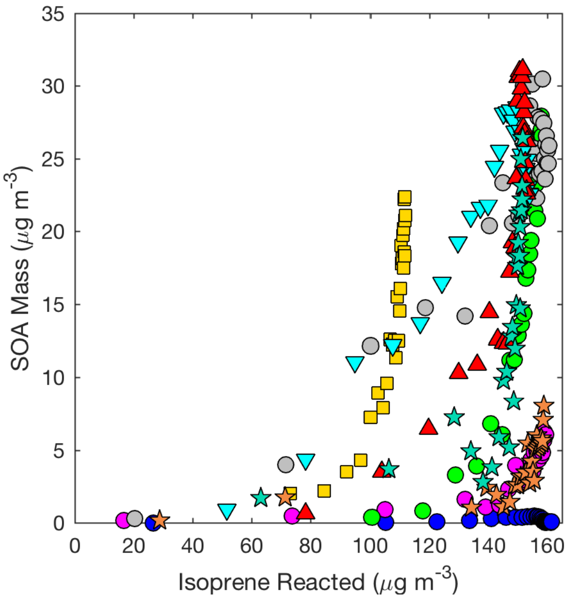

Figure 4. SOA mass yield (20 min averages) as measured by the DMA assuming a density of 1.4 g cm^{-3} for all LV pathway experiments: seed surface area - D1 (SA = 0 µm^{2}cm^{-3}, ●), D2 (SA = 1170 µm^2 cm^{-3}, ●), D3 (SA = 3420 µm^2 cm^{-3}, ●), & D4 (SA = 5770 µm^{2}cm^{-3}, ●), temperature - D5 (13 °C, ▼) & D6 (32 °C, ▲), isoprene loading - D7 (initial isoprene 110 µg m^{-3}, ♦), and new chamber with less wall charging - D10 (SA = 1580 µm^{2}cm^{-3}, ★) & D11 (SA = 4770 µm^{2}cm^{-3}, ★)

(Figure 4). ~~Thus, the~~ As shown in Figure 4, generally, SOA formation begins earlier (i.e., with less isoprene reacted) in experiments with larger seed aerosol. This is consistent with vapors partitioning more to particles relative to the chamber wall when seed aerosol is enhanced. The extent to which later-generation products are oxidized (i.e., the degree of oxidation) impacts the SOA yield as demonstrated by the varying slope (i.e., SOA yield) during each experiment in Figure 4. We tested the OH/isoprene ratio on the SOA yield. Experiment D7 was performed with 40 ppb of isoprene compared to 55-60 ppb used in the other experiments, while the OH precursor concentration was kept constant. The kinetic model predicts that the ~~SOA mass yield of dinitrates from experiment D7 is similar~~ production of important gas-phase SOA precursors from the LV pathway (e.g., isoprene dihydroxy dinitrates), when corrected for total isoprene reacted, is similar in experiment D7 to the other experiments (Figure S4)~~, and the~~. The empirical results are consistent with these predictions. Although a lower isoprene loading decreases the competition of isoprene with OH, other compounds also react with OH quickly (e.g., NO). Under the conditions used in this study, differences in isoprene loading are not expected to greatly influence the isoprene SOA mass yield. However, detailed kinetic modeling of past experimental conditions would be necessary to understand how the degree of oxidation of later-generation products in this study compares to other studies.

In summary, the results (Figure 5) suggest that one of the most important metrics for understanding the variability in SOA production from the LV pathway in various chamber experiments may be the initial seed surface area, instead of temperature

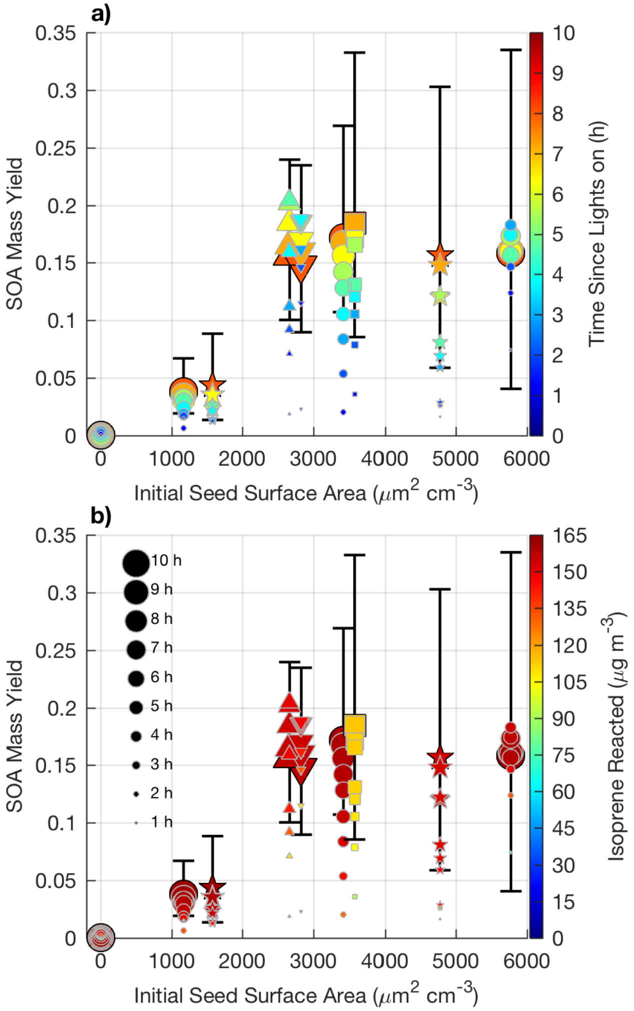

Figure 5. SOA mass yield (60 min averages) as a function of initial seed surface area for all LV pathway experiments. Colors represent time since lights on in panel a and extent of isoprene reacted in panel b. Marker size represents time since lights on. Uncertainty is shown in black lines as described in Section 4.1. Marker types indicate: 25-26°C (●), 13°C (▼), 32°C (▲), lower loadings of isoprene (■), and new chamber with less wall charging (★).

or OH/isoprene ratio. Other parameters such as humidity and seed composition may also be important for SOA yields, but were not tested in this study. Future experiments examining SOA yields should report the initial seed surface area and use a sufficient seed loading to reduce the impact of vapor wall deposition.

4.3 SOA Formation from the 2MGA Pathway

The SOA mass yields from methacrolein for all 2MGA pathway experiments (i.e., experiments targeting 2MGA and its oligomers) are shown in Figures 6 and 7. Results from past experiments (Chan et al., 2010) have already demonstrated that fluctuations in the NO_2/NO ratio impacts SOA formation through the production of MPAN. In this work, the NO_2/NO ratio is kept as consistent as possible to isolate other influences on SOA production. The kinetic model suggests that the conditions for each experiment produce a consistent level of ~~gas-phase 2-MGA precursor~~ HMML (Figure S4). Interestingly, because the experimental conditions heavily favored MPAN formation, the level of OH available to react with MPAN became the limiting reactant for aerosol formation in each experiment.

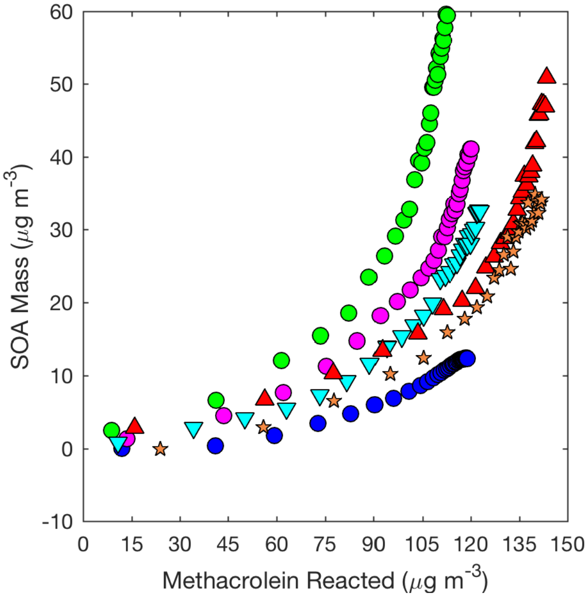

Figure 6. SOA mass yield (20 min averages) as measured by the DMA assuming a density of 1.4 µg cm^{-3} for 2MGA pathway experiments: seed surface area - M1 (SA = 0 $\mu m^2 cm^{-3}$, ●), M2 (SA = 1640 $\mu m^2 cm^{-3}$, ●), & M3 (SA = 2260 $\mu m^2 cm^{-3}$, ●), temperature - M5 (13 °C, ▼) & M6 (32 °C, ▲), and new chamber with less wall charging - M9 (SA = 1910 $\mu m^2 cm^{-3}$, ★).

Contrary to the LV pathway, SOA in the 2MGA pathway experiments do not require seed particles to form. The process of SOA formation from these two pathways is very different. Lactone SOA precursors may polymerize in the presence of organics and water, which possibly explains why SOA from the 2MGA pathway readily forms particles without significant seed surface area, whereas in the LV pathway experiments volatility-based SOA formation results in aerosol yields that are particularly

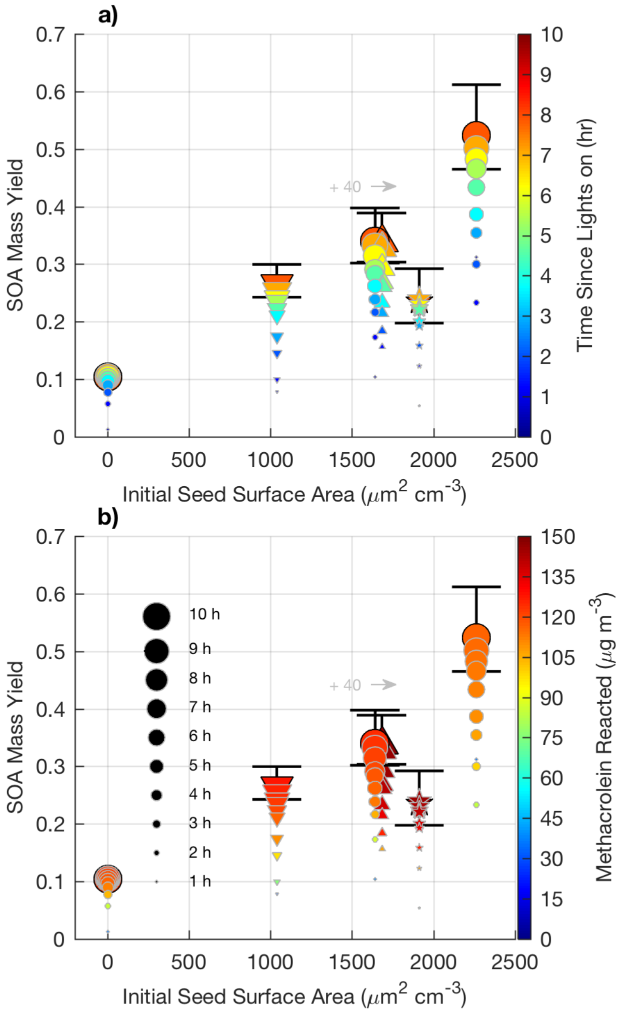

Figure 7. SOA mass yield (60 min averages) versus initial seed surface area for all 2MGA pathway experiments. Colors represent time since lights on (panel a) and extent of methacrolein reacted (panel b). Marker size represents time since lights on. Uncertainty is shown in black lines and described in Section 4.1. Markers represent: 25-26°C (●), 13°C (▼), 32°C (▲), and new chamber with less wall charging (★). Two experiments were performed at nearly the same seed surface area. To enhance viewing, experiment M6 (32°C, △) is shifted to the right by ~~100~~ 40 µm^2 cm^{-3}.

impacted by vapor partitioning. For the 2MGA pathway experiments, even though SOA formation occurred without initial seed aerosol, larger initial seed loadings still enhanced the SOA yield (Figure 7). Possibly, similar to the LV pathway, larger seed surface areas limit vapor wall loss of HMML or its oligomerization partners. Alternatively, the presence of higher ammonium sulfate seed aerosol may also increase organosulfate formation, which could impact SOA composition and yield.

Temperature was varied between 13°C to 32°C. The NO$_2$/NO ratio used in this work was sufficiently high such that this temperature change did not greatly influence MPAN or HMML formation (Figure S4). Thus, these experiments only test whether aerosol properties and SOA yields are affected by ~~the~~ temperature, as MPAN thermal decomposition is minimized. ~~Temperature~~ At the high NO$_2$/NO ratios used in this work, temperature does not impact SOA mass yield beyond given uncertainties (Figure 7). Based on known gas-phase chemistry, past studies (e.g., Clark et al. (2016)) with more moderate NO$_2$/NO ratios than that used in this work are expected to measure an enhanced SOA yield under colder temperatures due to a reduction in MPAN thermal decomposition and thereby an increase in HMML formation.

HMML, based on volatility alone, would exist mostly in the gas phase, but because HMML is very reactive (e.g., oligomerization or reaction with inorganic ions in the particle phase), HMML quickly produces aerosol (Kjaergaard et al., 2012; Nguyen et al., 2015). Based on HMML production simulated by the kinetic mechanism under the conditions used in these experiments, $\sim$~~0.25~~ 0.21 SOA mass yield from methacrolein is expected purely from the mass contained in HMML (MW = 102 g/mol, Figure S4). At first, the molecular weight of HMML itself is used because this is the mass of the majority of the oligomer monomers. This represents about half of the SOA mass yield ($\sim$0.5) measured from the experiment performed with the highest seed surface area. The rest of the aerosol is likely comprised of inorganic or organic compounds that react with HMML in the particle phase. For example, inorganic compounds such as water, nitrate, and sulfate can react with HMML through ring-opening reactions to produce total methacrolein SOA mass yields of $\sim$~~0.29~~0.25, $\sim$~~0.40~~0.34, and $\sim$~~0.49~~0.41, respectively (Figure 2). Additionally, HMML can react with 2MGA and other organic compounds through oligomerization processes (e.g., Chan et al. (2010); Nguyen et al. (2015); Zhang et al. (2011, 2012)) . Some of these organic oligomerization reactions bring into the particle phase additional organic compounds (e.g., organic acids) that ordinarily would exist primarily in the gas phase (Figure 2). The details of these particle-phase reactions are further discussed in Section 5.2.

In general, there is much greater variability in the SOA mass yields measured from the 2MGA pathway than the LV pathway. The additional variability is only partially explained by the initial seed surface area (Figure 7). Because the SOA yield is larger for experiments in which less methacrolein is oxidized (Figures 6 and 7b), potentially, the extent of methacrolein oxidization contributes to this variability. The kinetic model suggests that formation of ~~the~~ gas-phase ~~2MGA precursor~~ HMML is similar for all of the experiments (Figure S4), but potentially slight variations in the NO$_2$/NO ratio and/or OH particularly near the end of each experiment are not well captured by the model. The kinetic model used here only simulates gas-phase oxidation. Chemistry occurring on surfaces such as the chamber walls or in the particle phase may be especially important for capturing the variability in the 2MGA pathway experiments. Considering that the 2MGA pathway experiments are very susceptible to small differences in chamber conditions, regional and global models should parameterize SOA formation from the 2MGA pathway through gas-phase formation of HMML and subsequent particle-phase reactions.

5 Discussion

The gas-phase compounds measured by the CIMS (Section 5.1) and aerosol composition measured by the AMS (Section 5.2) provide important insight into isoprene SOA chemical composition formed from both the LV and 2MGA pathways. Additionally, comparison of the AMS and DMA results lends insight into possible biases in the AMS measurements of organic aerosol in Section 5.3. The SOA yields measured in this study are compared with past measurements in Section 5.4 and the atmospheric contribution of the LV versus 2MGA pathways toward SOA formation from isoprene OH-initiated oxidation under high-NO_x conditions is estimated in Section 5.5.

5.1 Specific Low-Volatility Nitrates and Dinitrates Detected in the Gas-Phase

Numerous nitrates and dinitrates are detected in the gas phase by the CF_3O^- CIMS (i.e., compounds highlighted in blue boxes in Figure 1). Many of these nitrates have been identified in previous studies (e.g., Lee et al. (2014)). Yields for the low-volatility later-generation nitrates are either highly uncertain or unknown. Quantification is difficult for these low-volatility compounds due to high losses to sampling lines or chamber walls and lack of available standards. ~~Lee et al. (2014), assuming~~ One study, Lee et al. (2014), was able to quantify the yield of dinitrates from the first-generation isoprene hydroxy nitrate standards. Assuming a sensitivity similar to ~~standards of the first-generation isoprene hydroxy nitrates,~~ the isoprene hydroxy nitrate standards, Lee et al. (2014) measured a dinitrate yield of 0.03-0.04 from OH-initiated oxidation of the δ-1-hydroxy,4-nitrate isomer.

~~However, these dinitrate yields are highly uncertain; Lee et al. (2014) assigned an upper limit for the yield of dinitrates from the δ-1-hydroxy,4-nitrate isomer to 0.29 - 0.39 and the β-4-hydroxy,3-nitrate isomer to 0.18.~~

Although most past studies have focused on dihydroxy dinitrates as the main contributor to isoprene high-NO SOA, other low-volatility nitrates are likely also important. In Figure 8, the CIMS signals for the other low-volatility nitrates are comparable or larger than the dihydroxy dinitrate signal. The relative sensitivities for these compounds are unknown, but these results suggest that detection and quantification of all low-volatility dinitrates and nitrates is important. The peroxy radical formed from OH-initiated oxidation of an isoprene hydroxy nitrate can undergo a 1,5 or 1,6 α-hydroxy H-shift to form a number of low-volatility nitrates that would occur in the ambient atmosphere (Wennberg et al., 2018). The NO concentrations are too high in these experiments for such shifts to occur. However, similarly, certain isomers of the alkoxy radical, formed from OH-initiated oxidation of a isoprene hydroxy nitrate, can undergo a 1,5 ~~or 1,6~~ α-hydroxy H-shift to form a dihydroxy carbonyl nitrate detected by the CIMS at m/z (-) 264 (Figure 1 and 8). Additionally, various low-volatility nitrates in the gas phase are detected, which are potentially ~~derived from the delta-isoprene~~ oxidation products from the δ-isoprene hydroxy alkoxy radical as depicted in Figure 1.

~~Further measurements of the yield of these low-volatility nitrates and dinitrates in the gas phase will be crucial for better understanding isoprene SOA formation under high-NO conditions~~Many multi-functional isoprene derived organic nitrates have been detected in ambient aerosol (Lee et al., 2016). Although these low-volatility nitrates and dinitrates have low molar yields from isoprene OH-initiated oxidation, their mass is substantially larger than isoprene and so their contribution to the isoprene

SOA mass yield is significant. The nitrate yield from straight chain hydrocarbons is reasonably well understood, but few experimental measurements of the nitrate yield from highly oxidized compounds exist (Orlando and Tyndall, 2012; Wennberg et al., 2018). Further measurements of the yield of these low-volatility nitrates and dinitrates in the gas phase will be crucial for better understanding isoprene SOA formation under high-NO conditions.

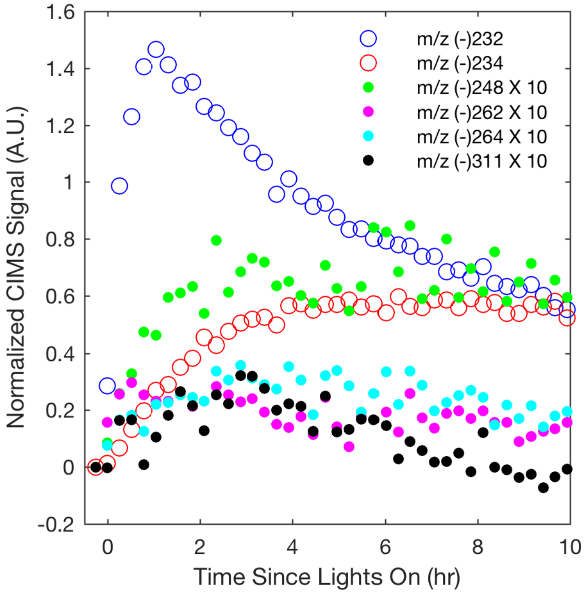

Figure 8. Normalized CIMS signal for known nitrates: C_5 hydroxy nitrate (m/z (-) 232 ○), methyl vinyl ketone/methacrolein nitrate (m/z (-) 234 ○), & C_5 dihydroxy dinitrate (m/z (-) 311 ●) and unknown nitrates, which are postulated in Figure 1 as C_5 dihydroxy nitrate (m/z (-) 248 ●), unknown (m/z (-) 262 ●), & C_5 dihydroxy carbonyl nitrate (m/z (-) 264 ●). As indicated in the legend, signals represented by filled circles are multiplied by 10.

5.2 Aerosol Composition of High-NO Isoprene SOA

Pieber et al. (2016) determined that inorganic aerosol such as ammonium nitrate or ammonium sulfate causes an interference on the AMS for the CO_2^+ ion signal. Although this interference is small for ammonium sulfate aerosol (<1%, (Pieber et al., 2016)), a correction may be needed for experiments with high initial seed aerosol loadings. Here organic signals from the AMS rise when ammonium sulfate seed is injected into the chamber. We expect this is due to the same interferences described in Pieber et al. (2016) and not due to contamination in ammonium sulfate solution or atomization technique. The background organic signal caused by the ammonium sulfate is subtracted from the overall results to produce Figures 9, 10, and 11.

The AMS spectra from the LV pathway confirm that SOA formed from the LV pathway is not dominated by 2-MGA and its oligomers (cyan and red bars in Figure 9 and S11). This is an important confirmation that isoprene SOA formed from the 2MGA and LV pathways are distinct. A small yield of isoprene epoxydiol (IEPOX) is produced from OH-initiated oxidation of isoprene hydroxy nitrates (Jacobs et al., 2014) and IEPOX SOA can be formed when particle liquid water is present (Nguyen et al., 2014a). NO levels remained high (> 100 ppb) throughout all LV pathway experiments (Figure S3), ensuring that the RO_2 fate in these experiments was always RO_2 + NO. AMS fragments associated with IEPOX, which were identified by Lin et al. (2012), are slightly enhanced under humid conditions in the LV pathway experiments (Figure 9). Some examples of organonitrate fragments ($C_xH_yNO_z^+$) are highlighted in Figure 9. Some of these organonitrate fragments are enhanced under humid conditions (e.g., CH_3NO^+). In general, the AMS spectra are similar between all LV pathway conditions (i.e. varied humidity-Figure 9 and varied temperature - Figure S11).

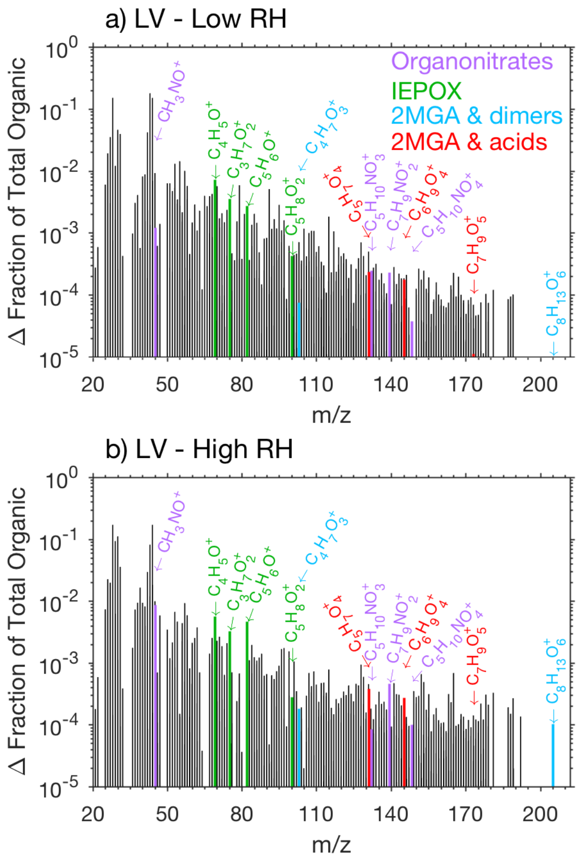

Figure 9. High resolution AMS mass spectra (averaged over 10h of photooxidation - the sulfate background) for experiment D3 (RH = 8%, panel a) and D9 (RH = 78%, panel b) in gray. Fragments are labeled as 2-MGA monomer/dimer (**cyan**), esterification of 2-MGA with acids (**red**), isoprene epoxydiol (IEPOX) tracers (**dark green**), and examples of organonitrate fragments - $C_xH_yNO_z$ (**purple**).

Prominent peaks in the AMS spectra from the 2MGA pathway clearly indicate that under dry conditions aerosol is comprised of various oligomerization products as mechanistically summarized in Figure 2. These oligomerization processes include 2-MGA oligomerization with HMML (cyan bars in Figure 10a) and, possibly, esterification of 2-MGA with carboxylic acids including formic, acetic, and pyruvic acids (red bars in Figure 10a), which yield products that have been detected in numerous studies (Chan et al., 2010; Zhang et al., 2011, 2012). Based on the AMS spectra, 2-MGA oligomerization appears to be more dominant without the presence of ammonium sulfate seed aerosol (Figure S13). Varying temperature from 13-32°C does not appear to substantially change the extent of 2-MGA oligomerization (Figure S14).

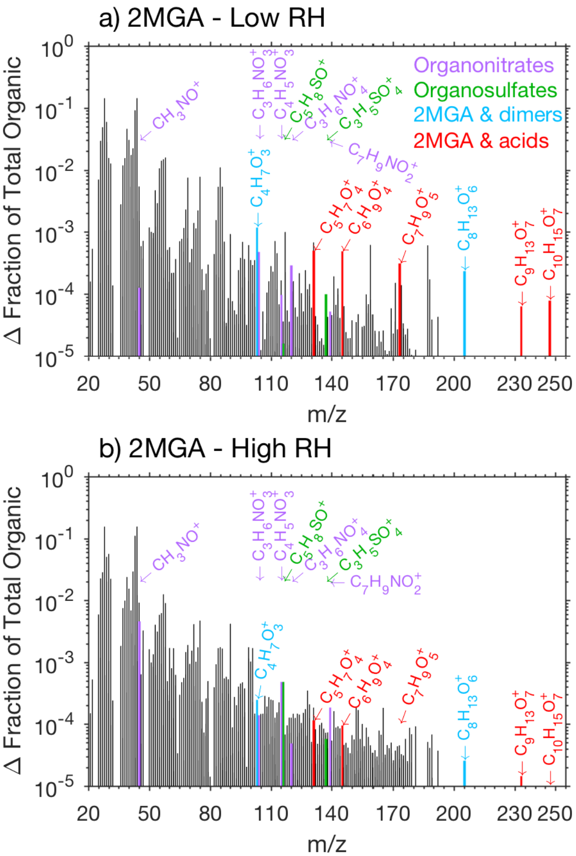

Figure 10. High resolution AMS mass spectra (averaged over 10h of photooxidation - the sulfate background) for experiment M2 (RH = 9%, panel a) and M8 (RH = 81%, panel b) in gray. Fragments are labeled as 2-MGA monomer/dimer (**cyan**), esterification of 2-MGA with acids (**red**), examples of organosulfate fragments (**dark green**), and examples of organonitrate fragments - $C_xH_yNO_z$ (**purple**).

Past studies have determined that HMML reaction with 2-MGA to form oligomers decreases under humid conditions while HMML ring-opening reactions with water and inorganic ions to form organic nitrates and organic sulfates increase (Zhang et al., 2011, 2012; Nguyen et al., 2015). Consistent with these past studies, the 2-MGA oligomer fragments on the AMS (cyan and red) are no longer prominent signals for all humid experiments (Figure 10 and Figure S12). 2-MGA oligomer fragments are not substantially different at 47%, 67%, or 81% RH, suggesting that the HMML oligomerization processes are impeded as soon as aerosol particles become deliquesced. Because isoprene is mostly emitted in regions with relatively high humidity, in the ambient atmosphere, HMML will more likely react with water and inorganic ions than undergo the various organic oligomerization reactions summarized in Figure 2.

5.3 Comparison of AMS and DMA Results

Based on the DMA measurements when assuming the same density, the SOA mass produced from the 2MGA pathway experiments is ∼2 times higher in magnitude than that from the LV pathway experiments (Figures 4 and 6). However, the AMS results (Figure 11) suggest that the SOA mass produced from the 2MGA pathway experiments is ≥8 times larger than that from the LV pathway experiments. This implies that the collection efficiency (CE) and/or the ionization efficiency on the AMS is quite different between these two regimes. Because the AMS is significantly more sensitive to aerosol formed from the 2MGA pathway, and not to SOA formed from the LV pathway, even ambient organic aerosol measurements have the potential to be impacted. Understanding whether the AMS is systematically underestimating organic aerosol from organic nitrates and dinitrates in general, or if this is only relevant to the isoprene system is crucial as the AMS is used throughout the world to quantify organic aerosol. Moreover, ambient measurements over the isoprene-rich Southeastern United States of particulate organic nitrates measured by the AMS are a factor of ∼5 lower than that measured by the thermal dissociation laser-induced fluorescence instrument (TD-LIF) (Lee et al., 2016). The relative CE differences between the LV and 2MGA pathways in this study and these field campaign results suggest further AMS calibration of organic nitrates is necessary.

In this work, a CE of 0.5 is assumed for both regimes consistent with past work (Nguyen et al., 2014b). The exact CE is not relevant as no mass yields are reported here from the AMS. Docherty et al. (2013) determined that the CE could be estimated based on the f_{44}/f_{57} ratio. The f_{44}/f_{57} ratio for all experiments (2MGA and LV) is ≥ 6, which is where the CE vs f_{44}/f_{57} curve plateaus at 0.2. Thus, the CE vs f_{44}/f_{57} relationship developed by Docherty et al. (2013) is not able to explain the large ~~CE difference~~ difference in AMS sensitivity between aerosol formed from the LV and 2MGA pathways.

5.4 Comparison to Previously Reported SOA Yields

SOA mass yields reported from past environmental chamber studies of OH-initiated oxidation of isoprene under high-NO_x conditions vary over the range of ~~0-0.09~~0.001-0.41 (Bregonzio-Rozier et al., 2015; Clark et al., 2016), suggesting isoprene SOA yields are highly dependent on chamber conditions (Carlton et al., 2009). In Table 2, past reported SOA mass yields are summarized along with the chamber conditions for both isoprene and methacrolein OH-initiated oxidation under high-NO_x conditions. Only experiments that explicitly measure an SOA mass yield are listed in Table 2. ~~By varying a large number of conditions, our results lend insight into the variation in these experiments.~~ Overall our results suggest that the initial seed surface area has the greatest impact on SOA yield. Unfortunately, the initial seed surface area was not commonly reported in past studies. The closest metric is aerosol volume, which can roughly be used to understand differences.

a) LV

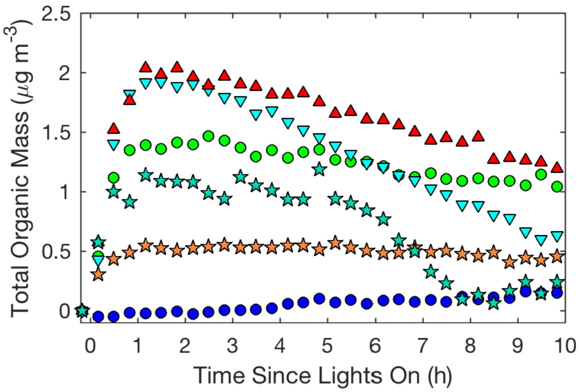

b) 2MGA

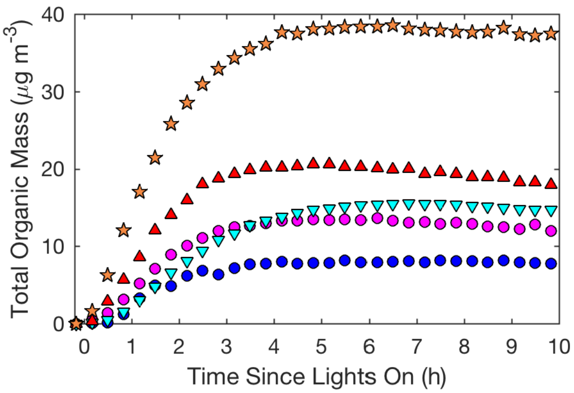

Figure 11. Total organic mass (20 minute averages) as measured by the AMS for LV pathway experiments (panel a): seed surface area - D1 (SA = 0 μm^2 cm^{-3}, ●) & D3 (SA = 3420 μm^2 cm^{-3}, ●), temperature - D5 (13 °C, ▼) & D6 (32 °C, ▲), and new chamber with less wall charging - D10 (SA = 1580 μm^2 cm^{-3}, ★) & D11 (SA = 4770 μm^2 cm^{-3}, ★) and 2MGA pathway experiments (panel b): seed surface area - M1 (SA = 0 μm^2 cm^{-3}, ●) & M2 (SA = 1640 μm^2 cm^{-3}, ●), temperature - M4 (13 °C, ▼) & M5 (32 °C, ▲), and new chamber with less wall charging - M9 (SA = 1910 μm^2 cm^{-3}, ★).

Table 2. Reported SOA mass yields and chamber conditions for isoprene and methacrolein OH-initiated oxidation under high-NO_x conditions

Study	CV (m^3)	Oxidant	$[VOC]_0$ (ppb)	$[NO]_0$ (ppb)	$[NO_2]_0$ (ppb)	Light ~~Source~~ Type	$[AS]_0$ ($\mu m^3/cm^3$)	Temp. (°C)	RH (%)	SOA Yield (fraction)
Isoprene										
Edney (2005)[a]	14.5	NO_x	1610-1680	~630	0	UV	<0.6-24[b]	29.7	30	0.002-0.028
Kroll (2005)	28	HONO	25-500	75-138	98-165	UV	10-25	~20	40-50	0.009-0.03
Dommen (2006)	27	NO_x	180-2500	0-700	40-806	X	0	20	<2-84	0.002-0.053
~~Kleindienst (2006)[a]~~ Kleindienst (2006)[a]	14.5	NO_x	1600	406-485	7-69	UV	0.1-27[b]	25	30	0.003-0.018 [c]
Chan (2010)	28	HONO or CH_3ONO	33-523	259-316	510-859	UV	11-19	20-22	9-11	0.031-0.074
Chhabra (2010)	28	HONO	81-286 [d]	518-591	374-434	UV	11-14	NR	<10	0.006-0.015
Zhang (2011)	137	NO_x	400-790	138-253	1-9	N	10-30	281-303	15-88	0.007-0.03
Nguyen (2011)	5	H_2O_2	~250	600	100	UV	0	22-26	<2-90	~ 0.07
Xu (2014)	10.6	H_2O_2	101-115	338-738	0	UV	0	~25	<5	0.015-0.085
~~Bregonzio-Rozier (2015)~~ Bregonzio -Rozier (2015)	4.2	NO_x or HONO	439-846	14-143	<1-79	X	0-16	16-24	<5	0.001-0.01
Clark (2016)	90	H_2O_2	250	500	0	UV	0	5-40	dry	0.1-0.41
Methacrolein										
Chan (2010)	28	HONO or CH_3ONO	20-285	164-725	365-799	UV	11-16	20-22	9-11	0.019-0.392
~~Bregonzio-Rozier (2015)~~Bregonzio -Rozier (2015)	4.2	NO_x or HONO	396-927	19-123	4-100	X	0-15	19-24	<5	0.005-0.042

CV = Chamber Volume. Acronyms are defined as follows: NR = not reported, UV = ultraviolet lights, N = natural, X = xenon arc lamps, and AS = ammonium sulfate seed aerosol volume. [a] Chamber was operated in dynamic mode (residence time = 6 h). [b] Ammonium sulfate was injected throughout the experiment to generate the lower limit of initial seed aerosol. SO_2 was added in some experiments to generate the upper limit of initial seed aerosol. [c] SOC is converted to SOA using factor (2.47) reported in Kleindienst et al. (2007). [d] VOC reacted was reported and tabulated instead of VOC initial.

As shown in Table 2, the range for isoprene SOA yields under high-NO$_x$ conditions even from the two most recent studies at comparable temperatures spans over an order of magnitude (0.004 at $\sim$21°C for Bregonzio-Rozier et al. (2015) and 0.1 at 27°C for Clark et al. (2016)). Our results are most consistent with those of Clark et al. (2016). As shown in Table 2, a variety of NO$_x$ regimes (i.e., non-consistent NO$_2$/NO ratios) are all labeled as high-NO$_x$ in these past studies. Each study likely produces SOA in varying degrees from the LV and 2MGA pathways, which greatly complicates direct comparison between these past studies. By varying a large number of conditions and completely separating SOA production between the 2MGA and LV pathways, our results lend insight into the variation in these past experiments.

Many of the past SOA yield measurements were performed with no seed aerosol. Consistent with past results, when no seed aerosol was injected into the chamber (experiments D1 and M1), the SOA mass yield for the LV pathway (0 from isoprene) and 2MGA pathway (0.1 from methacrolein) were quite low. Past experiments performed with no seed aerosol were only measuring SOA from the 2MGA pathway, which is ~~very~~ highly dependent on the NO$_2$/NO ratio (Chan et al., 2010)~~. The NO$_2$/NO ratio~~, which varied greatly between these past studies~~(Table 2)~~. Clark et al. (2016), who measured high SOA yields (0.1 at 27°C) in unseeded experiments is the exception. Possibly, the larger chamber volume (90 m^3) used by Clark et al. (2016) compared to most studies listed in Table 2 reduced vapor wall losses and contributed to the enhanced SOA yield. However, other chamber characteristics might also be important because Zhang et al. (2011) measured quite low isoprene SOA yields (0.007-0.03) using a chamber larger than the one used in the Clark et al. (2016) study.

While the zero or low seed aerosol loading experiments in this study generally compare well with the past, SOA yields measured here using higher initial seed surface areas are substantially greater than most studies, especially for the LV pathway. The SOA yield from the LV pathway is ~~$\simeq$~~ $\sim$0.15 in this study, while past isoprene SOA yields are largely $\leq$ 0.07 with the exception of studies optimizing for high RO$_2$ + NO$_2$ reactions (Chan et al., 2010) or mixed regimes - RO$_2$ + HO$_2$/NO (Xu et al., 2014). The SOA yield from the LV pathway in this work is even larger than the SOA yield from Clark et al. (2016) (0.1 at 27°C), which includes SOA from both the LV and 2MGA pathways. Possibly the larger chamber volume used by Clark et al. (2016) reduces vapor wall losses, but not to the extent that enhanced seed surface area does in this work. The higher yields measured in this study are not unexpected given that recent publications have recognized the importance of using high initial seed surface areas when measuring SOA yields to reduce the impact of vapor wall deposition (e.g., Zhang et al. (2014), Ehn et al. (2014)). The methacrolein SOA yields measured in this study from the 2MGA pathway are comparable to those measured by Chan et al. (2010), but larger than those measured by Bregonzio-Rozier et al. (2015).

~~The most recent isoprene SOA yield study, Bregonzio-Rozier et al. (2015) ,~~ Bregonzio-Rozier et al. (2015) measured low isoprene (0.001-0.01) and methacrolein (0.005-0.042) SOA mass yields ~~. They~~ and proposed that these lower yields were due to using xenon arc lamps as a light source, which are more representative of natural sunlight than the UV lamps used here and in most other studies. Dommen et al. (2006) also used xenon arc lamps and reported low yields. However, both of these studies used ~~0 or low~~ chambers with moderate to low chamber volumes (27-4.2 m^3) unlike the chamber used by Clark et al. (2016) and low levels of initial seed aerosol (0-16 µm^3/cm^3) unlike this work, which could also cause this low bias. Additionally, the stainless steel chamber used by Bregonzio-Rozier et al. (2015) may have higher vapor wall losses than the Teflon chambers used in other studies. Further work is necessary to understand how vapor wall losses compare across different types of environmental chambers.

As discussed by Carlton et al. (2009), isoprene SOA forms mostly from oxidation of 2nd and later-generation products (e.g., Ng et al., 2006). Towards the end of the experiment, SOA ~~mass~~ continues to grows even when isoprene is no longer reacting (e.g., the characteristic hook in Figure 4). Differences in the level of oxidation of 2nd and later-generation products could also explain some of the discrepancies between our results and past results. The isoprene SOA mass yields from the LV pathway are particularly sensitive to the extent of oxidation. More studies measuring the gas-phase yields and formation processes of low-volatility nitrates and dinitrates will be critical for further understanding isoprene SOA.

Many of the previous studies listed in Table 2 report the VOC/NO ratio when comparing experiments. A more useful metric is understanding the RO_2 fate and RO_2 lifetime. Simply injecting NO and/or NO_2 and reporting the initial concentrations are not sufficient to confirm that SOA was dominantly produced from the RO_2 + NO channel or in the case of HMML formation from the RO_2 + NO_2 channel. For example, if NO decreases to zero before the end of the experiment, SOA has formed in a mixed regime; RO_2 + NO reactions dominate in the beginning and RO_2 + HO_2 reactions dominate at the end. If large initial VOC loadings are used in the beginning of the experiment without comparable increases in NO, RO_2 + RO_2 reactions may become dominant.

Experiments here are specifically designed to test two different RO_2 fates, and the kinetic mechanism is used to confirm the fate of the RO_2. In the LV pathway experiments, high NO levels are maintained such that NO_2/NO ratio remains < 1.5 throughout the entire experiment and RO_2 dominantly and consistently across the experiments reacts with NO. In the 2MGA pathway experiments, high NO_2 levels are used such that the acyl radical derived from methacrolein dominantly and consistently across experiments reacts with NO_2. By controlling for the RO_2 fate, the effects of temperature, seed surface area, and relative humidity on SOA formation become easier to resolve. Design of future experiments should optimize and report the RO_2 fate for which the experiment was designed, in addition to key reaction parameters such as seed surface area, rather than simply reporting an initial VOC/NO ratio.

5.5 Estimating the Atmospheric Contribution of the LV versus 2MGA Pathways

This work was not only designed to independently study SOA formation from the two high-NO_x regimes (the 2MGA and LV pathways), but also to suggest alternative methods for parameterizing isoprene SOA under high-NO_x conditions in regional and global models. Because obtaining constant NO_2/NO ratios similar to the ambient atmosphere is near impossible for a chamber study (e.g., temporal variation in Figure S3), creating isoprene SOA parameterizations based on NO_2/NO ratio that realistically extrapolate to the ambient atmosphere is not realistic. Instead, this work highlights a potential alternative. Aerosol from the 2MGA pathway could be incorporated directly from gas-phase HMML formation and aerosol from the LV pathway could be included either from formation of surrogate compounds such as isoprene dihydroxy dinitrates or with a volatility basis set scheme. By treating the SOA from these two independent regimes separately, this study sets up the experimental basis for such an approach.

In this study, direct comparison of the results from the 2MGA and LV pathways is difficult due to the difference in the extent of oxidation between the two regimes caused by the use of different VOC precursors and the variation in OH levels (Table 1). Thus, the kinetic model is used here to estimate the contribution of each pathway to the total under consistent oxidant levels. A detailed global modeling study is needed to precisely capture the contribution of the LV versus the 2MGA pathways toward SOA formation from isoprene OH-initiated oxidation under high-NO$_x$ conditions. However, in order to demonstrate the significance of the new isoprene SOA yield from the LV pathway measured in this work, we roughly approximate the contribution of each pathway under typical atmospheric conditions. We use the same kinetic mechanism described in Section 3, but hold the following constant: RH = 70%, T = 298K, NO$_2$ = 0.3 ppb, NO = 0.05 ppb, isoprene = 5 ppb, OH = 1.5 x 10^6 molec cm^{-3}, CO = 135 ppb, O$_3$ = 37 ppb, and HO$_2$ = 25 ppt (Sanchez et al., 2018; Feiner et al., 2016; Pajunoja et al., 2016). Then ~~we simulate the formation of the~~ gas-phase ~~2-MGA and dinitrate SOA tracers~~ HMML and the gas-phase dinitrate SOA precursors are simulated as done for the experimental results in Figure S4.

To estimate the aerosol contribution ~~for~~ from the LV pathway, we assume that SOA production from the LV pathway scales with the ~~dinitrate tracer, so we multiply the dinitrate tracer by 7.1, which is the~~ production of isoprene dihydroxy dinitrates. Organic aerosol concentrations are higher in chamber experiments than the ambient atmosphere. By using low levels of VOC precursors compared to previous studies, this study attempts to reduce the organic aerosol concentrations to produce results more relevant to the ambient atmosphere. However, due to limitations in the DMA sensitivity, reducing the organic aerosol concentrations further to ambient levels is not possible. The ratio of the measured SOA yield (Figure 5) versus the simulated ~~SOA yield from the~~ gas-phase ~~dinitrate tracer~~ dihydroxy dinitrate SOA precursor yield (Figure S4) ~~. Then we~~ is about 5. F$_P$ is decreased by a factor of 2 for the dihydroxy dinitrates when C$_{OA}$ is reduced from ∼25 µg cm^{-3} in the chamber to ∼4 µg cm^{-3} measured in the Southeast U.S. (Zhang et al., 2018). Thus, we multiply the dihydroxy dinitrate SOA precursors by 2.5 and we convert to mass by multiplying by the molecular weight of dihydroxy dinitrate~~(226 g/mol). The dinitrate SOA tracer includes all dihydroxy dinitrates from isoprene OH-initiated oxidation.~~ . MCM v3.3.1 assumes a nitrate yield of 0.087-0.104 from NO reacting with the peroxy radical derived from OH + isoprene hydroxy nitrate. Low-volatility nitrates such as dihydroxy hydroperoxy nitrates form when HO$_2$ reacts with the peroxy radical derived from OH + isoprene hydroxy nitrate. Such products would not form in the chamber conditions used in this work where NO levels remained above 100 ppb, but would form in the ambient atmosphere. Considering these low-volatility species from mixed chemical regimes would further increase the SOA mass generated from the LV pathway.

For the 2MGA pathway, we convert to mass by multiplying ~~the~~ gas-phase ~~2MGA tracer~~ HMML by the molecular weight of 2-MGA (120 g/mol), 2-MGA-nitrate (165 g/mol), and 2-MGA-sulfate (200 g/mol), which are the expected condensed-phase products under the high humidity levels in the atmosphere. ~~The 2MGA tracer includes HMML and MAE, which in MCM v3.3.1 are produced in yields of 0.57 and 0.21, respectively from the reaction of MPAN + OH~~Laboratory studies confirm that 2-MGA forms under humid conditions and some of the 2-MGA partitions to the gas-phase as expected based on its volatility (Nguyen et al., 2015). For simplicity, we assume most of the HMML forms 2-MGA-nitrate and 2-MGA-sulfate, but acknowledge further experimental and modeling studies are needed to fully understand HMML/2-MGA aqueous phase chemistry.

Then based on the ~~assumptions above,~~ gas-phase SOA precursor distribution from the kinetic model ~~estimates that~~ and assumptions above, under typical atmospheric conditions the fraction of the total SOA mass from isoprene OH-initiated oxidation under high-NO~~conditions is~~$_x$ conditions is $\sim$0.7 ~~-0.8~~ from the LV pathway and ~~0.2-0.3~~ $\sim$0.3 from the 2MGA pathway~~depending on whether HMML ring-opens to react with water, nitrate, or sulfate.~~

~~Thus, in the atmosphere~~. This assumes that the dihydroxy dinitrates are valid surrogates for the isoprene SOA. Considering many multi-functional isoprene derived organic nitrates have been detected in ambient aerosol (Lee et al., 2016), all SOA precursors in Table S2 with $F_P > 0.05$ at 26°C are combined and converted to mass. Extrapolating these to ambient organic aerosol concentrations is more difficult because these compounds are more likely to exist in the particle phase because of accretion reactions and not volatility. When these products are assumed to exist entirely in the particle-phase and no factor is applied to correct for differences in organic aerosol concentration or for these products only representing about 1/3 of the isoprene SOA yield measured in this study (Figure S4), the LV pathway is estimated to contribute to $\sim$0.6 of the SOA formed under high-NO$_x$ conditions.

Thus, based on the simple calculations summarized above, the LV pathway ~~produces~~ may produce moderately more SOA mass than the 2MGA pathway in the atmosphere and consequently deserves equal attention. The conditions chosen here represent average atmospheric conditions around noon as measured during the SOAS field campaign, which occurred in the isoprene-rich Southeastern United States (Sanchez et al., 2018; Feiner et al., 2016; Pajunoja et al., 2016). A more complete assessment using global and regional modeling is needed to more definitively determine the fraction of SOA formed via the LV versus 2MGA pathways as location, time of day, season, ambient aerosol concentration and composition, etc. will all impact the amount of SOA formed from each pathway. Additional studies addressing organic nitrate hydrolysis and aerosol acidity are also necessary to fully understand the relative impact of the two pathways on SOA formation. Additionally, the kinetic model used in this work only estimates gas-phase potential SOA precursors. Future analysis using a more complex model that explicitly simulates both the gas and particle phases would be useful for extrapolating the SOA yields measured here to the ambient atmosphere, which typically has lower organic aerosol concentrations than chamber experiments. This would need to be combined with additional analysis of the chemical constituents in the particle phase. From past work (Kleindienst et al., 2009; Xu et al., 2014; D'Ambro et al., 2017) demonstrating that isoprene derived SOA under high-NO$_x$ conditions is lower in volatility than that derived under low-NO$_x$ conditions and the C* values estimated in this work (Table S2), accretion reactions appear to be important even in the LV pathway experiments. The degree to which accretion reactions occur in the LV pathway experiments to form even lower volatility products is quite uncertain and will greatly impact future analysis on how best to extrapolate isoprene SOA yields measured in chambers to the ambient atmosphere.

6 Conclusions

SOA from OH-initiated isoprene oxidation under high-NO$_x$ conditions forms from two major pathways: 1) low-volatility nitrates and dinitrates (LV pathway) and 2) 2-methyl glyceric acid and its oligomers (2MGA pathway). These SOA production pathways respond differently to experimental conditions, so this work examines the SOA yields from these two pathways independently. Results suggest that low-volatility nitrates and dinitrates produce significantly more aerosol than previously thought with the isoprene SOA mass yield from the LV pathway ~~$\simeq$~~$\sim$0.15. Sufficient initial seed aerosol is necessary to reduce the impact of vapor wall losses of low-volatility compounds and accurately measure the entire SOA mass yield. Even though previous studies have assumed that isoprene high-NO_x SOA largely forms from 2-MGA and its oligomers (Chan et al., 2010; Zhang et al., 2011, 2012), results from this study confirm low-volatility compounds are also important for isoprene SOA formed under high-NO_x conditions. The fate of isoprene's RO_2 radicals and the environmental conditions will determine which pathways are active in the atmosphere at a certain time and location.

Under dry conditions, substantial amounts of SOA form from HMML reaction with 2MGA to produce oligomers. The AMS results confirm that under humid conditions, these low-volatility oligomers are diminished in favor of higher-volatility monomer formation (and potentially subsequent volatilization of 2-MGA) to reduce the SOA mass. Thus, under atmospherically relevant humid conditions, aerosol formed from the 2MGA pathway is limited to HMML reaction with water or inorganic ions such as nitrate and sulfate. The importance of SOA from the 2MGA pathway will also depend on the NO_2/NO ratio, while SOA formed from the LV pathway will be important under all NO_2/NO ratios. Under typical atmospheric conditions (RH = 70%, T = 298K, NO_2/NO = 6, NO = 0.05 ppb, isoprene = 5 ppb, and OH = 1.5 x 10^6 molec cm^{-3}), we now estimate based on the simple assumptions discussed in Section 5.5 that the LV pathway produces moderately more SOA mass than the 2MGA pathway due to the high isoprene SOA yield from the LV pathway measured in this work.

Given the high isoprene SOA mass yield from the LV pathway (~~$\simeq$~~$\sim$0.15) measured here, low-volatility compounds are as important as 2MGA-based compounds for isoprene SOA formed under high-NO_x conditions. Thus, further studies investigating the formation rates and yields of these low-volatility compounds are needed. Consistent with past work (e.g., Lee et al. (2014)), a number of low-volatility nitrates and dinitrates, which are likely important precursors for SOA formed from the LV pathway, were detected in the gas phase by the CF_3O^- CIMS (Section 5.1). These low-volatility compounds are likely derived from OH-initiated oxidation of the first-generation isoprene hydroxy nitrates. Synthetic pathways toward standards of many of the isoprene hydroxy nitrates exist (Lee et al., 2014; Teng et al., 2017). Now that this study has confirmed that low-volatility products contribute significantly to isoprene SOA, measuring SOA mass yields under varying RO_2 fate using these isoprene hydroxy nitrate standards as the initial precursor instead of isoprene could be particularly valuable for decreasing the uncertainty in isoprene SOA yields. Additionally, an improved mechanistic understanding of isoprene SOA is needed. This would include an improved understanding of gas-phase reactions including measurements of highly functionalized peroxy radical isomerization rate constants~~and~~, quantification of nitrate and hydroperoxide yields from highly functionalized RO_2 radicals reacting with NO or HO_2, respectively~~.~~, and additional constraints on possible particle-phase accretion reactions leading to lower volatility products (e.g., hemiacetal formation).

There are some limitations for how results from this study should be interpreted. In the atmosphere, the RO_2 lifetime is longer than that in chamber experiments from this study and most past studies measuring SOA yields. Due to limitations in the sensitivity of the DMA and high NO levels needed to control the RO_2 fate, performing SOA yield chamber experiments at conditions that favor a long RO_2 lifetime is difficult. At longer RO_2 lifetimes, the hydroxy nitrate isomer distribution shifts toward a higher percentage of β-isomers over δ-isomers ~~(Teng et al., 2017)~~(Peeters et al., 2014; Teng et al., 2017). Additionally,

NO_x emissions are decreasing across many regions of the world due to improvements in emissions controls creating mixed regimes in the ambient atmosphere where a later-generation gas-phase product could form from RO_2 + NO reaction during the 1st-generation and RO_2 + HO_2 during the 2nd-generation. Field measurements confirm the presence of such products. For example, Xiong et al. (2015) discuss the presence of dihydroxy hydroperoxy nitrates detected in the particle phase by Lee et al. (2016) during SOAS, a field campaign that occurred during the summer in the Southeastern United States. Dihydroxy hydroperoxy nitrates likely form when hydroxy nitrates, produced from the RO_2 + NO pathway, react with OH and O_2 to form a peroxy radical that then reacts with HO_2. Additionally, because isoprene SOA from the LV pathway only forms once later-generation products get oxidized, the extent of oxidation is important, but also difficult to compare across different studies.

Comparisons of the DMA and AMS results imply that the collection and/or ionization efficiency on the AMS for SOA formed from the LV pathway is significantly lower than that formed from the 2MGA pathway. This could have important consequences on the interpretation of ambient organic aerosol measured by the AMS. Further work calibrating organic hydroxy nitrates on the AMS is needed to better understand why the organic fraction analysis varied so significantly between the two pathways.

Results from this work combined with past work provide further insight into how isoprene SOA should be parameterized in global and regional atmospheric chemistry models. Under humid conditions, SOA formation from the 2MGA pathway is produced mostly from HMML ring opening reactions to form monomer compounds 2-MGA, 2-MGA-nitrate, and 2-MGA-sulfate, which simplifies the parameterization of SOA from the 2MGA pathway as the organic oligomerization reactions can be ignored. The particle's liquid water and pH will be important to consider, as these metrics shift the equilibrium of 2MGA and its carboxylate and change the hydrolysis rates for the 2-MGA-nitrate and 2-MGA-sulfate. The gas-phase kinetics for MPAN formation and reaction with OH to form HMML have been reasonably well studied (e.g., Orlando et al. (1999, 2002); Nguyen et al. (2015)). HMML formation and generation of SOA in the atmosphere would be best incorporated into models by directly forming SOA through the MPAN + OH reaction. This would best parameterize the effects of temperature and NO_2/NO ratio on MPAN formation and also the influence of OH on HMML formation. This study confirms the need to perform experiments with adequate seed aerosol to limit vapor wall deposition processes when measuring SOA yields from the LV pathway. When regional chemical transport models use SOA yields that account for vapor wall deposition, there are differences in the contribution of isoprene to the total SOA budget and improvements in the agreement between simulated and observed total SOA and diurnal variability (Cappa et al., 2016). Incorporating the isoprene SOA yields from the LV pathway measured in this work into models will further improve the accuracy of simulated isoprene SOA. Moreover, the results from this study along with future experiments studying the formation of low-volatility nitrates and dinitrates on a mechanistic basis will be important for incorporating more explicit SOA formation into global models as has recently been done (e.g., Marais et al. (2016); Stadtler et al. (2018)), thus replacing previous parameterizations that typically were based on a single chamber condition (e.g.,Henze and Seinfeld (2006); Henze et al. (2008); Heald et al. (2008)).

Data availability. ~~Data used within this work are available upon request. Please email Rebecca Schwantes (rschwant@ucar.edu).~~ We welcome future collaboration with those who wish to use this data set for additional modeling purposes (e.g., creating volatility basis set parameters for global/regional models or for evaluating the results with a more complex box-model that includes aerosol chemistry). Please contact Rebecca Schwantes (rschwant@ucar.edu).

Author contributions. RHS designed the experiments. RHS and SMC performed the experiments. RHS analyzed the data with help from SMC, KHB, TBN, JHS, and YH. RHS did the kinetic modeling. YH, HM, WK, and RCF assisted RHS with DMA operation and data analysis. RHS wrote the manuscript with assistance from KHB, TBN, JHS, SMC, and YH.

Competing interests. The authors declare that they have no conflict of interest.

Acknowledgements. This work was supported by the National Science Foundation grant AGS-1523500. Sophia M. Charan is supported by the National Science Foundation Graduate Research Fellowship under grant 1745301. We thank Dennis Fitz for assistance with maintenance and data analysis of the luminol NO_2/acyl peroxynitrate analyzer. The National Center for Atmospheric Research is sponsored by the National Science Foundation.

References

Aiken, A. C., DeCarlo, P. F., Kroll, J. H., Worsnop, D. R., Huffman, J. A., Docherty, K. S., Ulbrich, I. M., Mohr, C., Kimmel, J. R., Sueper, D., Sun, Y., Zhang, Q., Trimborn, A., Northway, M., Ziemann, P. J., Canagaratna, M. R., Onasch, T. B., Alfarra, R. M., Prevot, A. S. H., Dommen, J., Duplissy, J., Metzger, A., Baltensperer, U., and Jimenez, J. L.: O/C and OM/OC ratios of primary, secondary, and ambient organic aerosols with high-resolution time-of-flight aerosol mass spectrometry, Environ. Sci. Technol., 42, 4478–4485, https://doi.org/10.1021/es703009q, 2008.

Atkinson, R.: Rate constants for the atmospheric reactions of alkoxy radicals: An updated estimation method, Atmos. Environ., 41, 8468–8485, https://doi.org/10.1016/j.atmosenv.2007.07.002, 2007.

Bregonzio-Rozier, L., Siekmann, F., Giorio, C., Pangui, E., Morales, S. B., Temime-Roussel, B., Gratien, A., Michoud, V., Ravier, S., Cazaunau, M., Tapparo, A., Monod, A., and Doussin, J.-F.: Gaseous products and secondary organic aerosol formation during long term oxidation of isoprene and methacrolein, Atmos. Chem. Phys., 15, 2953–2968, https://doi.org/10.5194/acp-15-2953-2015, 2015.

Burkholder, J. B., Sander, S. P., Abbatt, J., Barker, J. R., Huie, R. E., Kolb, C. E., Kurylo, M. J., Orkin, V. L., Wilmouth, D. M., and Wine, P. H.: Chemical Kinetics and Photochemical Data for Use in Atmospheric Studies, Evaluation No. 18, Tech. Rep. JPL Publication 15-10, Jet Propulsion Laboratory, Pasadena, CA, http://jpldataeval.jpl.nasa.gov, 2015.

Canagaratna, M. R., Jimenez, J. L., Kroll, J. H., Chen, Q., Kessler, S. H., Massoli, P., Hildebrandt Ruiz, L., Fortner, E., Williams, L. R., Wilson, K. R., Surratt, J. D., Donahue, N. M., Jayne, J. T., and Worsnop, D. R.: Elemental ratio measurements of organic compounds using aerosol mass spectrometry: characterization, improved calibration, and implications, Atmos. Chem. Phys., 15, 253–272, https://doi.org/10.5194/acp-15-253-2015, 2015.

Cantrell, C. A., Stockwell, W. R., Anderson, L. G., Busarow, K. L., Perner, D., Schmeltekopf, A., Calvert, J. G., and Johnston, H. S.: Kinetic Study of the NO_3-CH_2O Reaction and Its Possible Role in Nighttime Tropospheric Chemistry, J. Phys. Chem., 89, 139–146, https://doi.org/10.1021/j100247a031, 1985.

Cappa, C. D., Jathar, S. H., Kleeman, M. J., Docherty, K. S., Jimenez, J. L., Seinfeld, J. H., and Wexler, A. S.: Simulating secondary organic aerosol in a regional air quality model using the statistical oxidation model – Part 2: Assessing the influence of vapor wall losses, Atmos. Chem. Phys., 16, 3041–3059, https://doi.org/10.5194/acp-16-3041-2016, 2016.

Carlton, A. G., Wiedinmyer, C., and Kroll, J. H.: A review of secondary organic aerosol (SOA) formation from isoprene, Atmos. Chem. Phys., 9, 4987–5005, https://doi.org/10.5194/acp-9-4987-2009, 2009.

Chan, A. W. H., Chan, M. N., Surratt, J. D., Chhabra, P. S., Loza, C. L., Crounse, J. D., Yee, L. D., Flagan, R. C., Wennberg, P. O., and Seinfeld, J. H.: Role of aldehyde chemistry and NO_x concentrations in secondary organic aerosol formation, Atmos. Chem. Phys., 10, 7169–7188, https://doi.org/10.5194/acp-10-7169-2010, 2010.

Charan, S. M., Kong, W., Flagan, R. C., and Seinfeld, J. H.: Effect of particle charge on aerosol dynamics in Teflon environmental chambers, Aerosol Sci. Technol., 52:8, 854–871, https://doi.org/10.1080/02786826.2018.1474167, 2018.

Chhabra, P. S., Flagan, R. C., and Seinfeld, J.: Elemental analysis of chamber organic aerosol using an Aerodyne high-resolution aerosol mass spectrometer, Atmos. Chem. Phys., 10, 4111–4131, https://doi.org/10.5194/acp-10-4111-2010, 2010.

Clark, C. H., Kacarab, M., Nakao, S., Asa-Awuku, A., Sato, K., and Cocker, D. R.: Temperature effects on secondary organic aerosol (SOA) from the dark ozonolysis and photo-oxidation of isoprene, Environ. Sci. Technol., 50, 5564–5571, https://doi.org/10.1021/acs.est.5b05524, 2016.

Cox, R. A., Derwent, R. G., Kearsey, S. V., Batt, L., and Patrick, K. G.: Photolysis of methyl nitrite: kinetics of the reaction of the methoxy radical with O_2, J. Photochem., 13, 149–163, https://doi.org/10.1016/0047-2670(80)85006-4, 1980.

D'Ambro, E. L., Lee, B. H., Liu, J., Shilling, J. E., Gaston, C. J., Lopez-Hilfiker, F. D., Schobesberger, S., Zaveri, R. A., Mohr, C., Lutz, A., Zhang, Z., Gold, A., Surratt, J. D., Rivera-Rios, J. C., Keutsch, F. N., and Thornton, J. A.: Molecular composition and volatility of isoprene photochemical oxidation secondary organic aerosol under low- and high-NO_x conditions, Atmos. Chem. Phys., 17, 159–174, https://doi.org/10.5194/acp-17-159-2017, 2017.

Docherty, K. S., Jaoui, M., Corse, E., Jimenez, J. L., Offenberg, J. H., Lewandowski, M., and Kleindienst, T. E.: Collection efficiency of the aerosol mass spectrometer for chamber-generated secondary organic aerosols, Aerosol Sci. Technol., 47, 294–309, https://doi.org/10.1080/02786826.2012.752572, 2013.

Dommen, J., Metzger, A., Duplissy, J., Kalberer, M., Alfarra, M. R., Gascho, A., Weingartner, E., Prevot, A. S. H., Verheggen, B., and Baltensperer, U.: Laboratory observation of oligomers in the aerosol from isoprene/NO_x photooxidation, Geophys. Res. Lett., 33, L13 805, https://doi.org/10.1029/2006GL026523, 2006.

Donahue, N. M., Kroll, J. H., Pandis, S. N., and Robinson, A. L.: A two-dimensional volatility basis set – Part 2: Diagnostics of organic-aerosol evolution, Atmos. Chem. Phys., 12, 615–634, https://doi.org/10.5194/acp-12-615-2012, 2012.

Edney, E. O., Kleindienst, T. E., Jaoui, M., Lewandowski, M., Offenberg, J. H., Wang, W., and Claeys, M.: Formation of 2-methyl tetrols and 2-methylglyceric acid in secondary organic aerosol from laboratory irradiated isoprene/NO_X/SO_2/air mixtures and their detection in ambient PM2.5 samples collected in the eastern United States, Atmos. Environ., 39, 5281–5289, https://doi.org/10.1016/j.atmosenv.2005.05.031, 2005.

Ehn, M., Thornton, J. A., E., K., Sipila, M., Junninen, H., Pullinen, I., Springer, M., Rubach, F., Tillmann, R., Lee, B., Lopez-Hilfiker, F., Andres, S., Acir, I.-H., Rissanen, M., Jokinen, T., Schobesberger, S., Kangasluoma, J., Kontkanen, J., Nieminen, T., Kurten, T., Nielsen, L. B., Jorgensen, S., Kjaergaard, H. G., Canagaratna, M., Dal Maso, M., Berndt, T., Petaja, T., Wahner, A., Kerminen, V.-M., Kulmala, M., Worsnop, D. R., Wildt, J., and Mentel, T. F.: A large source of low-volatility secondary organic aerosol, Nature, 506, 476–479, https://doi.org/10.1038/nature13032, 2014.

Feiner, P. A., Brune, W. H., Miller, D. O., Zhang, L., Cohen, R. C., Romer, P. S., Goldstein, A. H., Keutsch, F. N., Skog, K. M., Wennberg, P. O., Nguyen, T. B., Teng, A. P., De Gouw, J., Koss, A., Wild, R. J., Brown, S. S., Guenther, A., Edgerton, E., Baumann, K., and Fry, J. L.: Testing atmospheric oxidation in an Alabama forest, J. Atmos. Sci., 73, 4699–4710, https://doi.org/10.1175/JAS-D-16-0044.1, 2016.

Gaffney, J. S., Bornick, R. M., Chen, Y.-H., and Marley, N. A.: Capillary gas chromatographic analysis of nitrogen dioxide and PANs with luminol chemiluminescent detection, Atmos. Environ., 32, 1445–1454, https://doi.org/10.1016/S1352-2310(97)00098-8, 1998.

Guenther, A. B., Jiang, X., Heald, C. L., Sakulyanontvittaya, T., Duhl, T., Emmons, L. K., and Wang, X.: The model of emissions of gases and aerosols from nature version 2.1 (MEGAN2.1): An extended and updated framework for modeling biogenic emissions, Geosci. Model Dev., 5, 1471–1492, https://doi.org/10.5194/gmd-5-1471-2012, 2012.

Hallquist, M., Wenger, J. C., Baltensperger, U., Rudich, Y., Simpson, D., Claeys, M., Dommen, J., Donahue, N. M., George, C., Goldstein, A. H., Hamilton, J. F., Herrmann, H., Hoffmann, T., Iinuma, Y., Jang, M., Jenkin, M. E., Jimenez, J. L., Kiendler-Scharr, A., Maenhaut, W., McFiggans, G., Mentel, T. F., Monod, A., Prevot, A. S. H., Seinfeld, J. H., Surratt, J. D., Szmigielski, R., and Wildt, J.: The formation, properties and impact of secondary organic aerosol: current and emerging issues, Atmos. Chem. Phys., 9, 5155–5236, https://doi.org/10.5194/acp-9-5155-2009, 2009.

Heald, C. L., Henze, D. K., Horowitz, L. W., Feddema, J., Lamarque, J.-F., Guenther, A., Hess, P. G., Vitt, F., Seinfeld, J. H., Goldstein, A. H., and Fung, I.: Predicted change in global secondary organic aerosol concentrations in response to future climate, emissions, and land use change, J. Geophys. Res. Atmos., 113, D05 211, https://doi.org/10.1029/2007JD009092, 2008.

Henze, D. K. and Seinfeld, J. H.: Global secondary organic aerosol from isoprene oxidation, Geophys. Res. Lett., 33, L09 812, https://doi.org/10.1029/2006GL025976, 2006.

Henze, D. K., Seinfeld, J. H., Ng, N. L., Kroll, J. H., Fu, T.-M., Jacob, D. J., and Heald, C. L.: Global modeling of secondary organic aerosol formation from aromatic hydrocarbons: high- vs. low-yield pathways, Atmos. Chem. Phys., 8, 2405–2420, https://doi.org/10.5194/acp-8-2405-2008, 2008.

Huang, Y., Zhao, R., Charan, S. M., Kenseth, C. M., Zhang, X., and Seinfeld, J. H.: Unified theory of vapor-wall mass transport in Teflon-walled environmental chambers, Environ. Sci. Technol., 52, 2134–2142, https://doi.org/10.1021/acs.est.7b05575, 2018.

Jacobs, M. I., Burke, W. J., and Elrod, M. J.: Kinetics of the reactions of isoprene-derived hydroxynitrates: gas phase epoxide formation and solution phase hydrolysis, Atmos. Chem. Phys., 14, 8933–8946, https://doi.org/10.5194/acp-14-8933-2014, 2014.

Jenkin, M. E., Hayman, G. D., and Cox, R. A.: The chemistry of CH_3O during the photolysis of methyl nitrite, J. Photochem. Photobiol., 42, 187–196, https://doi.org/10.1016/1010-6030(88)80062-5, 1988.

Jenkin, M. E., Saunders, S. M., and Pilling, M. J.: The tropospheric degradation of volatile organic compounds: A protocol for mechanism development, Atmos. Environ., 31, 81–104, https://doi.org/10.1016/S1352-2310(96)00105-7, 1997.

Jenkin, M. E., Hurley, M. D., and Wallington, T. J.: Investigation of the radical product channel of the $CH_3C(O)O_2$ + HO_2 reaction in the gas phase, Phys. Chem. Chem. Phys., 9, 3149–3162, https://doi.org/10.1039/B702757E, 2007.

Jenkin, M. E., Young, J. C., and Rickard, A. R.: The MCM v3.3.1 degradation scheme for isoprene, Atmos. Chem. Phys., 15, 11 433–11 459, https://doi.org/10.5194/acp-15-11433-2015, 2015.

Kjaergaard, H. G., Knap, H. C., Ornso, K. B., Jorgensen, S., Crounse, J. D., Paulot, F., and Wennberg, P. O.: Atmospheric fate of methacrolein. 2. Formation of lactone and implications for organic aerosol production, J. Phys. Chem. A., 116, 5763–5768, https://doi.org/10.1021/jp210853h, 2012.

Kleindienst, T. E., Edney, E. O., Lewandowski, M., Offenberg, J. H., and Jaoui, M.: Secondary organic carbon and aerosol yields from the irradiations of isoprene and α-pinene in the presence of NO_x and SO_2, Environ. Sci. Technol., 40, 3807–3812, https://doi.org/10.1021/es052446r, 2006.

Kleindienst, T. E., Jaoui, M., Lewandowski, M., Offenberg, J. H., Lewis, C. W., Bhave, P. V., and Edney, E. O.: Estimates of the contributions of biogenic and anthropogenic hydrocarbons to secondary organic aerosol at a southeastern US location, Atmos. Environ., 41, 8288–8300, https://doi.org/10.1016/j.atmosenv.2007.06.045, 2007.

Kleindienst, T. E., Lewandowski, M., Offenberg, J. H., Jaoui, M., and Edney, E. O.: The formation of secondary organic aerosol from the isoprene + OH reaction in the absence of NO_x, Atmos. Chem. Phys., 9, 6541–6558, https://doi.org/10.5194/acp-9-6541-2009, 2009.

Knote, C., Tuccella, P., Curci, G., Emmons, L., Orlando, J. J., Madronich, S., Baro, R., Jimenez-Guerrero, P., Luecken, D., Hogrefe, C., Forkel, R., Werhahn, J., Hirtl, M., Perez, J. L., San Jose, R., Giordano, L., Brunner, D., Yahya, K., and Zhang, Y.: Influence of the choice of gas-phase mechanism on predictions of key gaseous pollutants during the AQMEII phase-2 intercomparison, Atmos. Environ., 115, 553–568, https://doi.org/10.1016/j.atmosenv.2014.11.066, 2015.

Krechmer, J. E., Coggon, M. E., Massoli, P., Nguyen, T. B., Crounse, J. D., Hu, W., Day, D. A., Tyndall, G. S., Henze, D. K., Rivera-Rios, J. C., Nowak, J. B., Kimmel, J. R., Mauldin, R. L., Stark, H., Janye, J. T., Sipila, M., Junninen, H., St. Clair, J. M., Zhang, X., Feiner, P. A., Zhang, L., Miller, D. O., Brune, W. H., Keutsch, F. N., Wennberg, P. O., Seinfeld, J. H., Worsnop, D. R., Jimenez, J. L., and Canagaratna,

M. R.: Formation of Low Volatility Organic Compounds and Secondary Organic Aerosol from Isoprene Hydroxyhydroperoxide Low-NO Oxidation, Environ. Sci. Technol., 49, 10 330–10 339, https://doi.org/10.1021/acs.est.5b02031, 2015.

Kroll, J. H. and Seinfeld, J. H.: Chemistry of secondary organic aerosol: Formation and evolution of low-volatility organics in the atmosphere, Atmos. Environ., 42, 3593–3624, https://doi.org/10.1016/j.atmosenv.2008.01.003, 2008.

Kroll, J. H., Ng, N. L., Murphy, S. M., Flagan, R. C., and Seinfeld, J. H.: Secondary organic aerosol formation from isoprene photooxidation under high-NO_x conditions, Geophys. Res. Lett., 32, L18 808, https://doi.org/10.1029/2005GL023637, 2005.

Kroll, J. H., Ng, N. L., Murphy, S. M., Flagan, R. C., and Seinfeld, J. H.: Secondary organic aerosol formation from isoprene photooxidation, Environ. Sci. Technol., 40, 1869–1877, https://doi.org/10.1021/es0524301, 2006.

Kurten, T., Tiusanen, K., Roldin, P., Rissanen, M., Luy, J.-N., Boy, M., Ehn, M., and Donahue, N.: α-Pinene autoxidation products may not have extremely low saturation vapor pressures despite high O:C ratios, J. Phys. Chem. A., 120, 2569–2582, https://doi.org/10.1021/acs.jpca.6b02196, 2016.

Lambe, A. T., Chhabra, P. S., Onasch, T. B., Brune, W. H., Hunter, J. F., Kroll, J. H., Cummings, M. J., Brogan, J. F., Parmar, Y., Worsnop, D. R., Klob, C. E., and Davidovits, P.: Effect of oxidant concentration, exposure time, and seed particles on secondary organic aerosol chemical composition and yield, Atmos. Chem. Phys., 15, 3063–3075, https://doi.org/10.5194/acp-15-3063-2015, 2015.

Lee, B. H., Mohr, C., Lopez-Hilfiker, F. D., Lutz, A., Hallquist, M., Lee, L., Romer, P., Cohen, R. C., Iyer, S., Kurten, T., Hu, W., Day, D. A., Campuzano-Jost, P., Jimenez, J. L., Xu, L., Ng, N. L., Guo, H., Weber, R. J., Wild, R. J., Brown, S. S., Koss, A., de Gouw, J., Olson, K., Goldstein, A. H., Seco, R., Kim, S., McAvey, K., Shepson, P. B., Starn, T., Baumann, K., Edgerton, E. S., Liu, J., Shilling, J. E., Miller, D. O., Brune, W., Schobesberger, S., D'Ambro, E. L., and Thornton, J. A.: Highly functionalized organic nitrates in the southeast United States: Contribution to secondary organic aerosol and reactive nitrogen budgets, Proc. Natl. Acad. Sci., 113, 1516–1521, https://doi.org/10.1073/pnas.1508108113, 2016.

Lee, L., Teng, A. P., Wennberg, P. O., Crounse, J. D., and Cohen, R. C.: On rates and mechanisms of OH and O_3 reactions with isoprene-derived hydroxy nitrates, J. Phys. Chem. A, 118, 1622–1637, https://doi.org/10.1021/jp4107603, 2014.

Lin, Y.-H., Zhang, Z., Docherty, K. S., Zhang, H., Budisulistiorini, S. H., Rubitschun, C. L., Shaw, S. L., Knipping, E. M., Edgerton, E. S., Kleindienst, T. E., Gold, A., and Surratt, J. D.: Isoprene epoxydiols as precursors to secondary organic aerosol formation: acid-catalyzed reactive uptake studies with authentic compounds, Environ. Sci. Technol., 46, 250–258, https://doi.org/10.1021/es202554c, 2012.

Lin, Y.-H., Zhang, H., Pye, H. O. T., Zhang, Z., Marth, W. J., Park, S., Arashiro, M., Cui, T., Budisulistiorini, S. H., Sexton, K. G., Vizuete, W., Xie, Y., Luecken, D. J., Piletic, I. R., Edney, E. O., Bartolotti, L. J., Gold, A., and Surratt, J. D.: Epoxide as a precursor to secondary organic aerosol formation from isoprene photooxidation in the presence of nitrogen oxides, Proc. Natl. Acad. Sci. USA, 110, 6718–6723, https://doi.org/10.1073/pnas.1221150110, 2013.

Loza, C. L., Chhabra, P. S., Yee, L. D., Craven, J. S., Flagan, R. C., and Seinfeld, J. H.: Chemical aging of *m*-xylene secondary organic aerosol: laboratory chamber study, Atmos. Chem. Phys., 12, 151–167, https://doi.org/10.5194/acp-12-151-2012, 2012.

Mai, H. and Flagan, R. C.: Scanning DMA Data Analysis I. Classification Transfer Function, Aerosol Sci. Technol., 52, 1382–1399, https://doi.org/10.1080/02786826.2018.1528005, 2018.

Mai, H., Kong, W., Seinfeld, J. H., and Flagan, R. C.: Scanning DMA Data Analysis II. Integrated DMA-CPC Instrument Response and Data Inversion, Aerosol Sci. Technol., 52, 1400–1414, https://doi.org/10.1080/02786826.2018.1528006, 2018.

Marais, E. A., Jacob, D. J., Jimenez, J. L., Campuzano-Jost, P., Day, D. A., Hu, W., Krechmer, J., Zhu, L., Kim, P. S., Miller, C. C., Fisher, J. A., Travis, K., Yu, K., Hanisco, T. F., Wolfe, G. M., Arkinson, H. L., Pye, H. O. T., Froyd, K. D., Liao, J., and McNeill, V. F.: Aqueous-phase mechanism for secondary organic aerosol formation from isoprene: application to the southeast United States and co-benefit of SO_2 emission controls, Atmos. Chem. Phys., 16, 1603–1618, https://doi.org/10.5194/acp-16-1603-2016, 2016.

Nah, T., McVay, R. C., Pierce, J. R., Seinfeld, J. H., and Ng, N. L.: Constraining uncertainties in particle-wall deposition correction during SOA formation in chamber experiments, Atmos. Chem. Phys., 17, 2297–2310, https://doi.org/10.5194/acp-17-2297-2017, 2017.

Nannoolal, Y., Rarey, J., Ramjugernath, D., and Cordes, W.: Estimation of pure component properties Part 1. Estimation of the normal boiling point of non-electrolyte organic compounds via group contributions and group interactions, Fluid Phase Equilibria, 226, 45–63, https://doi.org/10.1016/j.fluid.2004.09.001, 2004.

Nannoolal, Y., Rarey, J., and Ramjugernath, D.: Estimation of pure component properties Part 3. Estimation of the vapor pressure of non-electrolyte organic compounds via group contributions and group interactions, Fluid Phase Equilibria, 269, 117–133, https://doi.org/10.1016/j.fluid.2008.04.020, 2008.

Ng, N. L., Kroll, J. H., Keywood, M. D., Bahreini, R., Varutbangkul, V., Flagan, R. C., and Seinfeld, J. H.: Contribution of first-versus second-generation products to secondary organic aerosols formed in the oxidation of biogenic hydrocarbons, Environ. Sci. Technol., 40, 2283–2297, https://doi.org/10.1021/es052269u, 2006.

Nguyen, T. B., Roach, P. J., Laskin, J., Laskin, A., and Nizhorodov, S. A.: Effect of humidity on the composition of isoprene photooxidation secondary organic aerosol, Atmos. Chem. Phys., 11, 6931–6944, https://doi.org/10.5194/acp-11-6931-2011, 2011.

Nguyen, T. B., Coggon, M. M., Bates, K. H., Zhang, X., Schwantes, R. H., Schilling, K. A., Loza, C. L., Flagan, R. C., Wennberg, P. O., and Seinfeld, J. H.: Organic aerosol formation from the reactive uptake of isoprene epoxydiols (IEPOX) onto non-acidified inorganic seeds, Atmos. Chem. Phys., 14, 3497–3510, https://doi.org/10.5194/acp-14-3497-2014, 2014a.

Nguyen, T. B., Crounse, J. D., Schwantes, R. H., Teng, A. P., Bates, K. H., Zhang, X., St. Clair, J. M., Brune, W. H., Tyndall, G. S., Keutsch, F. N., Seinfeld, J. H., and Wennberg, P. O.: Overview of the Focused Isoprene eXperiment at the California Institute of Technology (FIXCIT): mechanistic chamber studies on the oxidation of biogenic compounds., Atmos. Chem. Phys., 14, 13 531–13 549, https://doi.org/10.5194/acp-14-13531-2014, 2014b.

Nguyen, T. B., Bates, K. H., Crounse, J. D., Schwantes, R. H., Zhang, X., Kjaergaard, H. G., Surratt, J. D., Lin, P., Laskin, A., Seinfeld, J. H., and Wennberg, P. O.: Mechanism of the hydroxyl radical oxidation of methacryloyl peroxynitrate (MPAN) and its pathway toward secondary organic aerosol formation in the atmosphere, Phys. Chem. Chem. Phys., 17, 17 914–17 926, https://doi.org/10.1039/C5CP02001H, 2015.

Nielsen, O. J., Sidebottom, H. W., Donlon, M., and Treacy, J.: Rate constants for the gas-phase reactions of OH radicals and Cl atoms with n-alkyl nitrites at atmospheric pressure and 298 K, Int. J. Chem. Kinet., 23, 1095–1109, https://doi.org/10.1002/kin.550231204, 1991.

Orlando, J. J. and Tyndall, G. S.: Laboratory studies of organic peroxy radical chemistry: an overview with emphasis on recent issues of atmospheric significance, Chem. Soc. Rev., 41, 6294–6317, https://doi.org/10.1039/C2CS35166H, 2012.

Orlando, J. J., Tyndall, G. S., and Paulson, S. E.: Mechanism of the OH-initiated oxidation of methacrolein, Geophys. Res. Lett., 26, 2191–2194, https://doi.org/10.1029/1999GL900453, 1999.

Orlando, J. J., Tyndall, G. S., Bertman, S. B., Chen, W., and Burkholder, J. B.: Rate coefficient for the reaction of OH with $CH_2{=}C(CH_3)C(O)OONO_2$ (MPAN), Atmos. Environ., 36, 1895–1900, https://doi.org/10.1016/S1352-2310(02)00090-0, 2002.

Orlando, J. J., Tyndall, G. S., and Wallington, T. J.: The atmospheric chemistry of alkoxy radicals, Chem. Rev., 103, 4657–4689, https://doi.org/10.1021/cr020527p, 2003.

Pajunoja, A., Hu, W., Leong, Y. J., Taylor, N. F., Miettinen, P., Palm, B. B., Mikkonen, S., Collins, D. R., Jimenez, J. L., and Virtanen, A.: Phase state of ambient aerosol linked with water uptake and chemical aging in the southeastern US, Atmos. Chem. Phys., 16, 11 163–11 176, https://doi.org/10.5194/acp-16-11163-2016, 2016.

Pandis, S. N., Paulson, S. E., Seinfeld, J. H., and Flagan, R. C.: Aerosol formation in the photooxidation of isoprene and β-pinene, Atmos. Environ., 25A, 997–1008, https://doi.org/10.1016/0960-1686(91)90141-S, 1991.

Paulot, F., Crounse, J. D., Kjaergaard, H. G., Kurten, A., St. Clair, J. M., Seinfeld, J. H., and Wennberg, P. O.: Unexpected epoxide formation in the gas-phase photooxidation of isoprene, Science, 325, 730–733, https://doi.org/10.1126/science.1172910, 2009.

Peeters, J., Nguyen, T. L., and Vereecken, L.: HO_x radical regeneration in the oxidation of isoprene, Phys. Chem. Chem. Phys., 11, 5935–5939, https://doi.org/10.1039/b908511d, 2009.

Peeters, J., Muller, J.-F., Stavrakou, T., and Nguyen, V.: Hydroxyl radical recycling in isoprene oxidation driven by hydrogen bonding and hydrogen tunneling: The upgraded LIM1 mechanism, J. Phys. Chem. A., 118, 8625–8643, https://doi.org/10.1021/jp5033146, 2014.

Pieber, S. M., Haddad, I. E., Slowik, J. G., Canagaratna, M. R., Jayne, J. T., Platt, S. M., Bozzetti, C., Daellenbach, K. S., Frohlich, R., Vlachou, A., Klein, F., Dommen, J., Miljevic, B., Jimenez, J. L., Worsnop, D. R., Baltensperger, U., and Prevot, A. S. H.: Inorganic salt interference on CO_2^+ in Aerodyne AMS and ACSM organic aerosol composition studies, Environ. Sci. Technol., 50, 10 494–10 503, https://doi.org/10.1021/acs.est.6b01035, 2016.

Pierce, J. R., Engelhart, G. J., Hildebrandt, L., Weitkamp, E. A., Pathak, R. K., Donahue, N. M., Robinson, A. L., Adams, P. J., and Pandis, S. N.: Constraining particle evolution from wall losses, coagulation, and condensation-evaporation in smog-chamber experiments: Optimal estimation based on size distribution measurements, Aerosol Sci. Technol., 42, 1001–1015, https://doi.org/10.1080/02786820802389251, 2008.

Praske, E., Crounse, J. D., Bates, K. H., Kurten, T., Kjaergaard, H. G., and Wennberg, P. O.: Atmospheric fate of methyl vinyl ketone: Peroxy radical reactions with NO and HO_2, J. Phys. Chem. A., 119, 4562–4572, https://doi.org/10.1021/jp5107058, 2015.

Ribeiro, P. A., Raposo, M., Marat-Mendes, J. N., and Giacometti, J. A.: Constant-current corona charging of biaxially stretched PVDF films in humidity-controlled atmospheres., IEEE Transactions on Electrical Insulation, 27, 744–750, https://doi.org/10.1109/14.155791, 1992.

Sanchez, D., Jeong, D., Seco, R., Wrangham, I., Park, J.-H., Brune, W., Koss, A., Gilman, J., de Gouw, J., Misztal, P., Goldstein, A., Baumann, K., Wennberg, P. O., Keutsch, F. N., Guenther, A., and Kim, S.: Intercomparison of OH and OH reactivity measurements in a high isoprene and low NO environment during the Southern Oxidant and Aerosol Study (SOAS), Atmos. Environ., 174, 227–236, https://doi.org/10.1016/j.atmosenv.2017.10.056, 2018.

Sander, R.: Compilation of henry's law constants (version 4.0) for water as solvent, Atmos. Chem. Phys., 15, 4399–4981, https://doi.org/10.5194/acp-15-4399-2015, 2015.

Saunders, S. M., Jenkin, M. E., Derwent, R. G., and Pilling, M. J.: Protocol for the development of the Master Chemical Mechanism, MCM v3 (Part A): tropospheric degradation of non-aromatic volatile organic compounds, Atmos. Chem. Phys., 3, 161–180, https://doi.org/10.5194/acp-3-161-2003, 2003.

Schwantes, R. H., Schilling, K. A., McVay, R. C., Lignell, H., Coggon, M. M., Zhang, X., Wennberg, P. O., and Seinfeld, J. H.: Formation of highly oxygenated low-volatility products from cresol oxidation, Atmos. Chem. Phys., 17, 3453–3474, https://doi.org/10.5194/acp-17-3453-2017, 2017.

Seinfeld, J. H. and Pandis, S. N.: Atmospheric Chemistry and Physics: From Air Pollution to Climate Change, John Wiley & Sons, Inc., Hoboken, New Jersey, 3 edn., 2016.

Sharpe, S. W., Johnson, T. J., Sams, R. L., Chu, P. M., Rhoderick, G. C., and Johnson, P. A.: Gas-phase databases for quantitative infrared spectroscopy, composite spectrum for ISOPREN_25T (Ver 1.0, Oct, 01) and composite spectrum for ISOBUTENAL_25T (Ver 1.0, Dec, 04), Appl. Spectrosc., 58, 1452–1461, https://doi.org/10.1366/0003702042641281, 2004.

Sjogren, S., Gysel, M., Weingartner, E., Baltensperger, U., Cubison, M., Coe, H., Zardini, A., Marcolli, C., Krieger, U., and Peter, T.: Hygroscopic growth and water uptake kinetics of two-phase aerosol particles consisting of ammonium sulfate, adipic and humic acid mixtures, Aerosol Science, 38, 157–171, https://doi.org/10.1016/j.jaerosci.2006.11.005, 2007.

St. Clair, J. M., McCabe, D. C., Crounse, J. D., Steiner, U., and Wennberg, P. O.: Chemical ionization tandem mass spectrometer for the in situ measurement of methyl hydrogen peroxide, Rev. Sci. Instrum., 81, 094 102, https://doi.org/10.1063/1.3480552, 2010.

Stadtler, S., Kühn, T., Schröder, S., Taraborrelli, D., Schultz, M. G., and Kokkola, H.: Isoprene-derived secondary organic aerosol in the global aerosol–chemistry–climate model ECHAM6.3.0–HAM2.3–MOZ1.0, Geosci. Model Dev., 11, 3235–3260, https://doi.org/10.5194/gmd-11-3235-2018, 2018.

Sunol, A. M., Charan, S. M., and Seinfeld, J. H.: Computational simulation of the dynamics of secondary organic aerosol formation in an environmental chamber, Aerosol Sci. Technol., 52, 470–482, https://doi.org/10.1080/02786826.2018.1427209, 2018.

Surratt, J. D., Chan, a. W. H., Eddingsaas, N. C., Chan, M. N., Loza, C. L., Kwan, a. J., Hersey, S. P., Flagan, R. C., Wennberg, P. O., and Seinfeld, J. H.: Reactive intermediates revealed in secondary organic aerosol formation from isoprene, Proc. Natl. Acad. Sci. U. S. A., 107, 6640–6645, https://doi.org/10.1073/pnas.0911114107, 2010.

Taylor, W. D., Allston, T. D., Moscato, M. J., Fazekas, G. B., Kozlowski, R., and Takacs, G. A.: Atmospheric photo-dissociation lifetimes for nitromethane, methyl nitrite, and methyl nitrate, Int. J. Chem. Kinet, 12, 231–240, https://doi.org/10.1002/kin.550120404, 1980.

Teng, A. P., Crounse, J. D., and Wennberg, P. O.: Isoprene peroxy radical dynamics, J. Am. Chem. Soc., 139, 5367–5377, https://doi.org/10.1021/jacs.6b12838, 2017.

Wennberg, P., Bates, K. H., Crounse, J. D., Dodson, L. G., McVay, R. C., Mertens, L. A., Nguyen, T. B., Praske, E., Schwantes, R. H., Smarte, M. D., St Clair, J. M., Teng, A. P., Zhang, X., and Seinfeld, J. H.: Gas-Phase Reactions of Isoprene and Its Major Oxidation Products, Chem. Rev., 118, 3337–3390, https://doi.org/10.1021/acs.chemrev.7b00439, 2018.

Wennberg, P. O.: Let's abandon the high NO_x and low NO_x terminology, IGACnews, 50, 3–4, 2013.

Xiong, F., McAvey, K. M., Pratt, K. A., Groff, C. J., Hostetler, M. A., Lipton, M. A., Starn, T. K., Seeley, J. V., Bertman, S. B., Teng, A. P., Crounse, J. D., Nguyen, T. B., Wennberg, P. O., Misztal, P. K., Goldstein, A. H., Guenther, A. B., Koss, A. R., Olson, K. F., de Gouw, J. A., Baumann, K., Edgerton, E. S., Feiner, P. A., Zhang, L., Miller, D. O., Brune, W. H., and Shepson, P. B.: Observation of isoprene hydroxynitrates in the southeastern United States and implications for the fate of NO_x, Atmos. Chem. Phys., 15, 11 257–11 272, https://doi.org/10.5194/acp-15-11257-2015, 2015.

Xu, L., Kollman, M. S., Song, C., Shilling, J. E., and Ng, N. L.: Effects of NO_x on the volatility of secondary organic aerosol from isoprene photooxidation, Environ. Sci. Tech., 48, 2253–2262, https://doi.org/10.1021/es404842g, 2014.

Zhang, H., Surratt, J. D., Lin, Y. H., Bapat, J., and Kamens, R. M.: Effect of relative humidity on SOA formation from isoprene/NO photooxidation: Enhancement of 2-methylglyceric acid and its corresponding oligoesters under dry conditions, Atmos. Chem. Phys., 11, 6411–6424, https://doi.org/10.5194/acp-11-6411-2011, 2011.

Zhang, H., Lin, Y. H., Zhang, Z., Zhang, X., Shaw, S. L., Knipping, E. M., Weber, R. J., Gold, A., Kamens, R. M., and Surratt, J. D.: Secondary organic aerosol formation from methacrolein photooxidation: roles of NO_x level, relative humidity and aerosol acidity, Environ. Chem., 9, 247–262, https://doi.org/10.1071/EN12004, 2012.

Zhang, H., Yee, L. D., Lee, B. H., Curtis, M. P., Worton, D. R., Isaacman-VanWertz, G., Offenberg, J. H., Lewandowski, M., Kleindienst, T. E., Beaver, M. R., Holder, A. L., Lonneman, W. A., Docherty, K. S., Jaoui, M., Pye, H. O. T., Hu, W., Day, D. A., Campuzano-Jost, P., Jimenez, J. L., Guo, H., Weber, R. J., de Gouw, J., Koss, A. R., Edgerton, E. S., Brune, W., Mohr, C., Lopez-Hilfiker, F. D., Lutz, A., Kreisberg, N. M., Spielman, S. R., Hering, S. V., Wilson, K. R., Thornton, J. A., and Goldstein, A. H.: Monoterpenes are the largest source of summertime organic aerosol in the southeastern United States, PNAS, 115, 2038–2043, https://doi.org/10.1073/pnas.1717513115, 2018.

Zhang, Q., Jimenez, J. L., Canagaratna, M. R., Allan, J. D., Coe, H., Ulbrich, I., Alfarra, M. R., Takami, A., Middlebrook, A. M., Sun, Y. L., Dzepina, K., Dunlea, E., Docherty, K., DeCarlo, P. F., Salcedo, D., Onasch, T., Jayne, J. T., Miyoshi, T., Shimono, A., Hatakeyama, S., Takegawa, N., Kondo, Y., Schneider, J., Drewnick, F., Borrmann, S., Weimer, S., Demerjian, K., Williams, P., Bower, K., Bahreini, R., Cottrell, L., Griffin, R. J., Rautiainen, J., Sun, J. Y., Zhang, Y. M., and Worsnop, D. R.: Ubiquity and dominance of oxygenated species in organic aerosols in anthropogenically-influenced Northern Hemisphere midlatitudes, Geophys. Res. Lett., 34, L13 801, https://doi.org/10.1029/2007GL029979, 2007.

Zhang, X., Cappa, C. D., Jather, S. H., McVay, R. C., Ensberg, J. J., Kleeman, M. J., and Seinfeld, J. H.: Influence of vapor wall loss in laboratory chambers on yields of secondary organic aerosol, P. Natl. Acad. Sci. USA, 111, 5802–5807, https://doi.org/10.1073/pnas.1404727111, 2014.

Zhang, X., Schwantes, R. H., McVay, R. C., Lignell, H., Coggon, M. M., Flagan, R. C., and Seinfeld, J. H.: Vapor wall deposition in Teflon chambers, Atmos. Chem. Phys., 15, 4197–4214, https://doi.org/10.5194/acp-15-4197-2015, 2015.

Supplement to Low-volatility compounds contribute significantly to isoprene SOA under high-NO_x conditions

Rebecca H. Schwantes[1,5], Sophia M. Charan[2], Kelvin H. Bates[2,6], Yuanlong Huang[1], Tran B. Nguyen[3], Huajun Mai[1], Weimeng Kong[2], Richard C. Flagan[2], and John H. Seinfeld[2,4]

[1]Division of Geological and Planetary Sciences, California Institute of Technology, 1200 East California Boulevard, Pasadena, California 91125, United States
[2]Division of Chemistry and Chemical Engineering, California Institute of Technology, 1200 East California Boulevard, Pasadena, California 91125, United States
[3]Department of Environmental Toxicology, University of California - Davis, Davis, California 95616, United States
[4]Division of Engineering and Applied Science, California Institute of Technology, Pasadena, California 91125, USA
[5]Current Affiliation: National Center for Atmospheric Research, Boulder, Colorado, 80307, USA
[6]Current Affiliation: Faculty of Arts and Sciences, Harvard University, Cambridge, MA 02138, USA

Correspondence to: Rebecca H. Schwantes (rschwant@ucar.edu)

S1 Comparisons between Kinetic Model and Experimental Results

Table S1: Additional reactions and reaction rates included in the kinetic model, but not in MCM v3.3.1

Reaction	**Rate (cm^3 $molecule^{-1}$ s^{-1})**	**Source**
$CH_3ONO + h\nu \rightarrow HCHO + HO_2 + NO$	(1.4-2.3) x 10^{-4} s^{-1}	NA [a]
$CH_3ONO + OH \rightarrow H_2O + HCHO + NO$	3 x 10^{-13} * 0.5	See note [b]
$CH_3ONO + OH \rightarrow HCHO + HO_2 + HONO$	3 x 10^{-13} * 0.5	See note [b]
$HO_2 + NO_2 \rightarrow HONO$	5 x 10^{-16}	JPL
$HO_2 + HCHO \rightarrow HOCH_2OO$	9.7 x 10^{-15} exp(625/T)	IUPAC
$HOCH_2OO \rightarrow HO_2 + HCHO$	2.4 x 10^{12} exp(-7000/T) s^{-1}	IUPAC
$HOCH_2OO + HO_2 \rightarrow HMHP$	5.6 x 10^{-15} exp(2300/T) * 0.5	IUPAC
$HOCH_2OO + HO_2 \rightarrow HCOOH$	5.6 x 10^{-15} exp(2300/T) * 0.3	IUPAC
$HOCH_2OO + HO_2 \rightarrow HCOOH + HO_2 + OH$	5.60 x 10^{-15} exp(2300/T) * 0.2	IUPAC
$HOCH_2OO \rightarrow HCOOH$	7 x 10^{-13} * RO_2	IUPAC
$HOCH_2OO \rightarrow CH_2(OH)_2$	7 x 10^{-13} * RO_2	IUPAC
$HOCH_2OO \rightarrow HCOOH + HO_2$	5.50 x 10^{-12} * 2 * RO_2	IUPAC
$HOCH_2OO + NO \rightarrow HCOOH + HO_2 + NO_2$	5.60 x 10^{-12}	IUPAC
$HMHP + OH \rightarrow HOCH_2OO$	3.1 x 10^{-11} * 0.12	Jenkin (2007)
$HMHP + OH \rightarrow HCOOH + OH$	3.1 x 10^{-11} * 0.88	Jenkin (2007)
$HMHP + h\nu \rightarrow HCOOH + HO_2 + OH$	2.0 x 10^{-7} s^{-1}	JPL
$OH + OH \rightarrow O$	6.2 x 10^{-14} $(T/298)^{2.6}$ exp(945/T)	IUPAC
$OH + NO_2 + M \rightarrow HOONO + M$	Termolecular	IUPAC
$HOONO + M \rightarrow OH + NO_2 + M$	Termolecular	IUPAC
$OH + OH + M \rightarrow H_2O_2 + M$	Termolecular	IUPAC
$OH + NO_2 + M \rightarrow HNO_3 + M$	**Termolecular**	IUPAC
$NO_2 + O_3 \rightarrow NO_3$	**1.4 x 10^{-13} exp(-2470/T)*0.97**	Cantrell (1985)
$NO_2 + O_3 \rightarrow NO$	**1.4 x 10^{-13} exp(-2470/T)*0.03**	Cantrell (1985)
$NO_2 + NO_2 + M \rightarrow N_2O_4 + M$	Termolecular	IUPAC
$N_2O_4 + M \rightarrow NO_2 + NO_2 + M$	Termolecular	IUPAC
CISOPAO2 + NO → CISOPAO + NO2	**KRO2NO*0.88**	Wennberg (2018)
CISOPAO2 + NO → ISOPANO3	**KRO2NO*0.12**	Wennberg (2018)
ISOPBO2 + NO → ISOPBNO3	**KRO2NO*0.14**	Wennberg (2018)
ISOPBO2 + NO → ISOPBO + NO2	**KRO2NO*0.86**	Wennberg (2018)
CISOPCO2 + NO → CISOPCO + NO2	**KRO2NO*0.88**	Wennberg (2018)

Table S1: Additional reactions and reaction rates included in the kinetic model, but not in MCM v3.3.1

Reaction	**Rate (cm^3 molecule^{-1} s^{-1})**	**Source**
CISOPCO2 + NO → ISOPCNO3	**KRO2NO*0.12**	Wennberg (2018)
ISOPDO2 + NO → ISOPDNO3	**KRO2NO*0.13**	Wennberg (2018)
ISOPDO2 + NO → ISOPDO + NO2	**KRO2NO*0.87**	Wennberg (2018)
ISOPAO2 + NO → ISOPANO3	**KRO2NO*0.12**	Wennberg (2018)
ISOPAO2 + NO → ISOPAO + NO2	**KRO2NO*0.88**	Wennberg (2018)
ISOPCO2 + NO → CISOPCO + NO2	**KRO2NO*0.88**	Wennberg (2018)
ISOPCO2 + NO → ISOPCNO3	**KRO2NO*0.12**	Wennberg (2018)
OH + ISOPBNO3 → INB1O2	**3.0 x 10^{-11}*0.75**	Wennberg (2018)
OH + ISOPBNO3 → INB2O2	**3.0 x 10^{-11}*0.25**	Wennberg (2018)
OH + ISOPCNO3 → INCO2	**8.0 x 10^{-11}**	Wennberg (2018)
OH + ISOPDNO3 → INDO2	**4.15 x 10^{-11}*0.9**	Wennberg (2018)
OH + ISOPDNO3 → IND1O2	**4.15 x 10^{-11}*0.1**	Wennberg (2018)
IND1O2 + HO2 → INDOOH	**KRO2HO2*0.706**	Wennberg (2018)
IND1O2 + NO → INB1NO3	**KRO2NO*0.104**	Wennberg (2018)
IND1O2 + NO → IND1O + NO2	**KRO2NO*0.896**	Wennberg (2018)
IND1O2 + NO3 → IND1O + NO2	**KRO2NO3**	Wennberg (2018)
IND1O2 → IND1O	**8.00 x 10^{-13}*0.8*RO_2**	Wennberg (2018)
IND1O2 → INDOH	**8.00 x 10^{-13}*0.2*RO_2**	Wennberg (2018)
IND1O → C58ANO3 + HO2	**KDEC**	Wennberg (2018)
CISOPAO → HC4CCHO + HO2	**KDEC**	Wennberg (2018)
CISOPCO → HC4ACHO + HO2	**KDEC**	Wennberg (2018)
ISOPAO → HC4CCHO	**KDEC**	Wennberg (2018)
OH + MPAN → ACETOL + CO + NO3	**2.9 x 10^{-11}*0.25**	Wennberg (2018)
OH + MPAN → HMML + NO3	**2.9 x 10^{-11}*0.75**	Wennberg (2018)

Notes: HMHP = $CH_2(OH)(OOH)$ and all other names are identical to those used in MCMv3.3.1. All reactions in bold were already included in MCM v3.3.1, but have been revised for this work based on the source listed and as described in the text. ^{a} CH_3ONO photolysis was calculated from the GC-FID measurements. ^{b} Nielsen (1991), Cox (1980), and Jenkin (1988).

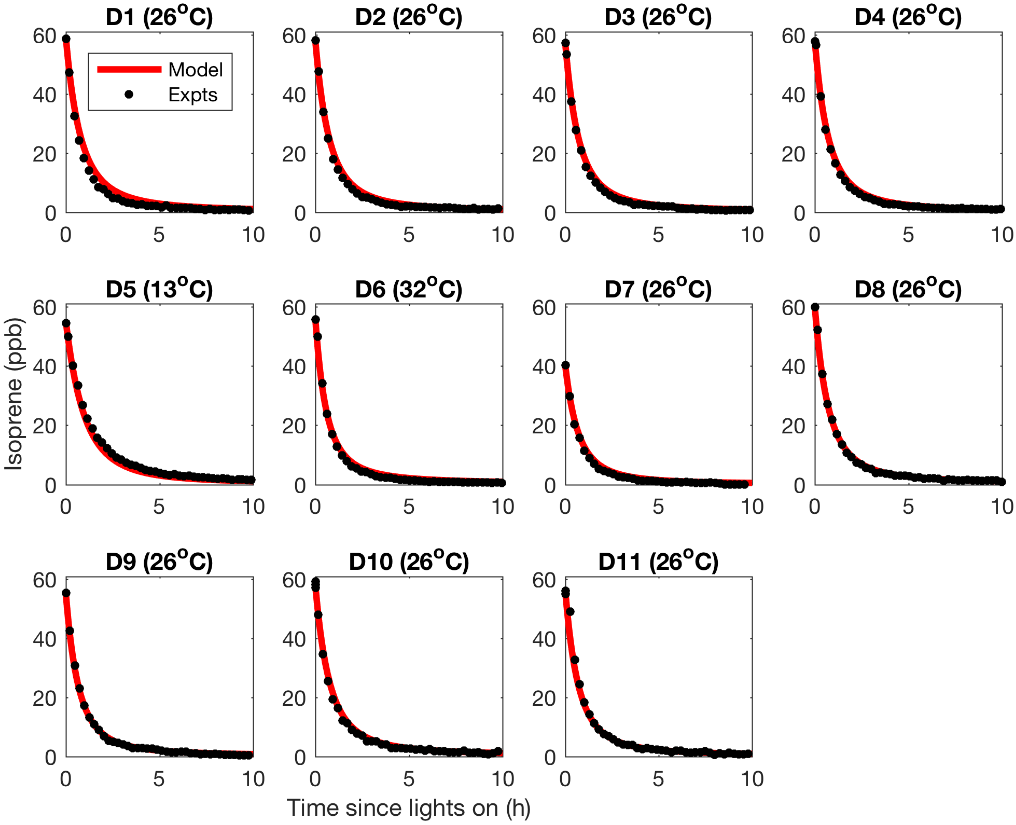

Figure S1. Isoprene observed (**black**) compared to simulated (**red**) for all LV (low volatility) pathway experiments.

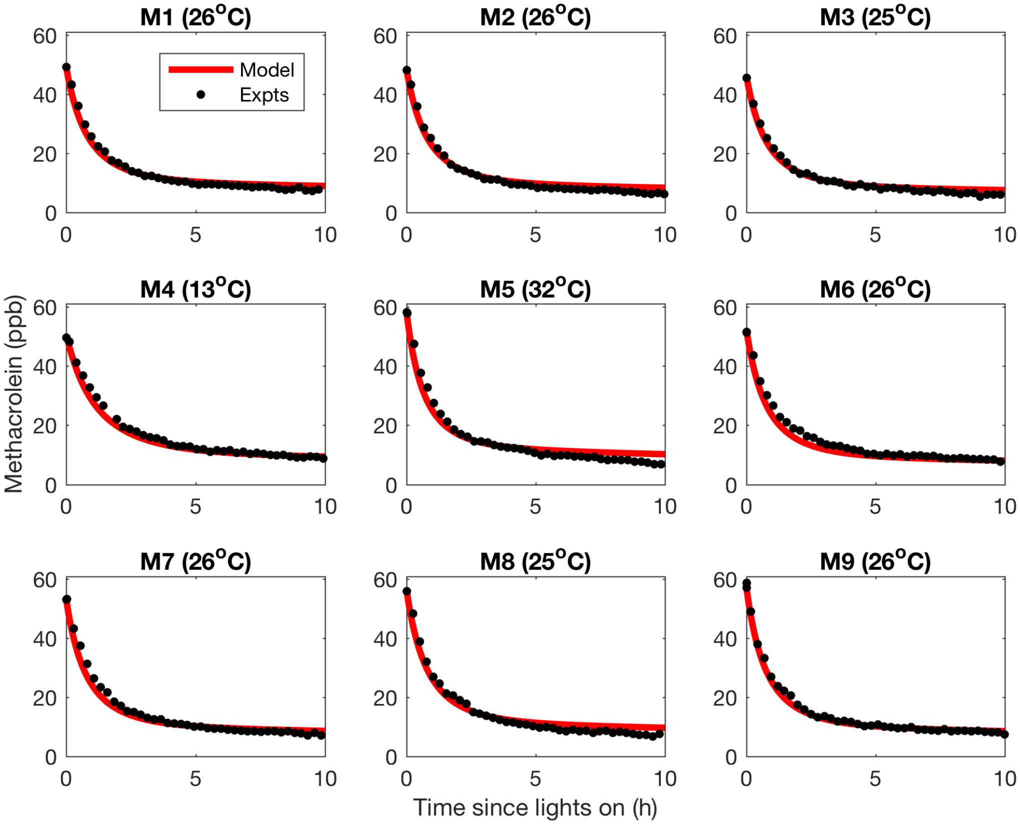

Figure S2. Methacrolein observed (**black**) compared to simulated (**red**) for all 2MGA (2-methyl glyceric acid and oligomers) pathway experiments.

As shown in Figure S3, NO_2 and NO compare reasonably well with the model in both the LV and 2MGA experiments. NO is measured using a Teledyne NO_x analyzer (T200) and NO_2 is measured using a luminol NO_2/acyl peroxynitrate analyzer developed by Fitz Aerometric Technologies. There is a large model bias in the NO_2/NO ratio (Figure S3), but this bias is largely caused by differences of only several ppb in the NO level between the model and observations. NO/NO_x and NO_2/NO_x are much more similar between the model and observations and are a more relevant metric for determining MPAN formation at high NO_2/NO ratios. Remaining biases are likely caused by unknown measurement interferences or unaccounted for wall deposition of NO_x reservoir species (e.g., N_2O_5, HNO_3, HO_2NO_2, etc.) in the kinetic model.

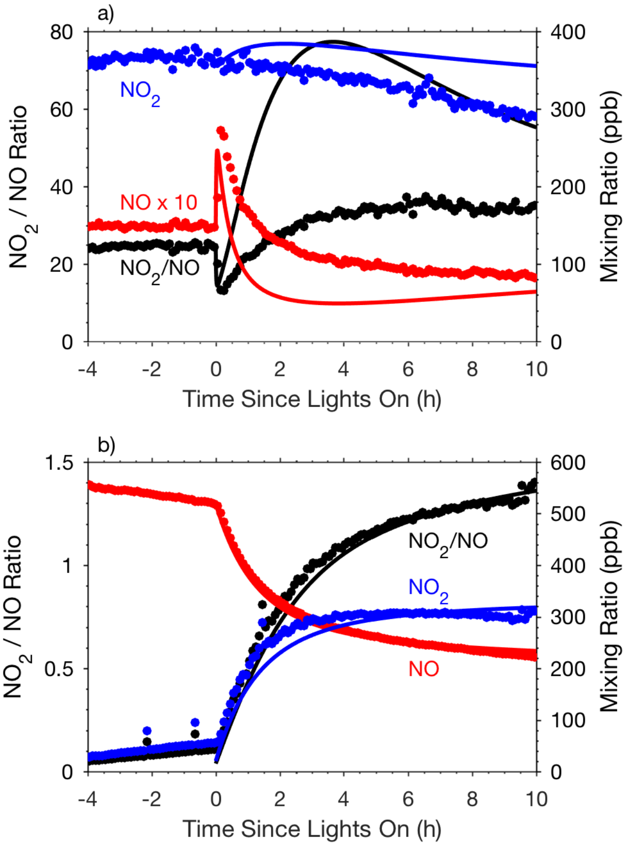

Figure S3. NO_2 (**blue**, right axis), NO (**red**, right axis), and NO_2 / NO ratio (**black**, left axis) for an example 2MGA experiment (M2, panel a) and an example LV experiment (D8, panel b) comparing experimental data (markers) and kinetic model results (lines). Note: in panel a, the NO mixing ratio is multiplied by 10 for ease of viewing.

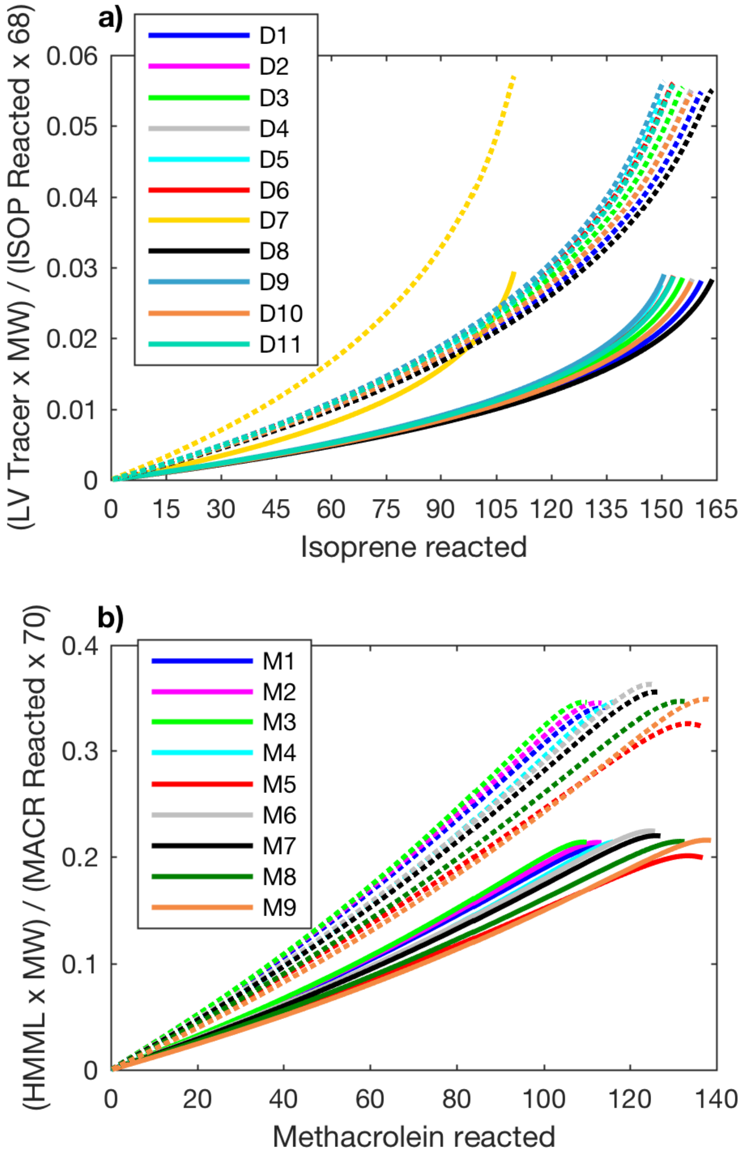

Figure S4. Simulated known gas-phase SOA precursors ~~converted to~~ divided by VOC reacted as a proxy of SOA mass yield for all LV pathway experiments (panel a) and all 2MGA pathway experiments (panel b). The kinetic model confirms experimental conditions were similar enough to produce relatively consistent yields of known gas-phase SOA precursors for both systems. ~~The dinitrate and HMML~~ In panel a, all LV pathway gas-phase tracers ~~were added into the chemical mechanism~~ listed in Table S2 with ~~no loss pathways (i.e, OH oxidation). OH oxidation of~~ an estimated fraction in the ~~dinitrates~~ particle-phase > 65% at 299 K are included as solid lines and > 5% as dashed lines. In panel b, HMML gas-phase SOA precursor is ~~slow enough that this has a minor impact~~ converted only based on the ~~results~~mass of HMML itself - 102 g/mol (solid lines) and 2MGA-nitrate mass - 165 g/mol (dashed lines). ~~The dinitrate tracer includes~~ In both panels for all ~~dihydroxy dinitrates from isoprene and~~ cases, the ~~2-MGA tracer includes HMML + MAE~~F_P values calculated in Table S2 are not used, so in this proxy for SOA yield all simulated gas-phase SOA precursors are assumed to exist 100% in the particle-phase.

Table S2: Estimated saturation mass concentration (C*) and fraction in particle phase (F_P) for organic nitrates and dinitrates in MCM v3.3.1.

MCM Name	**Structure**	**C*(299K)**	**C*(286K)**	**C*(305K)**	**F_P(299K)**	**F_P(286K)**	**F_P(305K)**
IVOC at 299 K							
ISOP34NO3	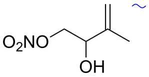	6.59E+05	1.99E+05	1.09E+06	0	0	0
ISOPDNO3	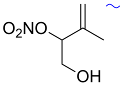	4.47E+05	1.32E+05	7.47E+05	0	0	0
ISOPBNO3	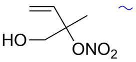	4.47E+05	1.32E+05	7.47E+05	0	0	0
ISOPCNO3	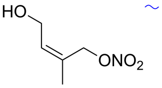	2.28E+05	6.40E+04	3.89E+05	0	0	0
ISOPANO3	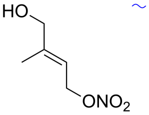	2.28E+05	6.40E+04	3.89E+05	0	0	0
MACRNB	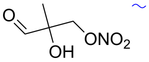	1.90E+05	5.15E+04	3.29E+05	0	0	0
HMVKANO3	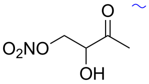	9.35E+04	2.46E+04	1.64E+05	0	0.001	0
MACRNO3	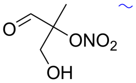	4.62E+04	1.13E+04	8.36E+04	0.001	0.002	0
MVKNO3	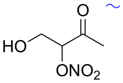	3.72E+04	9.17E+03	6.70E+04	0.001	0.002	0
C530NO3	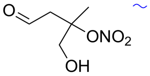	2.64E+04	6.16E+03	4.87E+04	0.001	0.004	0
C51NO3	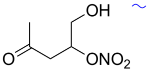	2.14E+04	5.03E+03	3.94E+04	0.001	0.004	0.001
C47CHO	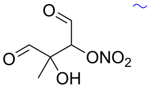	3.06E+03	5.82E+02	6.14E+03	0.009	0.038	0.004

Table S2: Estimated saturation mass concentration (C*) and fraction in particle phase (F_P) for organic nitrates and dinitrates in MCM v3.3.1.

MCM Name	**Structure**	**C*(299K)**	**C*(286K)**	**C*(305K)**	**F_P(299K)**	**F_P(286K)**	**F_P(305K)**
C4M2ALOHNO3	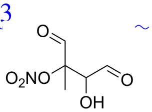	1.85E+03	3.39E+02	3.79E+03	0.014	0.063	0.006
C58ANO3	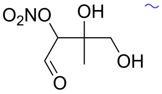	4.36E+02	7.01E+01	9.42E+02	0.059	0.245	0.025
INDHCHO	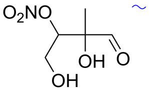	4.36E+02	7.01E+01	9.42E+02	0.059	0.245	0.025
INCNCHO	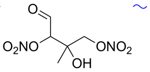	3.05E+02	4.68E+01	6.70E+02	0.082	0.327	0.034
INCCO	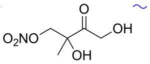	3.04E+02	4.82E+01	6.59E+02	0.082	0.32	0.035
SVOC at 299 K							
C58NO3	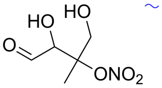	2.56E+02	3.93E+01	5.63E+02	0.096	0.366	0.041
C57NO3	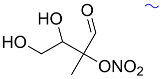	2.56E+02	3.93E+01	5.63E+02	0.096	0.366	0.041
INANCHO	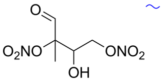	1.86E+02	2.74E+01	4.16E+02	0.128	0.453	0.054
INB1NACHO	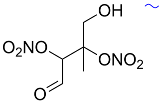	1.31E+02	1.89E+01	2.95E+02	0.172	0.546	0.075
INB1NBCHO	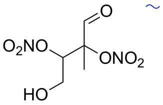	1.31E+02	1.89E+01	2.95E+02	0.172	0.546	0.075
INANCO	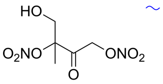	1.05E+02	1.51E+01	2.37E+02	0.206	0.601	0.092

Table S2: Estimated saturation mass concentration (C*) and fraction in particle phase (F_P) for organic nitrates and dinitrates in MCM v3.3.1.

MCM Name	**Structure**	**C*(299K)**	**C*(286K)**	**C*(305K)**	**F_P(299K)**	**F_P(286K)**	**F_P(305K)**
HMVKNO3	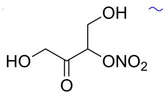	4.61E+01	6.33E+00	1.06E+02	0.371	0.782	0.183
INCNO3	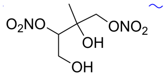	1.32E+01	1.53E+00	3.27E+01	0.673	0.937	0.422
INANO3	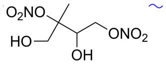	7.67E+00	8.50E-01	1.93E+01	0.78	0.964	0.552
INB1NO3	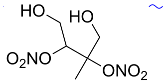	5.23E+00	5.66E-01	1.33E+01	0.838	0.976	0.642

Notes: C* is the saturation mass concentration in µg cm $^{-3}$ and F_P is the fraction of a compound estimated to be present in the particle phase.

In Table S2, vapor pressure is estimated using the vapor pressure and boiling point estimations from Nannoolal et al. (2004, 2008) using the online calculator located at: http://www.aim.env.uea.ac.uk/aim/ddbst/pcalc_main.php. The saturation mass concentration (C*) is calculated using the equation: C* = P^0 γ MW /(RT) where P^0 is the vapor pressure, γ is the activity coefficient, MW is the molecular weight, R is the gas constant, and T is the temperature (Seinfeld and Pandis, 2016). Here the activity coefficient (γ) is unknown and so assumed to be 1. The amount of each compound in the particle phase (F_P) is estimated using the equation: $F_P = (1 + C*/C_{OA})^{-1}$ where C_{OA} is the concentration of the organic aerosol (Seinfeld and Pandis, 2016). The reported F_P in Table S2 uses the measured 1 hr average C_{OA} after 10 hr of photooxidation - 27.16, 22.71, 23.87 µg cm $^{-3}$ for experiments D3 (299 K), D5 (286 K), and D6 (305 K), respectively.

S2 Corrections for Particle Coagulation and Particle Wall Deposition

For each experiment, after all gases and particles were injected into the chamber, purified air was added to facilitate mixing. Photooxidation was delayed by 4 h, during which particle wall deposition was measured. The first 0.5 h of this 4 h period was not used in the particle wall deposition calculation to ensure that air currents and particles/gases in the chamber had stabilized. A numerical model, similar to that reported by Nah et al. (2017), Sunol et al. (2018), and Charan et al. (2018) was used to simulate Brownian diffusion, particle settling, and electrostatic effects. The numerical model based on the aerosol dynamic equation (e.g., Sunol et al. (2018)) assumes $\beta(D_p,t)$ follows the Crump and Seinfeld (1981) equation for a spherical chamber. Prior to injection, all ammonium sulfate particles were passed through a soft x-ray source (TSI Model 3088) in order to impart a consistent initial charge distribution with a net charge of zero. For the particle coagulation/wall deposition correction, the initial charge distribution was assumed to be that computed by Leppa et al. (2017), which is an update to Lopez-Yglesias and Flagan (2013) and Wiedensohler (1988) and consistent with the charge distribution assumed in the DMA inversion (Section 2.2 of the main text). Only charges from -8 to 8 are considered, which is sufficient for the particles used in this study, which have a diameter range of 30 - 800 nm. All particles measured by the DMA were grouped into 15 size bins. The DMA collects data across 390 size bins, but reducing the size bin number decreased the analysis uncertainty by increasing the number of particles per size bin. The only unknown parameters in the numerical model then become the mean electrostatic field experienced within the chamber ($\bar{E}$) and the chamber eddy diffusion coefficient (k_e). The numerical model determines k_e and $\bar{E}$ by comparing the observed particle dynamics to that simulated and minimizing the optimization function J.

$$J = \int_0^{t_{final}} \sum_{D_p} \left(\left(\sum_{charges} N(D_p,t;ke,\bar{E})_{simulated} - N(Dp,t)_{observed} \right)^2 \frac{N(D_p,t)_{observed}}{\sum_{D_p} N(D_p,t)_{observed}} \right) dt \qquad (1)$$

The particle wall deposition coefficients ($\beta(D_p,t)$) can then be extrapolated from k_e and $\bar{E}$. Tabulated k_e and $\bar{E}$ values for all experiments are provided in Table ~~S1~~S3. Only experiments with an inferred chamber electric field within the range verified by the control experiments (i.e., $\bar{E}$ value < 15.7 V cm^{-1}) are reported. This consequently also removes experiments with abnormally high k_e values.

Table S3. Optimized mean electrostatic field experienced within the chamber ($\bar{E}$) and the eddy diffusion coefficient (k_e) for all experiments.

Experiment #	k_e (s^{-1})	$\bar{E}$ (V cm^{-1})
Control Dry Experiments		
C1	0.05	5.1
C2	0.10	8.9
C3	0.06	7.0
C4	0.21	15.7
Control Humid Experiments		
C5	0.07	7.9
C6	0.02	5.8
C7	0.11	11.8
C8	0.15	15.3
C9	0.31	20.9
Experiments optimized for LV pathway		
D1	NA	NA
D2	0.03	4.3
D3	0.03	5.6
D4	0.03	6.5
D5	0.27	13.3
D6	0.30	14.2
D7	0.02	4.5
D8	1.48	17.7
D9	1.09	27.6
D10	0.01	2.1
D11	0	0
Experiments optimized for 2MGA pathway		
M1	NA	NA
M2	0.29	11.6
M3	0.16	10.9
M4	0.32	10.6
M5	0.30	12.4
M6	1.02	18.7
M7	0.45	20.5
M8	0.33	19.6
M9	0	0

For experimental conditions, see Table 1 in main text.

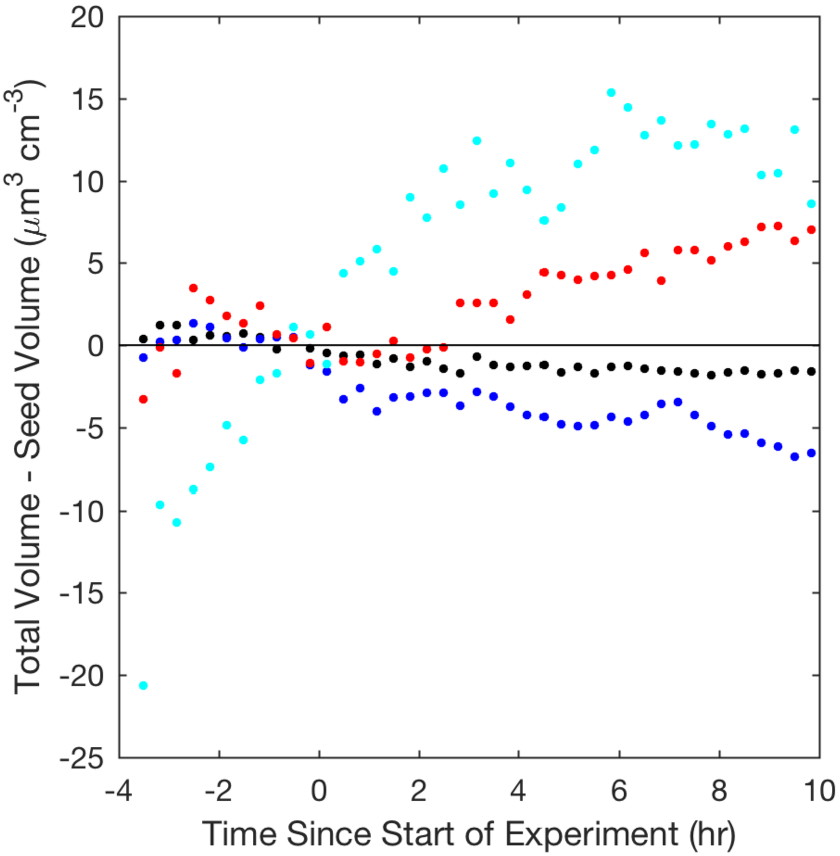

Figure S5. Total volume - seed volume (20 min averages) for the following particle wall deposition control experiments: C1 (V = 37 $\mu m^3 cm^{-3}$, ●), C2 (109 $\mu m^3 cm^{-3}$, ●), C3 (183 $\mu m^3 cm^{-3}$, ●), and C4 (375 $\mu m^3 cm^{-3}$, ●), respectively where V = initial corrected particle volume.

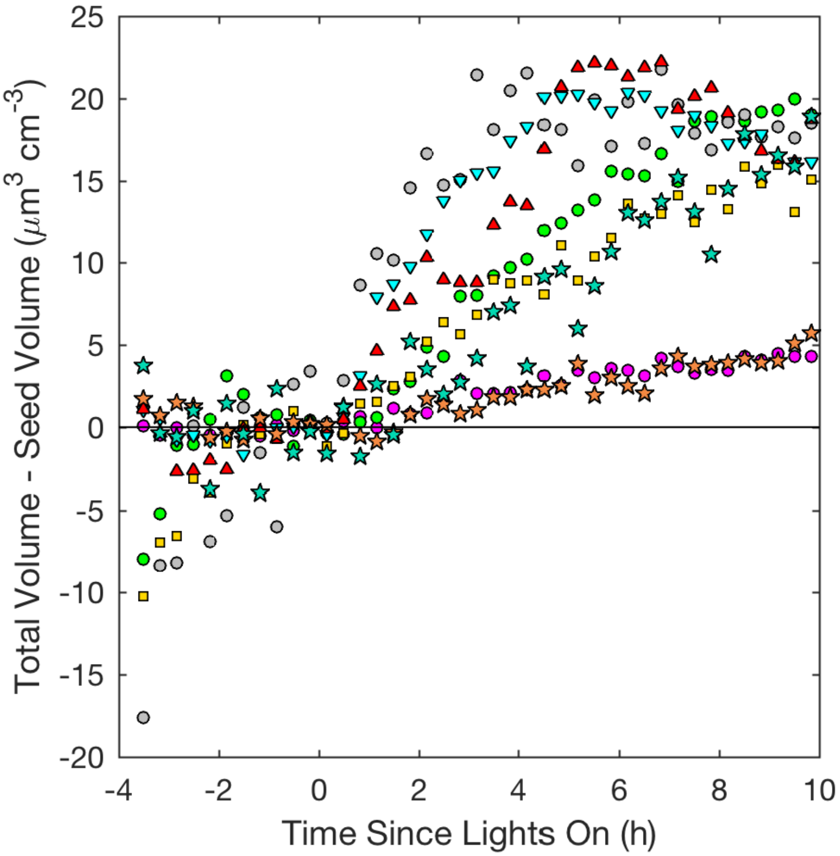

Figure S6. Total volume minus seed volume (20 min averages) as measured by DMA for all isoprene experiments with seed aerosol: seed surface area - D2 (SA = 1170 μm^2 cm^{-3}, ●), D3 (SA = 3420 μm^2 cm^{-3}, ●), & D4 (SA = 5770 μm^{2}cm^{-3}, ●), temperature - D5 (13 °C, ▼) and D6 (32 °C, ▲), isoprene loading - D7 (initial isoprene 110 μg m^{-3}, ♦), and new chamber with less wall charging - D10 (SA = 1580 μm^{2}cm^{-3}, ★) and D11 (SA = 4770 μm^{2}cm^{-3}, ★)

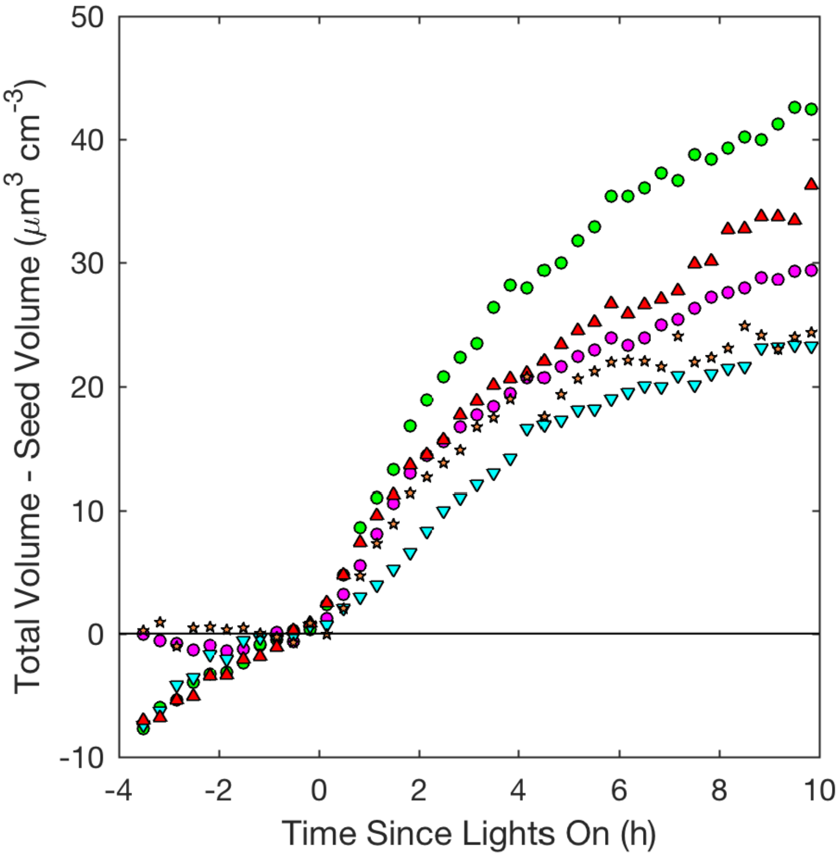

Figure S7. Total volume - seed volume (20 min averages) for all methacrolein experiments with seed aerosol: seed surface area - M2 (SA = 1640 μm^{2}cm^{-3}, ●), & M3 (SA = 2260 μm^{2}cm^{-3}, ●), temperature - M5 (13 °C, ▼) and M6 (32 °C, ▲), and new chamber with less wall charging - M9 (SA = 1910 μm^{2}cm^{-3}, ★).

S3 Additional Aerosol Composition Analysis from Aerosol Mass Spectrometer

The AMS results confirm that organic nitrates are present in the particle phase under dry conditions, but this technique is ill-suited for identifying specific organic nitrates present because $C_wH_xN_yO_z^+$ ions are produced in small yields (~5% of the nitrogen signal and <1% of the organic signal) and often occluded by more abundant peaks (Farmer et al., 2010). Organic nitrates fragment with a distinctly higher NO^+ / NO_2^+ ratio than inorganic ammonium nitrate (Farmer et al., 2010). Considering ammonium nitrate fragments to an NO^+ / NO_2^+ ratio of 2.4 for the Caltech AMS, the NO^+ / NO_2^+ ratio of 4-8 (Figure S8) implies organic nitrates are present during all the LV and 2MGA pathway experiments performed under dry conditions. Under humid conditions, nitric acid partitions to the particle phase (Figure S8) and the NO^+ / NO_2^+ (~2) shifts closer to that of ammonium nitrate.

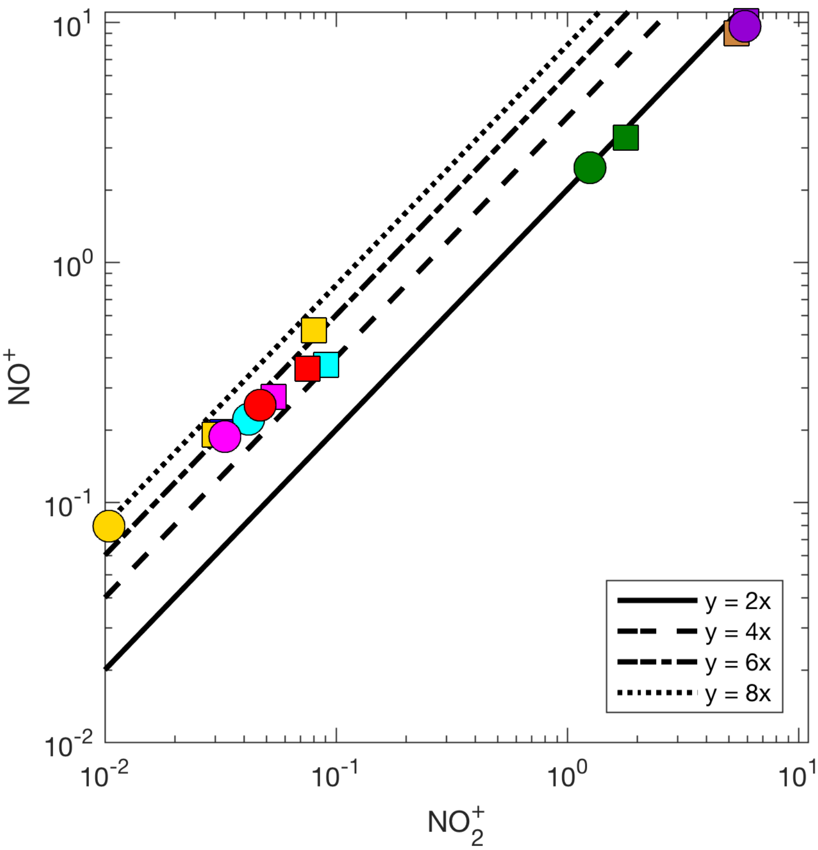

Figure S8. Average NO^+ vs NO_2^+ ratio from AMS during 10 h of photooxidation for LV pathway experiments (○) and 2MGA experiments (☐) with colors indicating no initial seed aerosol (**blue**), seed aerosol (**magenta**), 13°C (**cyan**), 32°C (**red**), RH ~50% (**green**), RH ~70% (**brown**), RH ~80% (**purple**), new chamber with negligible wall charging (**gold**)

As explained in Section 4.1 of the main text, SOA mass yields measured by the DMA under humid conditions were not reported due to the need for more characterization of particle coagulation and wall loss under humid, high-NO, and high-nitric acid conditions. The AMS results can provide a qualitative understanding of the SOA mass formed under various conditions. Due to uncertainties in the collection efficiency (CE), the AMS results should not be used for quantification of SOA mass in chamber experiments. Because humidity will enhance the CE (e.g., Docherty et al., 2013), for all humid experiments a Nafion dryer was used to dry the particles prior to AMS measurement. Changes in the CE due to differences in the organic composition between the experiments are possible. The AMS results are not corrected for particle wall loss. Additionally, as explained in Section 5.2 of the main text, an interference due to ammonium sulfate (Pieber et al., 2016) was subtracted from the organic signal. In general, this interference was higher and more variable in the humid experiments than the dry experiments.

For the LV pathway experiments, increases in humidity increase the aerosol mass measured by the AMS (Figure S9a). Given the low collection efficiency for the LV pathway compared to that from the 2MGA pathway (Section 5.3 of the main text), this increase is likely explained by slight enhancements in the particle phase of compounds, to which the AMS is more sensitive such as glyoxal and methylglyoxal. Zhang et al. (2011) determined the isoprene high-NO SOA mass yield under dry conditions was $\sim$ 2 times larger than that under humid conditions. Dommen et al. (2006) determined the isoprene SOA yield was not dependent on RH from 2-85%; however, Zhang et al. (2011) reevaluated data from Dommen et al. (2006) and concluded that when comparing only experiments performed under similar conditions, the SOA mass yield under dry conditions is $\sim$2 times greater than that formed under humid conditions. Here when comparing the AMS results for experiments M6 (RH = 47%) and M2 (RH = 8.9%), which have similar initial seed surface areas, SOA formation under dry conditions is $\sim$ 1-2 times higher than under humid conditions depending on the time of oxidation (Figure S9b).

In Figures S11-S14 and 9-10 in the main text, the average AMS mass spectra over the entire experiment (10h of photooxidation) is shown. The contribution of the highlighted fragments to the total tend to be fairly consistent over the entire 10h photooxidation period in both the LV and 2MGA pathway experiments.

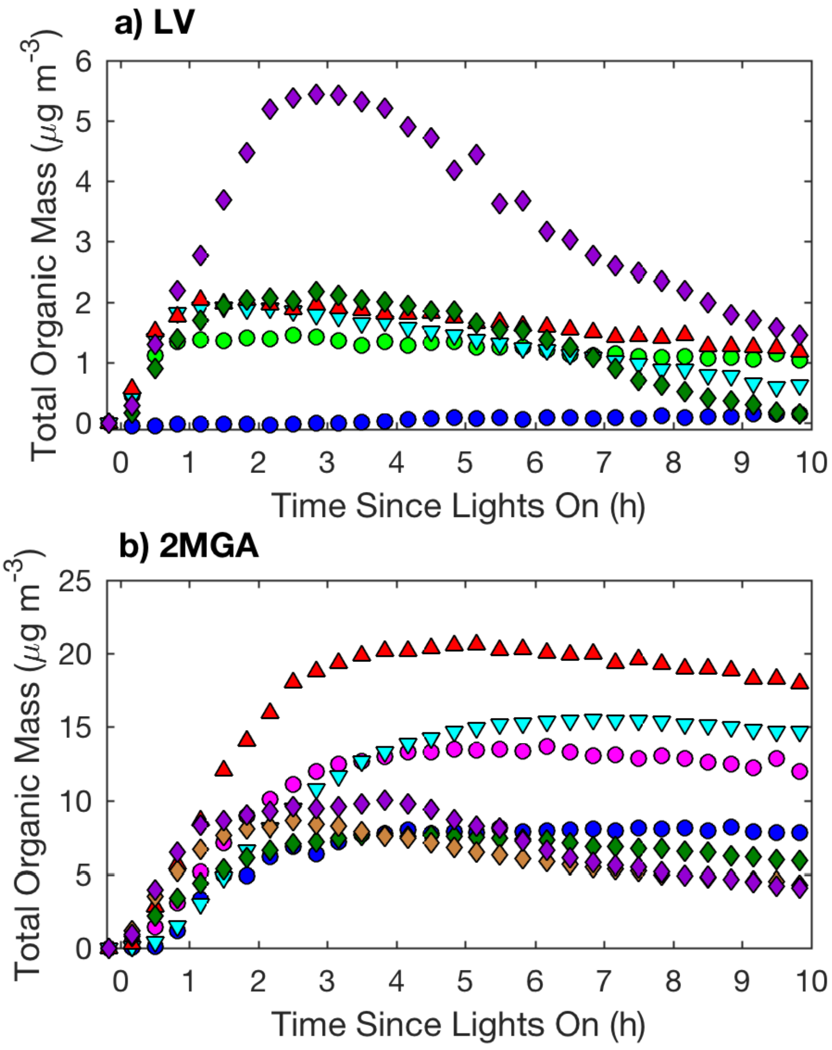

Figure S9. Total organic mass (20 minute averages) as measured by the AMS for LV pathway experiments (panel a): seed surface area - D1 (SA = 0 µm^2 cm^{-3}, ●) & D3 (SA = 3420 µm^2 cm^{-3}, ●), temperature - D5 (13 °C, ▼) & D6 (32 °C, ▲), and humidity - D8 (RH = 45%, ◆) & D9 (RH = 78%, ◆) and 2MGA pathway experiments (panel b): seed surface area - M1 (SA = 0 µm^2 cm^{-3}, ●) & M2 (SA = 1640 µm^2 cm^{-3}, ●), temperature - M4 (13 °C, ▼) & M5 (32 °C, ▲), and humidity - M6 (RH = 47%, ◆), M7(RH = 67%, ◆), & M8 (RH = 81%, ◆).

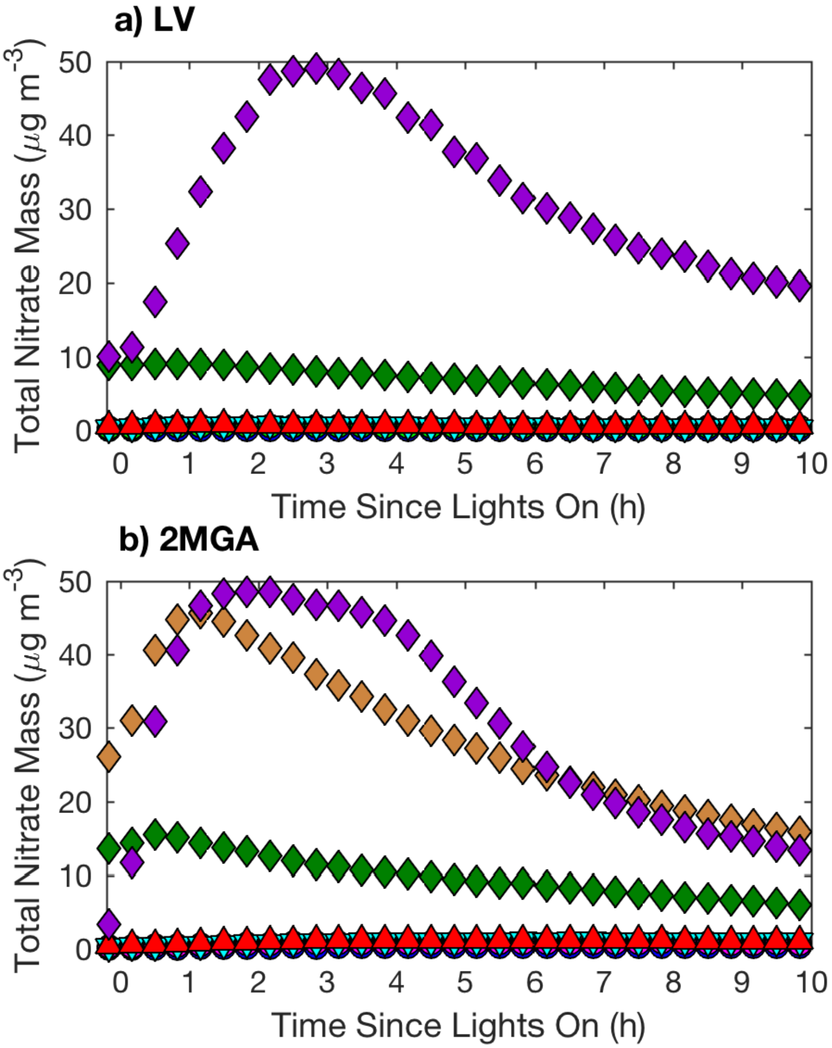

Figure S10. Total nitrate mass (20 minute averages) as measured by the AMS for LV pathway experiments (a): seed surface area - D1 (SA = 0 µm^2 cm^{-3}, ●) & D3 (SA = 3420 µm^2 cm^{-3}, ●), temperature - D5 (13 °C, ▼) & D6 (32 °C, ▲), and humidity - D8 (RH = 45%, ◆) & D9 (RH = 78%, ◆) and 2MGA pathway experiments (b): seed surface area - M1 (SA = 0 µm^2 cm^{-3}, ● & M2 (SA = 1640 µm^2 cm^{-3}, ●, temperature - M4 (13 °C, ▼) & M5 (32 °C, ▲), and humidity - M6 (RH = 47%, ◆), M7(RH = 67%, ◆), & M8 (RH = 81%, ◆).

a) LV - Low Temperature

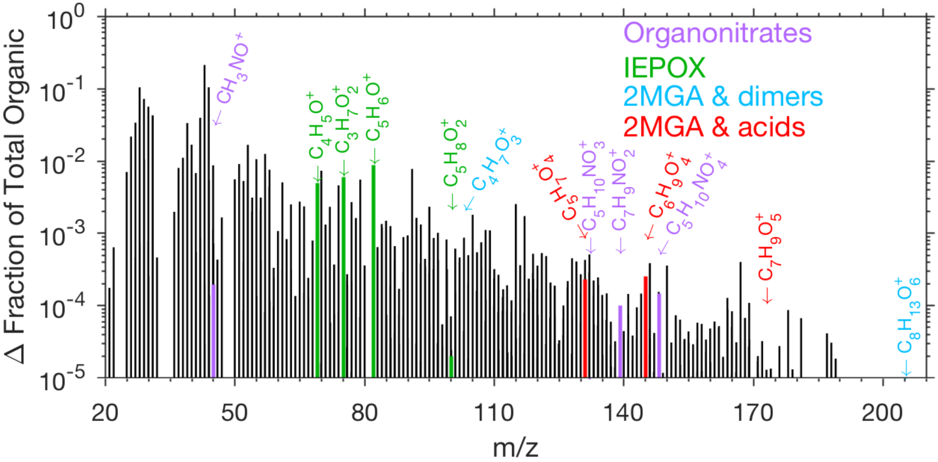

b) LV - High Temperature

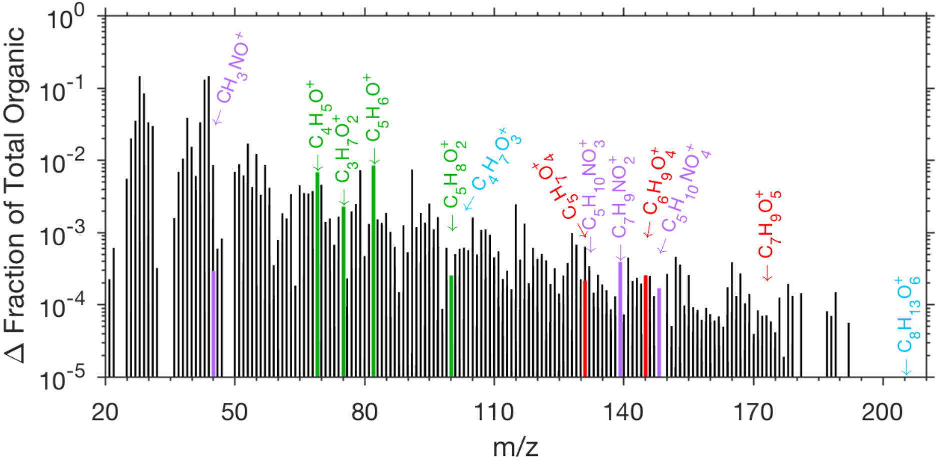

Figure S11. High resolution AMS mass spectra (averaged over 10h of photooxidation - the sulfate background) for experiment D5 (13 °C, panel a) and D6 (32 °C, panel b). Fragments are labeled as 2-MGA monomer/dimer (**cyan**), esterification of 2-MGA with acids (**red**), isoprene epoxydiol (IEPOX) tracers (**dark green**), and examples of organonitrate fragments - $C_xH_yNO_z$ (**purple**).

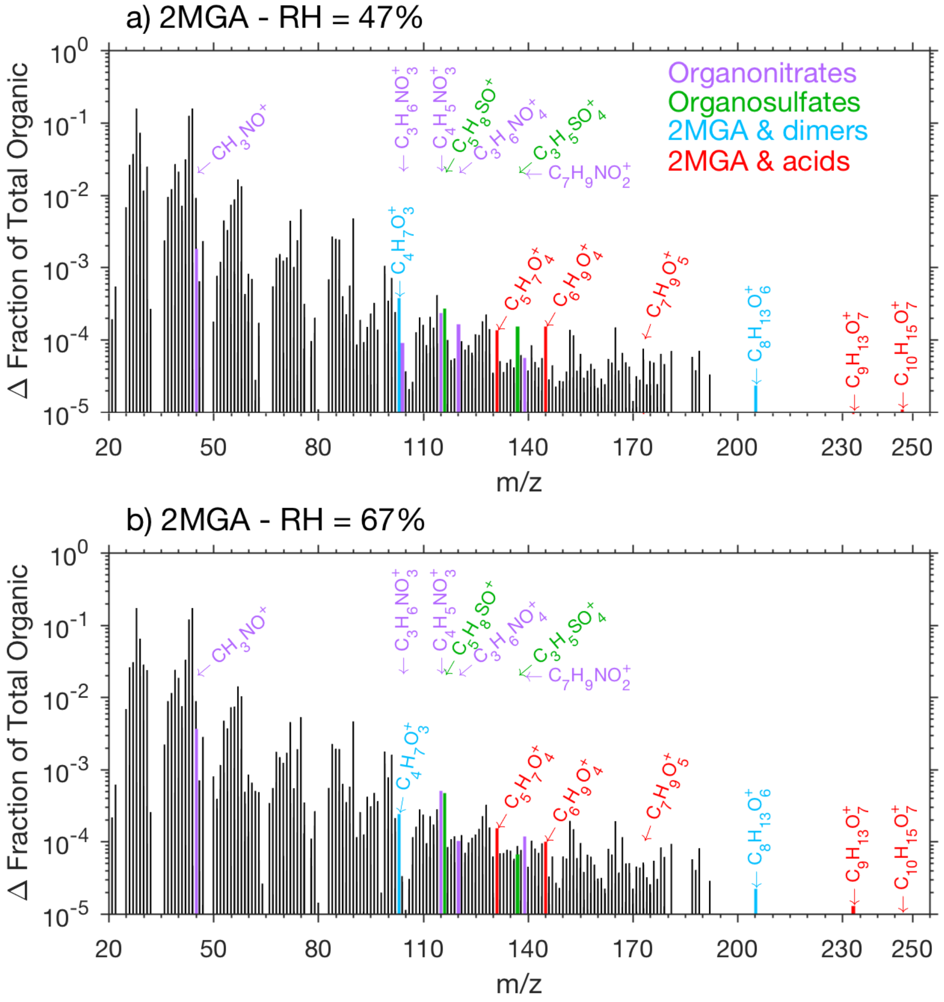

Figure S12. High resolution AMS mass spectra (averaged over 10h of photooxidation - the sulfate background) for experiment M6 (RH = 47%, panel a) and M7 (RH = 67%, panel b). Fragments are labeled as 2-MGA monomer/dimer (**cyan**), esterification of 2-MGA with acids (**red**), examples of organosulfate fragments (**dark green**), and examples of organonitrate fragments - $C_xH_yNO_z$ (**purple**).

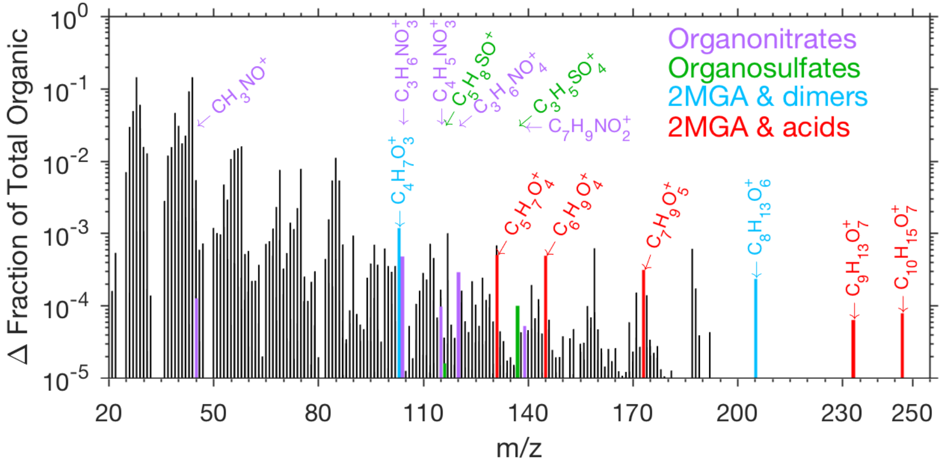

a) 2MGA - Ammonium Sulfate Seed

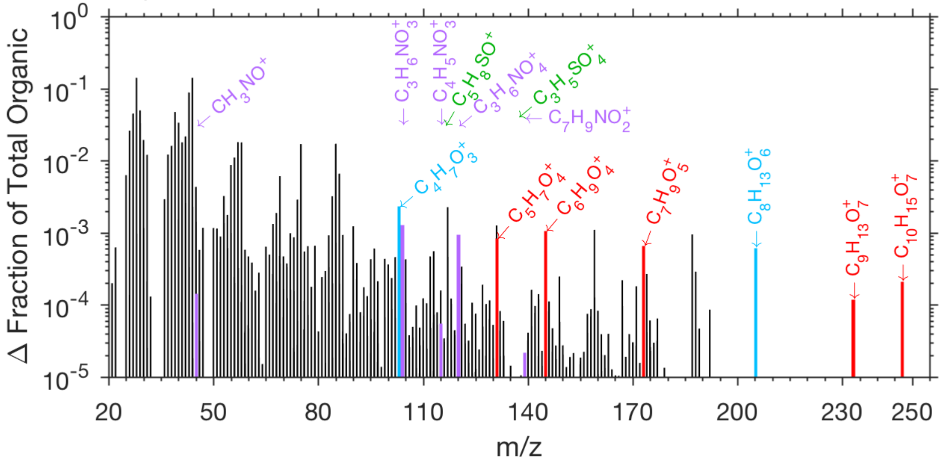

b) 2MGA - No Seed

Figure S13. High resolution AMS mass spectra (averaged over 10h of photooxidation - the sulfate background) for experiment M2 (1640 $\mu m^2\ cm^{-3}$, panel a) and AMS mass spectra (averaged over 10h of photooxidation) for experiment M1 (0 $\mu m^2\ cm^{-3}$, panel b). Fragments are labeled as 2-MGA monomer/dimer (**cyan**), esterification of 2-MGA with acids (**red**), examples of organosulfate fragments (**dark green**), and examples of organonitrate fragments - $C_xH_yNO_z$ (**purple**).

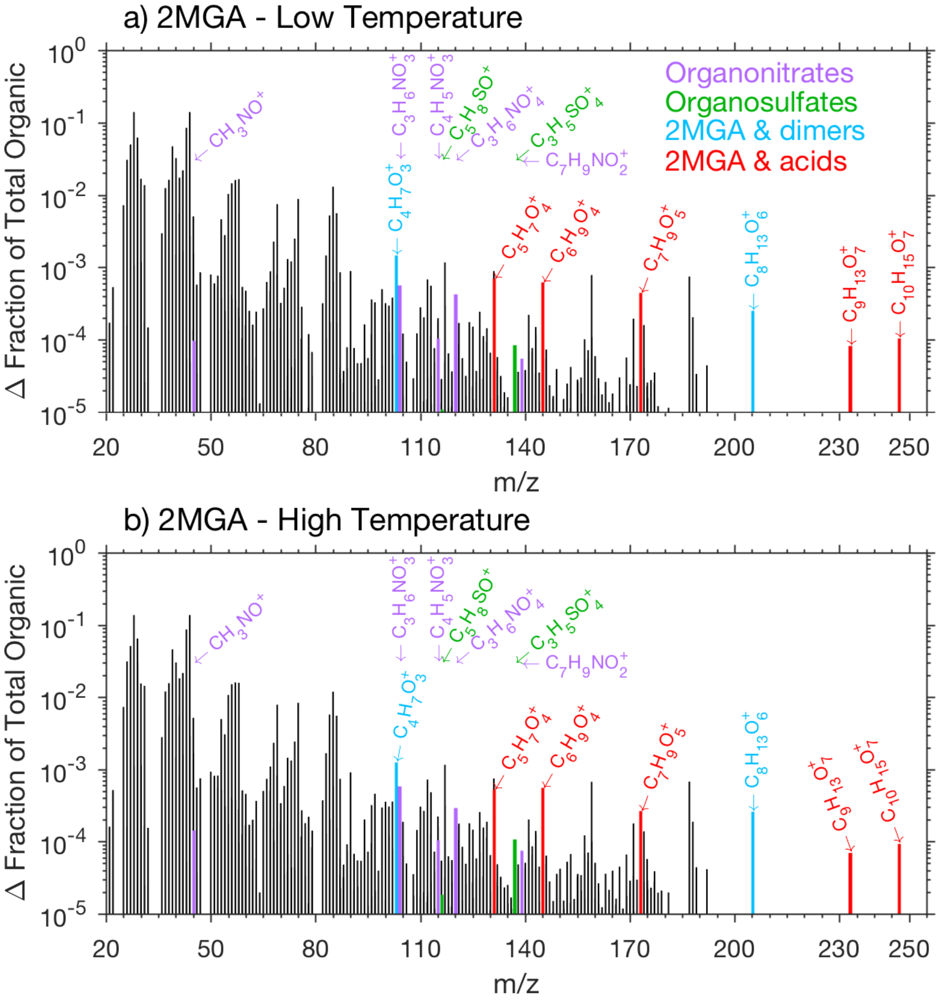

Figure S14. High resolution AMS mass spectra (averaged over 10h of photooxidation - the sulfate background) for experiment M4 (13 °C, panel a) and M5 (32 °C, panel b). Fragments are labeled as 2-MGA monomer/dimer (**cyan**), esterification of 2-MGA with acids (**red**), examples of organosulfate fragments (**dark green**), and examples of organonitrate fragments - $C_xH_yNO_z$ (**purple**).

References

Cantrell, C. A., Stockwell, W. R., Anderson, L. G., Busarow, K. L., Perner, D., Schmeltekopf, A., Calvert, J. G., and Johnston, H. S.: Kinetic Study of the NO_3-CH_2O Reaction and Its Possible Role in Nighttime Tropospheric Chemistry, J. Phys. Chem., 89, 139–146, https://doi.org/10.1021/j100247a031, 1985.

Charan, S. M., Kong, W., Flagan, R. C., and Seinfeld, J. H.: Effect of particle charge on aerosol dynamics in Teflon environmental chambers, Aerosol Sci. Technol., 52:8, 854–871, https://doi.org/10.1080/02786826.2018.1474167, 2018.

Cox, R. A., Derwent, R. G., Kearsey, S. V., Batt, L., and Patrick, K. G.: Photolysis of methyl nitrite: kinetics of the reaction of the methoxy radical with O_2, J. Photochem., 13, 149–163, https://doi.org/10.1016/0047-2670(80)85006-4, 1980.

Crump, J. G. and Seinfeld, J. H.: Turbulent deposition and gravitational sedimentation of an aerosol in a vessel of arbitrary shape, J. Aerosol Sci., 12, 405–415, https://doi.org/10.1016/0021-8502(81)90036-7, 1981.

Docherty, K. S., Jaoui, M., Corse, E., Jimenez, J. L., Offenberg, J. H., Lewandowski, M., and Kleindienst, T. E.: Collection efficiency of the aerosol mass spectrometer for chamber-generated secondary organic aerosols, Aerosol Sci. Technol., 47, 294–309, https://doi.org/10.1080/02786826.2012.752572, 2013.

Dommen, J., Metzger, A., Duplissy, J., Kalberer, M., Alfarra, M. R., Gascho, A., Weingartner, E., Prevot, A. S. H., Verheggen, B., and Baltensperer, U.: Laboratory observation of oligomers in the aerosol from isoprene/NO_x photooxidation, Geophys. Res. Lett., 33, L13 805, https://doi.org/10.1029/2006GL026523, 2006.

Farmer, D. K., Matsunaga, A., Docherty, K. S., Surratt, J. D., Seinfeld, J. H., Ziemann, P. J., and Jimenez, J. L.: Response of an aerosol mass spectrometer to organonitrates and organosulfates and implications for atmospheric chemistry, Proc. Natl. Acad. Sci. U. S. A., 107, 6670–6675, https://doi.org/10.1073/pnas.0912340107, 2010.

Jenkin, M. E., Hayman, G. D., and Cox, R. A.: The chemistry of CH_3O during the photolysis of methyl nitrite, J. Photochem. Photobiol., 42, 187–196, https://doi.org/10.1016/1010-6030(88)80062-5, 1988.

Jenkin, M. E., Hurley, M. D., and Wallington, T. J.: Investigation of the radical product channel of the $CH_3C(O)O_2$ + HO_2 reaction in the gas phase, Phys. Chem. Chem. Phys., 9, 3149–3162, https://doi.org/10.1039/B702757E, 2007.

Leppa, J., Mui, W., Grantz, A. M., and Flagan, R. C.: Charge distribution uncertainty in differential mobility analysis of aerosols, Aerosol Sci. Technol., 51, 1168–1189, https://doi.org/10.1080/02786826.2017.1341039, 2017.

Lopez-Yglesias, X. and Flagan, R. C.: Ion–aerosol flux coefficients and the steady-state charge distribution of aerosols in a bipolar ion environment, Aerosol Sci. Technol., 47, 688–704, https://doi.org/10.1080/02786826.2013.783684, 2013.

Nah, T., McVay, R. C., Pierce, J. R., Seinfeld, J. H., and Ng, N. L.: Constraining uncertainties in particle-wall deposition correction during SOA formation in chamber experiments, Atmos. Chem. Phys., 17, 2297–2310, https://doi.org/10.5194/acp-17-2297-2017, 2017.

Nannoolal, Y., Rarey, J., Ramjugernath, D., and Cordes, W.: Estimation of pure component properties Part 1. Estimation of the normal boiling point of non-electrolyte organic compounds via group contributions and group interactions, Fluid Phase Equilibria, 226, 45–63, https://doi.org/10.1016/j.fluid.2004.09.001, 2004.

Nannoolal, Y., Rarey, J., and Ramjugernath, D.: Estimation of pure component properties Part 3. Estimation of the vapor pressure of non-electrolyte organic compounds via group contributions and group interactions, Fluid Phase Equilibria, 269, 117–133, https://doi.org/10.1016/j.fluid.2008.04.020, 2008.

Nielsen, O. J., Sidebottom, H. W., Donlon, M., and Treacy, J.: Rate constants for the gas-phase reactions of OH radicals and Cl atoms with n-alkyl nitrites at atmospheric pressure and 298 K, Int. J. Chem. Kinet., 23, 1095–1109, https://doi.org/10.1002/kin.550231204, 1991.

Pieber, S. M., Haddad, I. E., Slowik, J. G., Canagaratna, M. R., Jayne, J. T., Platt, S. M., Bozzetti, C., Daellenbach, K. S., Frohlich, R., Vlachou, A., Klein, F., Dommen, J., Miljevic, B., Jimenez, J. L., Worsnop, D. R., Baltensperger, U., and Prevot, A. S. H.: Inorganic salt interference on CO_2^+ in Aerodyne AMS and ACSM organic aerosol composition studies, Environ. Sci. Technol., 50, 10 494–10 503, https://doi.org/10.1021/acs.est.6b01035, 2016.

Seinfeld, J. H. and Pandis, S. N.: Atmospheric Chemistry and Physics: From Air Pollution to Climate Change, John Wiley & Sons, Inc., Hoboken, New Jersey, 3 edn., 2016.

Sunol, A. M., Charan, S. M., and Seinfeld, J. H.: Computational simulation of the dynamics of secondary organic aerosol formation in an environmental chamber, Aerosol Sci. Technol., 52, 470–482, https://doi.org/10.1080/02786826.2018.1427209, 2018.

Wennberg, P., Bates, K. H., Crounse, J. D., Dodson, L. G., McVay, R. C., Mertens, L. A., Nguyen, T. B., Praske, E., Schwantes, R. H., Smarte, M. D., St Clair, J. M., Teng, A. P., Zhang, X., and Seinfeld, J. H.: Gas-Phase Reactions of Isoprene and Its Major Oxidation Products, Chem. Rev., 118, 3337–3390, https://doi.org/10.1021/acs.chemrev.7b00439, 2018.

Wiedensohler, A.: An approximation of the bipolar charge distribution for particles in the submicron size range, J. Aerosol Sci., 19, 387–389, https://doi.org/10.1016/0021-8502(88)90278-9, 1988.

Zhang, H., Surratt, J. D., Lin, Y. H., Bapat, J., and Kamens, R. M.: Effect of relative humidity on SOA formation from isoprene/NO photooxidation: Enhancement of 2-methylglyceric acid and its corresponding oligoesters under dry conditions, Atmos. Chem. Phys., 11, 6411–6424, https://doi.org/10.5194/acp-11-6411-2011, 2011.